XVI MEXICAN SYMPOSIUM ON MEDICAL PHYSICS

Physics in Precision Medicine - Advances in Imaging and Therapy

SCIENTIFIC PROGRAM

Content

Sponsors

The XVI Mexican Symposium on Medical Physics is sponsored by:

Academic Institutions and Professional Organizations

Universidad Autónoma de Yucatán (UADY)
Centro Latinoamericano de Física (CLAF)
American Association of Physicists in Medicine (AAPM)
International Organization for Medical Physics (IOMP)
Universidad Nacional Autónoma de México (UNAM)
Instituto de Física, UNAM

Commercial sponsors

EYMSA-Varian-PTW

IBA

Cyber Robotics

Welcome

The Medical Physics Division of the Mexican Physics Society and the School of Engineering of Universidad Autónoma de Yucatán are pleased to host the XVI Mexican Symposium on Medical Physics to be held virtually from October 28 to 30, 2020. The Symposium is sponsored by the International Organization for Medical Physics (IOMP), the American Association of Physicists in Medicine (AAPM), and the Centro Latinoamericano de Física (CLAF).

In its XVI iteration, the Symposium´s goal is to provide a space of collegiate discussion on the scientific and technological advances, perspectives, and challenges of Medical Physics in dawn of the era of precision medicine. The theme of the symposium is:

Physics in precision medicine: advances in diagnostic and therapy

Following the tradition of previous symposium, the Symposium will be preceded by a Pre-Symposium School on October 26 and 27 to provide continuing education on basic topics such as quality control and dosimetry. At the same time, we seek to offer attendants a deep view about the state of the art of our field. We are very thankful with the plenary and invited speakers, as well as with the faculty of the pre-symposium school for sharing with us their research and expertise.

In representation of the Organizing and Scientific Committees, we thank you for your contribution to the Symposium and hope that you enjoy it.

Orlando Soberanis-Dominguez, M.Sc. and Ivan M. Rosado-Méndez, Ph.D.

Chairs of Organizing and Scientific Committees
XVI Mexican Symposium on Medical Physics

Educational information

Target Audience:

- Scientists working on research projects related to Medical Physics
- Medical physicists working in hospitals, industry, and private companies
- Undergraduate and graduate students in Medical Physics or related programs working on projects related to Medical Physics
- Physicians and clinicians interested in Medical Physics

Educational Objectives:

Educational objective 1: To create a space of collegiate discussion on current research, clinical and professional challenges that Medical Physics face in the era of precision medicine.

Educational objective 2: To provide attendees with an extensive view of the state of the art of the different areas of medical physics, including diagnostic imaging, radiation therapy, nuclear medicine and analysis of physiological signals.

Educational objective 3: To contribute to the scientific training of attendees regarding scientific writing and presentation of scientific results through the publications of the Symposium's proceedings as well as oral and poster sessions.

Format and Educational Methods:

Pre-Symposium school: The Pre-Symposium school will include lectures from experts in different aspects of Medical Physics including radiation therapy, dosimetry, Monte Carlo simulation, quantitative imaging, physiological signal processing, and quality control. Lectures will be based on slide projections. The Pre-Symposium school will also include two workshops, one in Monte Carlo simulations and one on computed tomography quality control. These workshops will be based on exercises on personal computers performed by the participants guided by slide presentations provided by the instructors. Instructions on software installation and preparation for the workshops will be provided to the attendees at least two weeks before the symposium via email.

Symposium: Plenary and invited talks will provide attendees a comprehensive view on the state of the art of the various fields of Medical Physics. The information will be presented in slide projections. Scientific and poster sessions will provide a space for discussion on ongoing research in Medical Physics. The information will be presented in slide projections and posters.

Recertification credits for medical organizations

The enthusiasm of colleagues from the different branches of Medicine has been a driving force behind Medical Physics. The Organizing and Scientific Committees are fully convinced that the participation of fellow medical doctors is quintessential to foster multidisciplinary discussions that contribute to the progress of Medical Physics in Mexico. Thus, in recognition of this valuable contribution, we will be offering re-certification points from the following medical organizations:

Consejo Mexicano de Radiología e Imagen, A. C. - 5 puntos

Consejo Mexicano de Médicos Nucleares, A. C. - 18 puntos

Consejo Mexicano de Certificación en Radioterapia, A. C. - 25 puntos

Invited speakers and faculty of pre-symposium school

Dr. Thomas R. Mackie

Board of Visitors Vice Chair
Emeritus Professor, Medical Physics and Human Oncology
Director, Medical Devices Focus Area, Morgridge Institute for Research
University of Wisconsin-Madison
Faculty and plenary speaker

Dr. Mackie's career focuses on planning and delivery of radiation therapy to cancer patients. His group developed the 3-D treatment planning system that became the Philips Pinnacle treatment planning system, the most widely used radiation therapy treatment planning system in the world. His group was also the developer of tomotherapy, that combines technology from linear accelerators and computed tomography. More recently, Dr. Mackie has been working on developing a compact proton therapy machine for treating cancer. He has over 150 peer-reviewed publications, over 15 patents, and has trained many Ph.D. students. Dr. Mackie is a Fellow of the American Association of Physicists in Medicine and President of the John R. Cameron Medical Physics Foundation, a non-profit organization that supports the UW Medical Physics Department, medical physics in the developing world and high school science scholarships. In 2002, Dr. Mackie received the Ernst & Young Entrepreneur of the Year award.
https://directory.engr.wisc.edu/bme/Faculty/Mackie_Thomas/ https://en.wikipedia.org/wiki/Thomas_Rockwell_Mackie

Dr. Timothy J. Hall

Interim Chair and Professor Department of Medical Physics
Director, Graduate Medical Physics Program
Program Director, UW Radiological Sciences Training Program
Vice-Chair of the Quantitative Imaging Biomarker Alliance
Radiological Society of North America
Faculty and plenary speaker

Dr. Hall's work focuses on developing quantitative methods in medical ultrasound. This entails developing experimental methods for estimating specific physical properties of tissue such as the acoustic backscatter coefficient (to quantify acoustic scattering on an absolute scale), the effective scatterer size (to describe the tissue microstructure), and the nonlinear elastic modulus (to describe the tissue stiffness on an absolute scale). Also, within that effort are developments of test objects with known material properties (phantoms) that can be used to evaluate performance of these quantitative techniques, and performance descriptors that provide metrics to compare performance. The effort also involves integration of these methods into clinical imaging systems and tests in animal models, clinical trials in human subjects, and observer performance studies to test efficacy. Dr. Hall is funded by the NIH to investigate breast tissue properties with ultrasound and to develop uterine cervix assessments associated with pre-term birth and predicting successful post-date inductions.
https://www.medphysics.wisc.edu/blog/staff/hall-timothy/

Dr. Guillermina Ferro Flores

Gerencia de Aplicaciones Nucleares en la Salud
Instituto Nacional de Investigaciones Nucleares
Plenary speaker

Guillermina Ferro-Flores is the scientific leader of the "National Laboratory on Research and Development of Radiopharmaceuticals" at the National Institute of Nuclear Research in Mexico. She received her DSc in Medical Physics from the Autonomous University of the State of Mexico (UAEM). She conducted research stays at the Japan Atomic Energy Research Institute and at the University of Massachusetts Medical School. Her research is focused on the development of radiolabeled probes for therapy and molecular imaging. She has 110 peer-reviewed journal articles, several book chapters and seven patents, three under a broad international patent protection. Dr. Ferro-Flores is a member of the editorial board of the "Contrast Media & Molecular Imaging" journal. She has worked as a professor at the Faculty of Chemistry at UNAM, in the graduate medical physics program at UAEM and is currently a visiting professor of the master and doctorate program in physical ad mathematical sciences at the National Polytechnic Institute. She has participated as a head researcher in several projects sponsored by the Mexican National Council of Science and Technology and by the International Atomic Energy Agency (IAEA).

Dr. Daniel Razansky

Faculty of Medicine and Institute of Pharmacology and Toxicology
University of Zurich, Switzerland
Institute for Biomedical Engineering and Department of Information Technology and Electrical Engineering, ETH Zurich, Switzerland
Plenary speaker

Daniel Razansky is currently a Full Professor of Biomedical Imaging with double appointment at the Faculty of Medicine, University of Zurich (UZH) and Department of Information Technologies and Electrical Engineering, ETH Zurich, where he also serves as Director of the joint Animal Imaging Center of the ETH and UZH. He earned PhD in Biomedical Engineering and MSc in Electrical Engineering from the Technion - Israel Institute of Technology. Prof. Razansky's Lab pioneered a number of imaging technologies successfully commercialized worldwide, among them the multi-spectral optoacoustic tomography (MSOT) and hybrid optoacoustic ultrasound (OPUS). He has authored over 200 peer-review journal articles and holds 15 patented inventions in bio-imaging and sensing. Prof. Razansky's research has been recognized by the German Innovation Prize and multiple awards from the ERC, NIH, SNF, DFG and HFSP. He is a co-founding Editor of the Photoacoustics journal and serves on Editorial Boards of a number of journals published by Springer-Nature, Elsevier, IEEE and AAPM. He is an elected Council Member of the European Society for Molecular Imaging (ESMI), serves on the IEEE Technical Committee on Biomedical Imaging and Image Processing and has chaired numerous international conferences of the OSA, WMIS, ESMI and IFMBE. He is also an elected Fellow of the OSA and SPIE.

Dr. María-Ester Brandan

Investigadora Titular C, T. C.
Coordinadora de grupo de Dosimetría y Física Médica
Instituto de Física
Universidad Nacional Autónoma de México
Faculty of pre-symposium school

Dr. Brandan's present and past research include a broad spectrum of subjects in experimental nuclear physics, radiation dosimetry and medical physics. She was the creator and coordinator for 20 years of the UNAM M.Sc. (Medical Physics) program aimed at specializing physicists into medical applications. She is a member of the Mexican Academy of Sciences, Fellow of the American Physical Society and the American Association of Physicists in Medicine and a Fellow (member) of TWAS, the Academy of Sciences for the Developing World. She has been awarded the Mexican Physics Society Medal for the Development of Physics in Mexico and received the UNAM 2013 Premio Universidad Nacional in the area of Research in Exact Sciences. She is a current commissioner of ICRU, the International Commission on Radiation Units & Measurements.
https://www.fisica.unam.mx/~brandan/

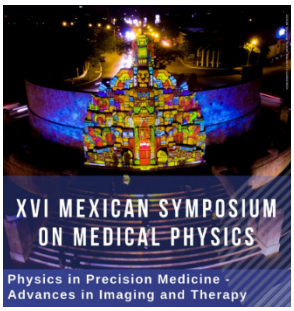

Dr. Héctor Garnica-Garza

Investigador Cinvestav 3C
Centro de Investigación y Estudios Avanzados
Monterrey, Nuevo León
Faculty of pre-symposium school

Dr. Garnica-Garza heads the X-ray Imaging Laboratory at the Center for Research and Advanced Studies of the National Polytechnic Institute. His research interests center on the use of Monte Carlo simulation, as applied to the transport of radiation, to model radiotherapy treatment devices, irradiation techniques and imaging modalities. He holds a Ph.D. in Medical Physics from Wayne State University.

Dr. Ana Leonor Rivera López

Investigadora de Carrera Titular B
Departamento de Estructura de la Materia
Instituto de Ciencias Nucleares
Faculty and invited speaker

Dr. Rivera López is a Physics specialist in Complex Systems and Signal Analysis using techniques in the time domain (statistics, correlations and networks), Spectral analysis (Fourier transform) and in Phase space (Wigner and wavelets distribution function). In the line of Medical Physics, she has studied non-invasive physiological time series of electrocardiograms, blood pressure, electroencephalograms, genetics and human voices. In 1996, she obtained his doctorate in science (Physics) from the Universidad Nacional Autónoma de México (UNAM) directed by Dr. Bernardo Wolf (specialist in mathematical optics) and Dr. Serguei Chumakov (from the Levedev Institute of the USSR Academy of Sciences, physicist -Mathematical specialist in quantum optics). As a student, she won the "Gabino Barreda" medal for being the best average of her generation of Master in Space Studies. As a research, in 2018, she obtained "Sor Juana Ines de la Cruz" Medal from UNAM. She is a National Researcher Level II (SNI). She currently works at the Institute of Nuclear Sciences of the UNAM and is the Academic Coordinator of Center for Complexity Sciences of UNAM. She was responsible for the creation of the curriculum of the UNAM degree in technology, being the first academic coordinator.

Jorge Castillo-López, M. Sc.

Clinical Medical Physicists
Servicio de Radiodiagnóstico
Instituto Nacional de Cancerología
Faculty of pre-symposium school

Jorge Castillo-López is a clinical medical physicist with five years of experience in medical imaging. His research interests include contrast-enhanced digital mammography and internal dosimetry. He is also a professor of the clinical residency for medical physicist at the National Institute for Cancer, training students on the physics of radiological images, MRI and ultrasound. He holds two Master of Science degrees, one in medical physics from the National Autonomous University of Mexico and the other nuclear physics from the Higher Institute of Applied Science and Technology (InSTEC) in La Habana, Cuba. During his time as student he worked on Dual-energy subtraction for microCT and Patient-specific dosimetry for 131I thyroid cancer therapy.

Dr. Eenas Omari

Clinical medical physicist
Medical College of Wisconsin
Invited speaker

Following her clinical training, Dr. Eenas Omari joined Loyola University in Chicago, where she took on lead roles in commissioning an MRI linac and the clinical implementation of the MRgRT program. She was the lead physicist implementing MRI guided real-time on-table adaptive radiotherapy (ROAR). Dr. Omari is also the co-lead of the Radiation Oncology Department's treatment planning service. Dr. Omari's research interests include image guided radiotherapy (IGRT) with an emphasis on MRI and Ultrasound imaging. She is also actively working on the development of MRI compatible immobilization devices and enhancing the MRgRT clinical workflow. As a faculty member, Dr. Omari mentors therapy physics residents and holds various lectures in the area of imaging and therapy physics for medical residents. Dr. Omari has over 30 published peer-reviewed papers, conference proceedings, and abstracts. She is a member of the AAPM and has been awarded to become an Associate of the Science Council mentorship program (SCAMP) for 2019-2020.

Dr. Paulina Galavis

Assistant Professor
Department of Radiation Oncology
New York University Langone Health
Invited speaker

Dr. Paulina Galavis received her Ph.D. in medical physics from the University of Wisconsin-Madison in 2013. Her dissertation focused on Robust Segmentation for Target Definition. Upon graduation, she went on to complete a residency program in therapeutic medical physics at the New York University, Langone Health. Dr. Galavis joined the Medical Physics Faculty at NYU in 2015, where she currently works as Assistant Clinical Professor in Radiation Oncology. She is American Board of Radiology (ABR) certified in therapeutic medical physics. Her research interests include radiomics, target definition for radiation therapy, treatment assessment, small field dosimetry, and patient safety.

Dr. Eric Ehler

Assistant Professor
Director of Physics Residency Program
Department of Radiation Oncology
University of Minnesota, Medical School
Invited speaker

Dr. Eric Ehler is an American Board of Radiology (ABR) certified clinical physicist. He earned his PhD in Medical Physics at the University of Wisconsin - Madison in 2009 followed by a clinical residency in Therapeutic Medical Physics at the University of Minnesota which he completed in 2011. He is currently an Assistant Professor in the University of Minnesota Department of Radiation Oncology. His clinical and research interests include pediatric radiotherapy, 3D printing, intrafraction tumor motion and compensation, small field dosimetry, and machine learning
https://med.umn.edu/bio/departmentofradiationoncology/eric-ehler

Dr. Guerda Massillon

Investigador Titular A, T. C.
Instituto de Física
Universidad Nacional Autónoma de México
Invited speaker

Dr. Massillon's research is Basic Dosimetry and its application in Medical Physics. She has received several national and international awards for her research such as: "Fellow" of the Interamerican Network of Academies of Sciences (IANAS) 2011; "Young Scientist Prize" of the International Union of Pure and Applied Physics (IUPAP) 2015; "Research Fellow" of the Royal Society, England 2015; "Marie Curie Medal", 2017; National System of Researchers SNI (CONACyT, Mexico) level II and PRIDE C of UNAM. As institutional work she is the actual president of the Medical Physics Division of the Mexican Physics Society, editorial board member of Physica Medica: European Journal of Medical Physics and a member of the TG-235 working group of the AAPM (American Association of Physicists in Medicine).

XVI Mexican Symposium On Medical Physics

Physics in Precision Medicine: Advances in Imaging and Therapy

Schedule

IMPORTANT: EVERY MORNING YOU WILL RECEIVE A LIST OF LINKS TO JOIN EACH BLOCK. THE PLATFORM ONLY ALLOWS BLOCKS WITH A MAXIMUM DURATION OF 2.5 HRS.

Blok number	Color code
Block 1	
Block 2	
Block 3	
Block 4	
Block 5	

	Monday October 26	Tuesday October 27	Wednesday October 28	Thursday October 29	Friday October 30
8:30-9:00			Opening ceremony		
9:00-9:30	Class 1	Class 4	Plenary Talk 1	Plenary Talk 3	Plenary Talk 4
9:30-10:00					
10:00-10:30			Invited Talk 1	Invited Talk 3	Invited talk 5
10:30-11:00			Networking	Networking	Networking
11:00-11:30	Break	Break	Scientific sess. 1	Scientific sess. 3	Sponsor Talk 3
11:30-12:00	Class 2	Class 5			
12:00-12:30					Scientific sess. 5
12:30-13:00			Sponsor Talk 1		
13:00-13:30				Sponsor Talk 2	DFM ASSEMBLY
13:30-14:00	Lunch	Lunch	Lunch & Networking		
14:00-14:30				Lunch	Lunch
14:30-15:00	Class 3	Class 6			
15:00-15:30			Invited Talk 2	Invited Talk 4	Sponsor Talk 4
15:30-16:00			Scientific sess. 2	Scientific sess. 4	
16:00-16:30					Scientific sess. 6
16:30-17:00			Poster Session	Poster Session	
17:00-17:30					
17:30-18:00					Closing ceremony
18:00-18:30			Plenary Talk 2	Student competition	Round Table DFM-SMFM
18:30-19:00					
19:00-19:30					
19:30-20:00					

Pre-symposium school

MONDAY, OCTOBER 26, 2020

Radiation therapy and dosimetry (Moderator: Dr. Guerda Massillon)

Learning objectives:

1. Discuss the value of innovation in radiation therapy and clinical translation of new technologies
2. Discuss the physical principles behind beam quality assessment with thermoluminescent dosimetry
3. Review basic concepts of Monte Carlo methods in radiation therapy

9:00 – 11:00 Innovation in Medical Physics: From the Lab to the Clinic to the Enterprise
Dr. Thomas R. Mackie (University of Wisconsin-Madison, USA)

Abstract: Radiation oncology and radiology have relied on advances in science and engineering from medical physics researchers. Medical physicists and clinicians are trained to have an orientation of professionalism that goes beyond the rewards of receiving grants, training students and publishing results. A relatively large number of medical physicists have successfully passed their ideas onto existing companies or started for-profit and not-for-profit enterprises that bring their technology into practical use. The more that a medical physicist knows about business and regulatory principles the more likely their success. This lecture will discuss innovation and development of research ideas into practice illustrated through examples. The importance of finding worthwhile problems to solve, involving potential customers in critiquing your solutions, and protecting your intellectual property will be emphasized. Principles of business formation, financing, product design, project management, regulation and reimbursement will be framed. The value of the lean startup methodology applied to the development of capital-intensive medical devices will be highlighted. Analysis of the root causes of business failures in radiation oncology and radiology will also be discussed.

11:00– 11:30 Break

11:30 – 13:30 Advances in thermoluminescent dosimetry – Teletherapy beam quality assessment
Dr. María-Ester Brandan (Instituto de Física, UNAM, Mexico)

Abstract: The basics of thermoluminescent (TL) dosimetry will be presented, based on the experience and protocols developed in our laboratory at the UNAM Physics Institute. I will review the current use of TL dosimeters in radiotherapy and present novel results from our group assessing the mean energy of secondary radiation produced in a linac using TL dosimeters.

13:30 – 14:30 Lunch

14:30 – 16:30 Monte Carlo Simulation in Voxelized Geometries: Applications in Radiation Therapy and Diagnostics Radiology
Dr. Héctor Garnica (CINVESTAV-Monterrey, Mexico)

Abstract: Monte Carlo simulation of radiation transport plays a crucial role in the Medical Physics field, from radiotherapy treatment planning to the modeling of the devices that generate the radiation used both in treatment as well as in diagnostics. In this workshop, the implementation of Monte Carlo simulations using CT scanner-derived patient information will be discussed, with emphasis on the methods employed to extract the CT image data required

by most Monte Carlo radiation transport codes currently available. Among the topics to be discussed are: mechanics of photon transport in voxelized geometries, conversion from CT number to material density and composition, and x-ray source modeling. Applications with specific examples in radiotherapy treatment planning, CT scanner modeling and breast imaging will also be discussed.

TUESDAY, OCTOBER 27, 2020

Diagnostic imaging and physiological signal analysis (Moderator: Dr. Ivan Rosado-Mendez)

Learning objectives:

1. Discuss the physical principles of Quantitative Ultrasound imaging
2. Cover the basic principles of non-invasive biomarkers based on physiological measurements
3. Review recent quality control protocols of x-ray computed tomography

9:00 – 11:00 Physics of Quantitative Ultrasound Imaging

Dr. Timothy Hall (University of Wisconsin-Madison, USA)

Abstract: Ultrasound is one of the most widely used medical imaging modalities because of its relatively low cost, portability, and safety. Despite these advantages, in some applications utility of the information obtained depends on the imaging system configuration, the skills of the operator, as well as the skills of the clinician interpreting the data. This class will present the physics of novel quantitative imaging techniques based on ultrasound imaging, broadly known as Quantitative Ultrasound (QUS) that aim at overcoming these limitations. Special emphasis will be given to a technique known as Ultrasound Backscatter Spectroscopy, which allows obtaining acoustic and structural properties of tissue to inform on its microscopic changes during disease and/or treatment. This is achieved through the spectral analysis of backscatter echo signals generated by ultrasound equipment as part of the conventional image formation process. The class will close with a discussion of ongoing pre-clinical and clinical applications of QUS in tissues such as breast and cervix.

11:00 – 11:30 Break

11:30 – 13:30 Introduction to non-invasive biomarkers from physiological signals

Dr. Ana Leonor Rivera (Instituto de Ciencias Nucleares, UNAM, Mexico)

Abstract: Human health is determined by the functionality of its various organs and the interaction between them that can be understood from the physical point of view as a complex system. Health can be considered as a condition that allows an adequate dynamic balance between robustness, supported by systems that allow it to maintain homeostasis and survive in a wide range of conditions, but also by its ability to rapidly and effectively adapt to a changing external environment. This balance between robustness and adaptability can be measured by biomarkers. Alterations in the range of these biomarkers may appear before symptoms arise and open up promising possibilities for applications in preventive medicine. In this short course we will take a glance of methods that allow to find relevant parameters that can be used as biomarkers characteristic of health from non-invasive physiological time series like electrocardiograms, breathing, and blood pressure signals. We introduce signal analysis techniques in the time domain using the distribution moments, autocorrelation functions, Poincaré diagrams, and the spectral analysis (Fourier transform). We will see how deviations

from the range of these biomarkers can be used as early warnings auxiliaries in the diagnosis of diseases like Diabetes Mellitus type 2.

13:30 – 14:30 Lunch

14:30 – 17:30 Workshop on CT quality control

M. en C. Jorge Castillo (Instituto Nacional de Cancerología, Mexico)

Abstract: Computed tomography (CT) is a broadly used imaging modality, including clinical diagnosis, interventional procedures, therapy planning and hybrid imaging with nuclear medicine systems. Quality control, which is the main topic of this course, is a major tool to ensure that each study achieves a clinically relevant image quality at the proper radiation dose. Upon completion of this workshop, attendees should be able to demonstrate understanding about the influences of acquisition parameters on image quality, routine quality controls and annual survey of a CT unit. The workshop is divided in two parts: theory and practice. The first part will be imparted online and every participant should complete it before accessing practical session. Hands on will include an annual survey of a CT unit used for radiation therapy planning.

Symposium

WEDNESDAY, OCTOBER 28, 2020

08:00 – 18:00 Registration
08:30 – 09:00 Opening ceremony

Plenary Talk 1

Moderator: Dr. Ivan Rosado-Mendez

09:00 – 10:00 Quantitative Imaging Biomarkers: standardization and clinical use.
Dr. Timothy Hall, Co-chair of the Quantitative Imaging Biomarker Alliance, Radiological Society of North America, USA.

Invited Talk 1 (Moderator: Dr. Ivan Rosado)

Moderator: Lizbeth Ayala, M.Sc.

10:00 – 10:30 Magnetic resonance imaging guided adaptive radiotherapy (MRgART).
Dr. Eenas Omari, Loyola University Medical Center, USA.

10:30 – 11:00 Networking

Scientific session 1 (SS1)

Moderator: Dr. Héctor Morales Bárcenas

11:00 – 12:30 Use of non-ionizing radiation in medicine

11:00-11:15 Non-invassive Pressure Estimation with Lumason and Sonazoid Microbubbles. Gupta et al., T. Jefferson University, USA.

11:15-11:30 Disrupting Biofilms in Synovial Fluid with Ultrasound Triggered Microbubble Destruction. Forsberg et al., T. Jefferson University, USA.

11:30-11:45 Feasibility of Clinical Risk Assessment based on Pressure-gradient Estimation using 3D Contrast-enhanced Ultrasound. Nam et al., Thomas Jefferson University, USA.

11:45-12:00 Estimation of Effective Scatterer Size and Acoustic Concentration Quantitative Ultrasound Parameters Using Dynamic Programming. Jafarpisheh et al., Concordia University, Canada.

12:00-12:15 Application of dynamic-programing estimation of acoustic attenuation and backscatter coefficient of breast carcinoma. Castañeda-Martínez et al., UNAM, Mexico.

Sponsor Talk 1

12:30 – 13:30 Aplicación de nuevos criterios de análisis para el control de calidad paciente específico
Camilo Beltrán – Aplicaciones PTW para América Latina

13:30 – 15:00 LUNCH & NETWORKING

Invited Talk 2

Moderator: Dr. Miguel Ángel Ávila Rodríguez

15:00 – 15:30 Reproducibility and standardization in Radiomics: Are we there yet?
Dr. Paulina Galavis, NYU Langone Health, USA.

Scientific session 2 (SS2)

Moderator: Dr. Héctor Alva Sánchez

15:30 – 16:30 Physics and dosimetry of medical images (ionizing radiation) – Part 1

15:30–15:45 Breast density quantification using dual-energy digital mammography. Pacheco et al., UNAM, Mexico

15:45-16:00 Use of Timepix detectors in preclinical CT/PET/SPECT imaging. Sefc et al., CAPI, Czech Republic.

16:00-16:15 Design of a bilateral filter for noise reduction in contrast-enhanced micro-CT. Ayala et al., UNAM, Mexico.

16:15-16:30 Characterization of a Fricke-gel solution as a potential low-dose dosimeter. Medina et al., UNAM, Mexico.

Poster Session 1

16:30 – 18:00 Poster Session

Plenary Talk 2

Moderator: Dra. Olga Ávila

18:00 – 19:00 Advances in molecular imaging
Dr. Guillermina Ferro-Flores, Instituto Nacional de Investigaciones Nucleares, Mexico.

THURSDAY, OCTOBER 29, 2020

08:00 – 18:00 Registration

Plenary Talk 3

Moderator: Dra. María Ester Brandan

09:00 – 10:00 Is Upright Radiotherapy Medically and Financially Better?
Dr. Thomas R. Mackie (Emeritus Professor, University of Wisconsin.

Invited Talk 3

Moderator: Dra. Olinca Galván

10:00 – 10:30 Utilization of 3D Printing in Clinical Medical Physics.
Dr. Eric Ehler, University of Minnesota, USA.

10:30 – 11:00 Networking

Scientific session 3 (SS3)

Moderator: Dr. José Manuel Lárraga

11:00 – 13:00 Physics and dosimetry of medical images (ionizing radiation) – Part 2, and Physics and dosimetry of radiation therapy – Part 1

11:00-11:15 A Three-Dimensional Electronic Detector Array Readout Configuration for Radiotherapy based on Active Matrices. Challco et al., UNI, Peru

11:15-11:30 Monte Carlo modelling of kV and MV imaging systems of the Varian TrueBeam STx Linac. Zapien-Campos et al., UNAM, Mexico.

11:30-11:45 Optical transport studies in monolithic LYSO crystals for PEM detectors. Lara et al., IPN, Mexico.

11:45-12:00 Lipomics: a coloidal system with potential as a hydrophilic-lipophilic drugs carrier. Ramírez-Hernández et al., UNAM, Mexico.

12:00-12:15 Preparation and Preclinical Evaluation of 64Cu-NOTA-iPSMA as a Theranostic Radiopharmaceutical for Prostate Cancer. Góngora-Servín et al., UNAM, Mexico.

Sponsor Talk 2

13:00 – 14:00 Talk by IBA

14:00 – 15:00 Networking

Invited Talk 4

Moderator: Dra. Marisela Vega de Lille

15:00 – 15:30 A fundamental approach of low-energy radiation dosimetry
Dr. Guerda Massillon-JL, Instituto de Física, UNAM, México.

Scientific session 4 (SS4)

Moderator: Dr. Mariana Hernández

15:30 – 16:30 Physics and dosimetry of radiation therapy – Part 2

15:30–15:45 OSL nanoDot Response at High Dose Gradient Regions: Validation with phantom and *in vivo* tests. Agüero et al., FEMN, Argentina.

15:45-16:00 Image Guided Radiotherapy Protocols and Doses: A CEMENER Experience. Palacios et al., CEMENER, Argentina.

16:00-16:15 A Proposed Method to Assure the Efficiency of Thermotherapy Treatments. Pérez-Ahumada et al., UNAM, Mexico.

Poster Session 2

16:30 – 18:00 Poster session

Best Student Paper Competition (SC)

Moderator: Dr. Guerda Massillon

18:00 – 19:00

18:00-18:15 Short-term Cardiorespiratory Variability During the Menstrual Cycle. Barajas-Martínez et al., UNAM, Mexico

18:15-18:30 A preclinical model for radio-osteoporosis induction. Hernández-Ramírez et al., UNAM, Mexico.

18:30-18:45 Sleep staging with a hyperdimensional specialized dense network. Hernández-Cano et al., UNAM, Mexico.

FRIDAY, OCTOBER 30, 2020

08:00 – 12:00 Registration

Plenary Talk 4

Moderator: Dr. Crescencio García

09:00 – 10:00 Advanced optoacoustic methods for biological discovery and precision diagnostics
Dr. Daniel Razansky, Institute for Biomedical Engineering, ETH Zurich, Switzerland.

Invited Talk 5

Moderator: Dr. Rubén Fossion

10:00 – 10:30 Non-invasive biomarkers from physiological signals
Dr. Ana Leonor Rivera, Instituto de Ciencias Nucleares, UNAM, Mexico.

10:30 – 11:00 Networking

Sponsor Talk 3

11:00 – 12:00 Física Médica 3.0: desafíos y beneficios de la combinación de inteligencia humana y artificial
Cleverson Lopes – Gerente de Marketing Varían Latin America

Scientific session 5 (SS5)

Moderator: Dr. Rubén Fossion

12:00 – 13:00 Biological physics, physiological measurements and mathematical methods in medical physics

12:00-12:15 Parallels Between Homeostatic Regulation and a Balance Robot Toy Model. Legaria-Peña et al., UNAM, Mexico.

12:15-12:30 Design of a Faraday Cage for Biomedical Measurements Based on Site Electromagnetic Field Mapping. Cruz-Valenzuela et al., UNAM, Mexico.

12:30-12:45 Spectral and Statistical analysis of actigraphic recordings of acute insomnia patients. Marín-García et al., UNAM, Mexico.

12:45-13:00 Analysis of the exponent Hurst in RR series of healthy subjects and congestive patients in sleep and wake state and in healthy subjects during physical activity. Salcedo-Martínez et al., UPIBI-IPN, Mexico.

13:00-14:00 ASSEMBLY OF THE MEDICAL PHYSICS DIVISION OF THE MEXICAN PHYSICS SOCIETY

14:00 – 15:00 Lunch & Networking

Sponsor Talk 4

15:00 – 16:00 Talk by Cyber Robotics

Scientific session 6 (SS6)

Moderator: César Ruiz, M.Sc.

16:00 – 17:00 Educational and professional issues

16:00–16:15 2D Radiotherapy in Mexico Today. García-Zúñiga et al., Hospital Central "Ignacio Morones Prieto", Mexico.

16:15-16:30 Professional and academic follow up of 100+ graduates of the UAEM-ININ masters and doctorate program in medical physics in Mexico. E. Mitsoura, UAEM, Mexico.

16:30-16:45 Academic offer in the UNAM M. Sc. (Medical Physics) program. M. E. Brandan, UNAM, Mexico.

16:45-17:00 International experiences on a budget: the role of online technologies in the training of young scientists in developing countries. Porras-Chaverri et al., U. de Costa Rica, Costa Rica.

17:00 – 17:30 Break & Networking

17:00 – 18:00 Awards and Closing ceremony

Round table

Moderator: Adriana Moreno, M.Sc.

18:00 – 20:00 Towards better professional recognition of the Medical Physicist in Mexico (This activity will be open to the public)

Plenary talks

Plenary talk 1

9:00 – 10:00 Wednesday, October 28, 2020.

Quantitative Imaging Biomarkers: standardization and clinical use

Dr. Timothy Hall
Co-chair of the Quantitative Imaging Biomarker Alliance, Radiological Society of North America, USA.

Abstract: As patient management moves toward personalized treatment strategies, the need for objective and quantitative information to accurately diagnose disease and monitor its response to therapy is more important than ever. Objective information derived from medical images have the potential to offer this information in the form of Quantitative Imaging Biomarkers (QIBs). QIBs are quantitative features extracted from medical images that can be linked to the phenotype of a disease in each patient. This talk will present current efforts of the Radiological Society of North America's Quantitative Imaging Biomarker Alliance (QIBA) to standardize the use of QIBs to maximize their reproducibility, clinical value, and impact. This effort involves all major imaging modalities, and all stakeholders in the design, use, and evaluation of medical imaging systems. One key aspect of this work is the integration of concepts from metrology into the physics and clinical aspects of image acquisition and feature extraction. The effort can be described as 'converting imaging systems into measurement systems'. Examples from several modalities will be presented with an overview toward future efforts.

Plenary talk 2

19:00 – 20:00 Wednesday, October 28, 2020.

Advances in molecular imaging

Dra. Guillermina Ferro-Flores
Instituto Nacional de Investigaciones Nucleares, Mexico.

Abstract: Molecular imaging detects and records the distribution in time and space of molecular processes for diagnostic and therapeutic applications. The techniques in which molecular imaging is applied include magnetic resonance imaging (MRI), optical imaging (OI), positron emission tomography (PET), and single-photon emission computed tomography (SPECT). Radionuclide-based molecular imaging involves SPECT and PET. Nuclear imaging is a technique that, in comparison to other imaging modalities, offers greater sensitivity and has no tissue penetration limits. Protein-protein, protein-peptide and protein-hormone interactions are crucial for the performing of biological processes. Several of these specific interactions are responsible for diseases, including cancer. In general, the development of synthetic inhibitors of protein interactions is an active research field in medicinal chemistry due to the advantage of obtaining low molecular- weight compounds for specific binding to protein surfaces. The development of radiolabeled protein-inhibitor peptides for molecular imaging and targeted therapy with rapid clinical translation is an interesting and active research field in the radiopharmaceutical sciences. In this presentation, recent achievements concerning the design, translational research and theranostic applications of structurally-modified small radiopeptides such as prostate-specific membrane antigen (PSMA) inhibitors, antagonists of chemokine-4 receptor ligands (CXCR-4-L) and fibroblast activation protein (FAP) inhibitors with high affinity for cancer-associated target proteins, will be reviewed and discussed.

Plenary talk 3

9:00 – 10:00 Thursday, October 29, 2020.

Is Upright Radiotherapy Medically and Financially Better?

Dr. Thomas R. Mackie
Emeritus Professor, University of Wisconsin.

Abstract: Treating patients in the upright position is not new but has been limited by image guidance in the upright position and specialized immobilization. Treatment planning images can now be acquired with MRI or CT scanners that allow upright patient positioning with secure immobilization. There are medical advantages to treatment in the upright position for conventional external beam photon radiotherapy. It has been shown that lung radiotherapy would be advantageous because the lung is more inflated, there is less normal tissue integral dose, the lung moves less in the upright position, and patients who cannot control coughing are more comfortable and less likely to choke. Treating the breast in a slightly forward leaning posture may better space the lung and heart as compared to supine treatments and be easier to set up as compare to prone treatments. Upright proton and carbon radiotherapy offer many cost advantages by eliminating the need for an expensive gantry. The potential size of upright megavoltage x-ray units is small enough that two treatment rooms can be contained within the size of a typical contemporary vault lowering facilities costs especially for green-field sites.
Disclosures: I am chairman of Leo Cancer Care. I am also co-founder and chairman of Asto CT, which has developed a multi-axis CT scanner for veterinary use. I also have financial investment in these companies.

Plenary talk 4

9:00 – 10:00 Friday, October 30, 2020.

Advanced optoacoustic methods for biological discovery and precision diagnostics

Dr. Daniel Razansky
Institute for Biomedical Engineering and Department of Information Technology and Electrical Engineering, ETH Zurich, Switzerland.

ABSTRACT: Rapid progress of the Multi-Spectral Optoacoustic Tomography (MSOT) technology has enabled unprecedented insights into in vivo biological dynamics and molecular processes. This fast-emerging imaging modality is capable of entirely non-invasive longitudinal observations at penetration and spatiotemporal scales not covered by other bio-imaging techniques. The talk covers most recent advances pertaining ultrafast imaging instrumentation, intelligent reconstruction algorithms as well as smart optoacoustic contrast and sensing approaches. Our current efforts are geared toward exploring potential of the technique in studying multi-scale dynamics of the brain and heart, monitoring of therapies, fast tracking of cells and targeted molecular imaging applications. MSOT further allows for a handheld operation thus offers new level of precision for clinical diagnostics of patients in a number of indications, such as breast and skin lesions, lymph node metastases, thyroid conditions and inflammatory bowel disease.

Invited talks

Invited talk 1

10:30 – 11:00 Wednesday, October 28, 2020.

Magnetic resonance imaging guided adaptive radiotherapy (MRgART)

Dr. Eenas Omari
Loyola University Medical Center, USA.

Abstract: Magnetic resonance imaging guided radiation therapy (MRgRT) has been playing a major role in offline treatment planning. In recent years, linear accelerators (linac) with onboard MRI has become clinically available. In addition, real-time MRI guided adaptive radiation therapy (MRgART) has led to a major paradigm shift resulting in personalized daily patient treatment. In this work, we first familiarize the audience with the emerging technology and discuss its advantages and drawbacks. We then discuss the steps to take in implementing an MRgRT program. This includes the acceptance and commissioning of a 0.35 T MRI linac and the clinical implementation of real-time on-table adaptive radiotherapy.

Invited talk 2

15:00 – 15:30 Wednesday, October 28, 2020.

Reproducibility and standardization in Radiomics: Are we there yet?

Dr. Paulina Galavis
NYU Langone Health, USA.

Abstract: Radiomics is a rapidly growing field in cancer research that looks for ways to personalize patient's treatments based on the extraction of texture features from routine clinical images. However, the implementation of Radiomics-based models in routine patient care poses important challenges, since they are multi-step processes that include image selection, region of interest (ROI) segmentation, texture-feature extraction, model development, and model-validation. Each of these processes needs extensive evaluation to ensure consistency and accuracy of the final Radiomics-based model, so that it becomes reproducible and translatable into the clinical practice. Image selection and ROI segmentation are a critical component in Radiomics, because they define the quality of the extracted features, which then become the input of the model. In this short review, after presenting a brief description of the Radiomics, we will concentrate in particular on the status of various technical aspects of imaging modality and segmentation selection, including their shortcomings and possible solutions with emphasis to radiation therapy.

Invited talk 3

10:30 – 11:00 Thursday, October 29, 2020.

Utilization of 3D Printing in Clinical Medical Physics

Dr. Eric Ehler
University of Minnesota, USA.

Abstract: 3D printing is a method of semi-automated custom fabrication. The advantages of this technology for medical physics is apparent; objects can be constructed for specific clinical needs and constructed with moderate expertise. The cost of 3D printing is cheaper compared to other custom fabrication methods or purchasing from established vendors. Phantoms can be constructed for specific quality control tasks and radiation dosimetry measurements, including patient specific measurements. Beyond phantoms, 3D printing can be used for procedure devices in the form of radiation bolus, immobilization devices, surgical planning models, and rudimentary radiation detectors. Real clinical uses of 3D printing will be presented as well.

Invited talk 4

15:00 – 15:30 Thursday, October 29, 2020.

A fundamental approach of low-energy radiation dosimetry

Dr. Guerda Massillon-JL
Instituto de Física, UNAM, México.

Abstract: Nowadays, low-energy photons (x-rays and gamma) are widely used in different areas including biomedical research and medical applications such as mammography, fluoroscopy, general radiography, computed tomography, and brachytherapy treatment amongst others. These photons interact with matter transferring energy to orbital electrons (called primary electrons), which generate secondary electron cascades along their paths via electron-electron interactions. In general, the absorbed dose (energy deposited per unit mass: 1Gy=1J/kg) deposited along the electron track is defined as the product of the secondary electron yield and the linear energy transfer (LET) or the mass restricted stopping power averaged over the electron energy spectrum. From a standpoint of basic research, the physical processes by which very low energy electrons interact with matter are not well understood. Besides, accurate cross sections for the interaction of electrons energies below 1 keV with compound materials of dosimetric interest is scarce both, from theoretical and experimental studies. This is due, in part, to the complexity of electron interaction processes at these low energies, which require a quantum mechanical treatment. Thus, it is necessary to identify a model that allows us to understand the interaction processes of ionizing radiation with matter at energies where classical approaches do not hold. During the last 5 years, we have used a novel approach to radiation dosimetry based on fundamental quantum mechanics. In this talk, recent results will be presented and discussed. Work partially supported by Royal Society-Newton Advanced Fellowship grant NA150212 and PAPIIT-UNAM grant IN118120.

Invited talk 5

10:30 – 11:00 Friday, October 30, 2020.

Non-invasive biomarkers from physiological signals

Dr. Ana Leonor Rivera
Instituto de Ciencias Nucleares, UNAM, Mexico.

Abstract: From the point of view of Complex Sciences, human health is determined by the interaction of multiple organs and systems that try to preserve the homeostatic state of balance between the robustness and the adaptability to changes in the environment. Actually, technological devices can monitor continuously diverse physiological variables that reflect the dynamics of these homeostatic balance. Time series analysis of these variables allow to find relevant parameters that can be used as biomarkers characteristic of health. To do this, here we analyze the non-invasive physiological time-series records from rigorously screened healthy control subjects available on CALMECAC data base (records of electrocardiography, breathing, oxygen saturation, perfusion index, blood pressure wave-form, temperature and actigraphy) in three different conditions: supine, standing up, and controlled breathing at 0.1 Hz test. Analysis of the detrended time series were evaluated by the statistical moments and the homeostatic measurement parameter α that combines the variability of the heart rate (HRV) and the SBP, Fourier spectral analysis, and the resonance parameter β that measures the resonance peak at 0.1 Hz for controlled breathing. Alterations in the range of these biomarkers may appear before symptoms arise and opens up promising possibilities for applications in preventive medicine

Round Table

Towards better professional recognition of the Medical Physicist in Mexico

Joint activity of the Mexican Society of Physicists in Medicine (SMFM) and
the Medical Physics Division of the Mexican Physics Society

Mission:

Foster an inter-disciplinary discussion on the current status and challenges of the recognition of the Medical Physicists in Mexican health institutions.

Goal:

Device specific measures to improve the recognition of the Medical Physicist as a unique and essential profession in the health system

Participants:

Moderator: Adriana Moreno – President of SMFM
Radiologist: Dr. Flor Tanoira – President of the Colegio de Radiología e Imagen de Yucatán
Radiation Oncologist: Dr. Juan Miguel Pech León
Clinical medical physicist (radiation oncology): Orlando Soberanis, M. Sc.
Clinical medical physicist (radiology): Dr. Xochitl Lopez
Graduate program coordinators: Eleni Mitsoura, M. Sc. (UAEM) and Dr. Luis Medina (UNAM)

Poster sessions

Poster session 1

16:30 – 18:00 Wednesday, October 28, 2020.

1. Wed-01 Relative efficiency of TLD-100 glow peaks induced by low photon energy beams. Arzaga-Barajas et al., UNAM, Mexico.
2. Wed-02 Assessment of ^{99m}Tc-Octreotide through a hybrid quantification method. Ramírez Nava et al., IPN, Mexico.
3. Wed-03 Scatter and attenuation corrections for a PEM system: A thesis protocol. Morón Fernández et al., UNAM, Mexico.
4. Wed-05 M3D: Mammography phantom to assess mean glandular dose using thermoluminescent dosimetry. López-Pineda et al., UNAM, Mexico.
5. Wed-06 Development of the CMC for air kerma for X-Ray reference beams in the RQR-M qualities of the IEC 61267:2005 in the SSDL-ININ. Cabrera-Vertti et al., ININ, Mexico
6. Wed-07 Determination of image features in cone beam computerized tomography used in lung stereotactic radiotherapy: a phantom study. Valdes-Corona et al., UAEM, Mexico.
7. Wed-08 Does Cone Beam Computed Tomography image have the potential to monitor response to lung stereotactic body radiotherapy? Initial analysis. Zepeda-Barrios et al., UAEM, Mexico.
8. Wed-09 Depth of Interaction in Monolithic Scintillators for Positron Emission Tomography. Díaz-Martínez et al., UNAM, Mexico.
9. Wed-11 Subsurface laser engraving to pixelate scintillation crystals used in PET/PEM detectors Hernández-Cordero et al., UNAM, Mexico.
10. Wed-12 Comparison between NEMA NU-2 and the new report of AAPM TG 126 for PET-CT Image Quality. Galicia Larios et al., UNAM, Mexico.
11. Wed-13 Tumor Sphericity as Predictor of Tumor Changes In Patients With HPV-Positive Oropharyngeal Carcinoma. Galavis et al., NYU Langone Health, US.
12. Wed-14 Design of a free-air ionization chamber to medium energy X-ray for operation at the SSDL-ININ atmospheric conditions. De la Cruz et al., IPN, Mexico.
13. Wed-17 On the stability of asymmetry of thermal emission in diabetic foot disease. Ortiz-Sosa et al., UNAM, Mexico.
14. Wed-18 Synthesis and Characterization of Au@SiO2 Nanoparticles and their Possible Application in Photothermal Therapy. Gutiérrez-Velázquez et al., UNISON, Mexico.
15. Wed-20 Design and Building of a Phantom for the Recording of Internal Temperature, in an Ultra-Low Magnetic Field MR System. Martínez Martínez et al., UNAM, Mexico.
16. Wed-21 Development of Anatomical Phantoms for an Ultra-Low Field Magnetic Resonance Imaging System. Avendaño García et al., UNAM, Mexico.
17. Wed-22 Modified Petal Resonator Surface Coil for UHF-MRI. Solís Nájera et al., UNAM, Mexico.
18. Wed-23 Ultrasound-Sensitive Prophylaxis for Prevention of Post-Operative Infection in Spinal Fusion Surgery. Delaney et al., Thomas Jefferson University, US.
19. Wed-24 Initial experience on the application of quantitative tests for ultrasound quality control in Mexican hospitals. Manríquez-Padilla et al., UNAM, Mexico.
20. Wed-26 Multiple Scattering and Scattering Cross Section Models in Ultrasound. Fonseca-Rodríguez et al., UAM-I, Mexico.
21. Wed-27 Breast ultrasound image segmentation methods. Bass et al., UNAM, Mexico.
22. Wed-28 On the graphic representation of clinical data: the metabolic syndrome case. Fuentes-Oliver et al., UNAM, Mexico.

16:30 – 18:00 Thursday, October 29, 2020.

1. Thu-01 Response of BANG3-Pro gel induced by 6 MV X-ray radiotherapy beam. Flores-Mancera et al., UNAM, Mexico.
2. Thu-02 Implementation of the hexapod table in patients of the Oaxaca state Center of Oncology and Radiotherapy. Sánchez-Hernández et al., Centro Oncológico Oaxaca, Mexico.
3. Thu-05 Quality assurance of the calculation algorithm of a radiotherapy treatment planning system before its clinical implementation. Jiménez-Acosta et al., Hospital Médica Sur, Mexico.
4. Thu-08 Dosimetry response and water influence of delaminated-Gafchromic EBT3 irradiated at kilovoltage. Santibañez et al., Universidad de la Frontera, Chile.
5. Thu-09 Initial characterization of 6X-FFF beam in a Varian C-Series machine and comparison with a TrueBeam linear accelerator. Velázquez Trejo et al., Centro Médico Nacional del Bajío, IMSS, Mexico.
6. Thu-11 Comments on the precise definition of the concept of absorbed dose. Montes-Rodríguez et al., IPN, Mexico.
7. Thu-12 Determination of α/β for a Mexican Cohort of PCa Patients Treated with External Radiotherapy. Adame González et al., IPN, Mexico.
8. Thu-13 Imparted dose in blood components with a 137Cs irradiator. Cruz et al., UNAM, Mexico.
9. Thu-14 Dosimetry in fractionated irradiation of rat brain to evaluate radiobiological response. Iglesias Ojeda et al., UNAM, Mexico.
10. Thu-16 Influence of beam quality on absorbed depth-dose curves in liquid water induced by kilovoltage x-ray beams. Moreno-Ramírez et al., UNAM, Mexico.
11. Thu-17 Impact of Detector-specific correction factors in Non-Conventional Radiation Fields for Dose Distribution Calculation in Radiosurgery. Sánchez-Díaz et al., UNAM, Mexico.
12. Thu-18 Audit of non-conventional radiation fields applying AAPM/IAEA 483 formalism. Nolasco Altamirano et al., CICATA, Mexico.
13. Thu-19 Emulation of Gynecological Brachytherapy Doses with External Beam. Schnell et al.University of Oklahoma, US.
14. Thu-20 Out-of-Field Dosimetry in IMRT with OSL. Rojas López et al., Instituto Balseiro, Argentina.
15. Thu-21 Implementation of total body irradiation using VMAT. Muñoz-Moral et al., UNAM, Mexico.
16. Thu-22 Personal dose assessment using thermoluminescent dosimetry. Silva Fierro et al., UNAM, Mexico.
17. Thu-23 Dosimetric evaluation of a dental 70 kV X-ray tube. Hernández et al., UNAM, Mexico.
18. Fri-01 Functional network of patients with temporal lobe epilepsy: characterization of the database. Ríos et al., UNAM, Mexico.
19. Fri-02 Parkinson´s Disease Image Analysis. Rojas-Jiménez et al., UPIBI-IPN, Mexico.
20. Fri-09 ECG Waveform Analysis Algorithm. Rojas-Jiménez et al., UPIBI-IPN, Mexico.
21. Fri-10 Sleep in Crayfish: Relationships between Brain Electrical Activity and Autonomics Variables. Osorio-Palacios et al., UNAM, Mexico.
22. Fri-11 Facial Palsy Estimation Algorithm. Martínez-Ángeles, Universidad de Guadalajara, Mexico.
23. Fri-12 Dominant vs Submissive: Autonomic-like responses in crayfish. Oliver-Domínguez et al., UNAM, Mexico.
24. Fri-14 High dose-rate effect (1200 MU min-1) on delay expression of cytokine pro-inflammatory IL-1β in rats brain. Aguirre-Maldonado et al., UNAM, Mexico.
25. Fri-15 Measurement of activity concentration of polonium-210 in species of the phylum Mollusca from Mexico. Mandujano-García et al., UAZ, Mexico.
26. Fri-20 From planning to operating of an ABT BG-75 self-shielding cyclotron service of 7.5 MeV one dose dispenser. Vázquez et al., GRUPO VITAMEX, Mexico.
27. Fri-21 Turning undergraduate research assistants into scientific researchers: a wooden-block based method. Porras-Chaverri et al., Universidad de Costa Rica, Costa Rica.

Abstracts: Oral Contributions

SS1-1 – WEDNESDAY October 28, 2020: 11:00-11:15

Noninvassive Pressure Estimation with Lumason and Sonazoid Microbubbles

Ipshita Gupta[1,2], John Eisenbrey,[1] Maria Stanczak,[1] Priscilla Machado,[1] Corinne Wessner,[1] Jonathan Fenkel,[1] Colette Shaw,[1] Susan Schultz,[3] Michael Soulen,[3] Mehnoosh Torkzaban[1], Kibo Nam[1], Kirk Wallace[4], Flemming Forsberg[1]
[1]Thomas Jefferson University, Philadelphia, PA, USA, [2]Drexel University, Philadelphia, PA, USA, [3]Hospital of the University of Pennsylvania, PA, USA, [4]GE Global Research, Niskayuna, NY, USA
Email: flemming.forsberg@jefferson.edu

Research Area of Interest: C. Use of non-ionizing radiation in medicine

Keywords: subharmonic, ultrasound contrast agents, pressure estimation.

Introduction: Ultrasound contrast agents (UCAs) are gas-filled microbubbles designed to act as echo-enhancers [1]. At medium acoustic pressures (> 200 kPa) the UCAs start to oscillate nonlinearly [1]. This behavior forms the basis for subharmonic contrast imaging, which receives at half the transmit frequency ($f_o/2$). Subharmonic signals decrease linearly with increasing hydrostatic pressures, which our group has utilized for noninvasive pressure estimation termed SHAPE [2]. This study investigated SHAPE for diagnosing portal hypertension using the UCA Sonazoid (GE Healthcare, Oslo, Norway) and compared this UCA to Lumason (Bracco, Milan Italy) as an alternative UCA, since it is approved for liver imaging in the USA, but has been reported to respond differently to changes in hydrostatic pressure [3].

Methods: A modified Logiq 9 scanner (GE, Waukesha, WI, USA) with a 4C curvilinear array transmitted a 2.5 MHz Gaussian windowed binomial filtered square wave and acquired the subharmonic response (at 1.25 MHz). *In vitro* contrast signals from Sonazoid and Lumason were measured in a 2.25 L water tank at hydrostatic pressures from 10-220 mmHg. Linear regression analysis was performed as a function of tank pressure. *In vivo*, 178 participants scheduled for a transjugular liver biopsy and hepatic venous pressure gradient (HVPG) measurements enrolled in an IRB and FDA (IND no 124,465) approved study. After standard of care HVPG measurements, subjects received an infusion of Sonazoid at a rate of 0.024 µL/kg/min and SHAPE data was collected after optimization from a portal and a hepatic vein. The SHAPE gradient (the difference between hepatic and portal signals) was compared to HVPG values. ROC analysis was performed to determine the accuracy of SHAPE for diagnosing clinically significant portal hypertension (i.e., HVPG > 10 mmHg).

Results and Discussion: *In vitro*, Sonazoid showed an inverse linear relationship between subharmonic amplitude and ambient pressure, with a slope of -0.11 dB/mmHg and a correlation of -0.81 (Fig. 1). However, Lumason exhibited an increase in subharmonic amplitude from 0–100 mmHg hydrostatic pressure (slope = 0.06 dB/mmHg, r = 0.81), a plateau between 100–140 mmHg, and a decrease from 140–220 mmHg (slope = -0.26 dB/mmHg, r = -0.98). It is not known why an ascending phase has only been observed with Lumason, but it may be due to the higher vapor pressure of the gas used inside these bubbles i.e., sulphur hexafluoride (1062 kPa vs. 333 kPa for perfluorobutane used in Sonazoid).

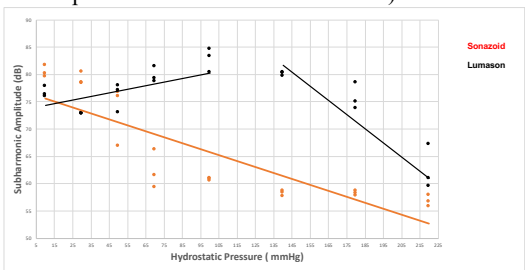

Figure 1: In vitro changes in subharmonic amplitude with hydrostatic pressure for Sonazoid and Lumason along with the best linear fit.

In vivo, complete data were acquired from 125 subjects (80 men and 45 women, median age 60.5 years). Patients diagnosed with portal hypertension had a significantly higher mean SHAPE gradient than patients with lower HVPGs (0.27 ± 2.13 vs. -5.34 ± 3.29 dB; $p < 0.001$). The area under the ROC curve were 0.95 [95% CI: 0.89 - 0.99, $p < 0.001$] for clinically significant portal hypertensive patients The optimal operating point was determined to be -0.11 dB, resulting in a sensitivity of 91% (95% CI: 88%-93%) and a specificity of 82% (95% CI: 75%-85%).
Conclusion: SHAPE with Sonazoid is an accurate noninvasive technique for detecting clinically significant portal hypertension. The difference in subharmonic behavior of Lumason compared with other UCAs warrants further investigation.

References:

[1] Cosgrove D. Ultrasound contrast agents: an overview. Eur J Radiol, 2006, 60:324-30.
[2] Eisenbrey JR, et al. Chronic liver disease: noninvasive subharmonic aided pressure estimation of hepatic venous pressure gradient. Radiology, 2013, 268:581-8.
[3] Nio AQX, et al. Optimal control of SonoVue microbubbles to estimate hydrostatic pressure. IEEE Trans Ultrason Ferroelectr Freq Control, 2019, Oct 21.

SS1-2 – WEDNESDAY October 28, 2020: 11:15-11:30

Disrupting Biofilms in Synovial Fluid with Ultrasound Triggered Microbubble Destruction

Flemming Forsberg,[1] Dylan Curry,[1] Priscilla Machado,[1] Maria Stanczak,[1] John R. Eisenbrey,[1] Thomas P. Schaer,[2] Noreen J. Hickok,[1]

[1]*Thomas Jefferson University, Philadelphia, PA, USA,* [2]*New Bolton Center, Penn Vet University of Pennsylvania, Kennett Square, PA, USA*

Email: flemming.forsberg@jefferson.edu

Research Area of Interest: C. Use of non-ionizing radiation in medicine

Keywords: ultrasound contrast agents, joint infections, biofilms.

Introduction: : Infectious arthritis is difficult to treat in both human and veterinary clinical practice, due to the ability of Staphylococcus aureus (as well as other gram-positive and gram-negative isolates) to form free-floating bacterial biofilms in both human and equine synovial fluid (SynF). Bacteria within these biofilm phenotypes show increased antimicrobial tolerance even at high antibiotic concentrations. We recently demonstrated that enzymatic dispersal of SynF biofilm restores the activity of antimicrobials. Hence, this study investigated the ability to restore antimicrobial efficacy in infected joints by combining antibiotics and ultrasound triggered microbubble destruction (UTMD) to disrupt and disperse biofilms in SynF.

Methods: In *vitro*, $1x10^7$ colony forming units (CFU) of *S. aureus* (ATCC25923, Manassas, VA) were added to human SynF followed by incubation (90 min, 37°C) to allow for bacterial aggregation. The culture had 100 µl of Definity microbubbles (Lantheus Medical Imaging, N. Billerica, MA), and 30 µg/ml of amikacin added. Samples were insonated either at a high mechanical index (MI) of 1.06 for 10 min or a low MI of 0.04 for 6 min. Bacterial cultures were allowed to incubate for an additional 6 hours before collection and counting. *In vivo,* 6 castrated Yorkshire pigs (~2 months of age; average body weight 35 kg) were sedated and their left femorotibial joint was inoculated with $1x10^6$ CFU of *S. aureus* in 1 ml of saline using aseptic technique under an IACUC approved protocol. SynF was collected from all animals 24 hours post-inoculation. Two animals received 1 ml of amikacin (250 mg) injected into the joint (as controls). The remaining animals received 100 µl of Definity and 1 ml of amikacin intra-articularly into the left femorotibial joint followed by a UTMD procedure. UMD was performed using an S9 Pro ultrasound scanner with a curvilinear probe (SonoScape, Shenzhen, China) and a flash replenishment sequence (low MI (< 0.15) harmonic imaging (transmitting at 3.5 MHz) with 4 second-high MI (> 0.6) destructive pulses for the duration of contrast visualization). A sample of SynF was collected from all animals after the therapeutic intervention and prior to sacrifice. All SynF samples underwent cytological analysis and quantitative bacteriology. Bacterial load (CFU/ml) at 8 hours post-treatment was determined by serial dilutions using 3M Petri-films. Three serial dilutions were performed in triplicate after a 5 min sonication to break up bacterial aggregates and plate counting. The biofloat aggregates were processed for confocal and scanning electron microscopy.

Results and Discussion: The combination of ultrasound, microbubbles, and antibiotics resulted in large decreases in bacterial numbers (>2-4 logs) *in vitro* as compared to antibiotic alone. Dilution of the SynF, as occurs *in vivo* with addition of the antibiotics and the microbubbles was required for the largest effect. *In vivo* the infection protocol consistently caused clinical septic arthritis by 24 hours post-inoculation with animals exhibiting a noticeable hind limb lameness and the infected stifle joints were hot to the touch with variable degrees of joint effusion. Nucleated cell counts and cytology parameters were all within ranges consistent with septic arthritis. Free-floating bacterial aggregates were occasionally observed in the joint aspirates obtained prior to initiating the UTMD intervention. No biofloats were detected on joint aspirates obtained several hours following intra-articular therapy and no bacterial growth was noted in any dilution of replicates in the post-treatment SynF samples, while the pre-treatment samples and amikacin only animals had bacterial counts above 2000 CFU/ml.

Conclusion: In this study, we demonstrated that both human (*in vitro*) and porcine (*in vivo*) SynF allow for robust biofilm aggregate. Mechanical disruption and dispersal of SynF biofilm aggregates *in vitro* and *in vivo* restores antimicrobial activity. Overall, UTMD augmented therapy demonstrates synergism with the aminoglycoside amikacin against previously tolerant biofilm aggregates against a clinically relevant pathogen. Mechanical disruption using UTMD is a minimally invasive procedure and has the potential to augment current antimicrobial treatment regimens, which could lead to a decrease in morbidity and mortality associated with infectious arthritis in particular and biofilm infections in general.

SS1-3 – WEDNESDAY October 28, 2020: 11:30-11:45

Feasibility of Clinical Risk Assessment based on Pressure-gradient Estimation using 3D Contrast-enhanced Ultrasound

Kibo Nam[1,a]
[1]*Thomas Jefferson University, Philadelphia, PA 19107, USA* [a] kibo.nam@jefferson.edu

Research Area of Interest: C. Use of non-ionizing radiation in medicine

Keywords: Pressure estimation, subharmonics, contrast-enhanced ultrasound, therapy response, vulnerable plaque

Introduction: A pressure-gradient creates a force across a surface, which can be a risk marker indicating a flow blockage or a rupture in the body. One of the factors hypothesized to affect the response of breast cancer to neoadjuvant chemotherapy (NAC) is the interstitial fluid pressure (IFP) gradient. Increased IFP in cancer inhibits an effective uptake of therapeutic agents and reduces the efficacy of therapy [1]. Similarly, in prediction of vulnerable plaques, the pressure gradient between the plaque and the blood vessel can be considered. The hemodynamic pressure may weaken a plaque cap and combined with factors such as plaque composition and cap thickness, it can lead a plaque to a sudden rupture [2]. Contrast-enhanced ultrasound (CEUS) has been used to estimate hydrostatic pressures exploiting the inverse relationship between the amplitude of subharmonic signal from the contrast agent and the ambient pressure [3]. Thus, we evaluated the feasibility of clinical risk assessment based on pressure-gradient estimation using 3D CEUS in two studies.

Methods: In the first study, eleven patients underwent CEUS exams after 0, 10 (1 cycle), 60 (7 or 9 cycles), and 100% (12 or 16 cycles) of NAC. The study was approved by the IRB of our institution and was compliant with the HIPAA. All patients provided written informed consent. Ultrasound exams were performed using a Logiq 9 (GE Healthcare, Waukesha, WI, USA) with a 4D10L probe. Modified software enabled RF data collection from 3D subharmonic imaging before and during an infusion of Definity (Lantheus, N Billerica, MA, USA) for pressure estimation. In the second study, twenty-seven rabbits (9 Watanabe Heritable Hyperlipidemic rabbits and 18 New Zealand White rabbits) received a high-cholesterol diet for 2 weeks prior to a balloon catheter-injury to denude the endothelium of the aorta, followed by 8-10 weeks of high-cholesterol diet to create arteriosclerotic plaques. The study was approved by the Institutional Animal Care and Use Committee and was supervised by our Laboratory Animal Services Department. 3D CEUS exams of the resulting plaques were performed 12, 16, and 20 weeks post-injury using a Logiq 9 scanner with a 4D10L probe before and during an infusion of Definity. The ratios of maximum subharmonic amplitude before and during the infusion were calculated and the difference between the tumor and surrounding area (first study) or between the plaque and blood vessel area (second study) was obtained. The results were compared to clinical outcomes (first study) or were correlated with the pressure gradient across the plaque cap obtained from direct measurements (second study). The aortic and plaque pressures were directly measured using a 0.75 F fiber-optic pressure catheter (FISO Technologies, Quebec City, Quebec, Canada) and an intra-compartmental pressure monitoring system (Stryker, Newbury, Berkshire, UK), respectively.

Results and Discussion: In the first study, six patients showed complete response, while five showed non/partial response based on imaging assessment. Comparing all 3D CEUS results to imaging responses, only the results after 10% completion of the therapy showed significance (3.23 ± 1.41 dB vs. -0.88 ± 1.46 dB; $p < 0.01$). In the second study, ten rabbits died prematurely following the balloon-injury procedure or due to toxicity from the high-cholesterol diet, while two rabbits were excluded for other conditions. Five rabbits were scanned in the 12, 16, and 20 week groups, respectively. Even after 20 weeks the plaques that developed were very small (0.3~1.4 cm by 0.07~0.19 cm). The 3D CEUS results achieved only moderate correlation with pressure across the plaque cap ($r = -0.19$). While the first study showed the potential of pressure gradient from 3D CEUS as an early risk predictor for NAC response outcome, the second study only showed the feasibility of pressure gradient estimation in plaques. That could be because small sizes of the rabbit plaques, which necessitated including some of the surrounding area around the plaques in order to calculate accurate FFTs for pressure estimation. In addition, most plaques were hypo-echoic in CEUS. This may be because the contrast agents could not enter due to the small size of blood vessels within plaques in these animal models.

Conclusion: The studies demonstrated the feasibility of clinical risk assessment based on pressure-gradient estimation using 3D CEUS albeit with small sample sizes.

References:

[1] Heldin, C.H., et al., 2004. "High interstitial fluid pressure: an obstacle in cancer therapy", Nat. Rev. Cancer 4, 806–813.
[2] Fuster, V., et al., 1998. "Atherothrombosis: mechanisms and clinical therapeutic approaches", Vasc. Med. 3, 231-239.
[3] Dave, J.K., et al., 2017. "Non-invasive intra-cardiac pressure measurements using subharmonic-aided pressure estimation: proof of concept in humans", Ultrasound Med. Biol. 43, 2718-2724.

SS1-4 – WEDNESDAY October 28, 2020: 11:45-12:00

Estimation of Effective Scatterer Size and Acoustic Concentration Quantitative Ultrasound Parameters Using Dynamic Programming

Noushin Jafarpisheh[1, a], Ivan M. Rosado-Mendez[2], Timothy J. Hall[2], and Hassan Rivaz[1],
[1]*Department of Electrical and Computer Engineering, Concordia University, Montreal, CA;*
[2]*Instituto de Física, Universidad Nacional Autónoma de México, Mexico City, MEX 04510*
[a]*n_jafarp@encs.concordia.ca*

Research area of interest: C
Keywords: Quantitative ultrasound, low variance, form factor.

Introduction: We recently proposed dynamic programming (DP) to estimate acoustic backscattering and attenuation in the context of quantitative ultrasound (QUS) [1,2]. Herein, we build on that work by estimating effective scatterer size, acoustic concentration, and effective attenuation. The general formula of attenuation is:

$$A(f,z) = exp(-4\alpha f z) \quad (1)$$

where A is the total attenuation, f is the frequency, z is the depth and α is the attenuation coefficient. The power law model for parametrizing backscatter coefficients is:

$$B(f) = B_0 G(f) \quad (2)$$

where B_0 is the magnitude and $G(f)$ is the frequency dependence of backscatter coefficients. The following equation defines $G(f)$ in terms of a form factor model:

$$G(f) = f^4\, F\left(f, a_{eff}\right) \quad (3)$$

We exploit the reference phantom method (RPM) to have a system independent algorithm.

Methods: As the microstructure of real tissue is often modeled using scatterers with spherically-symmetrical, Gaussian impedance correlation functions [3], a Gaussian form factor model has been selected as follows:

$$F\left(f, a_{eff}\right) = exp\left(-0.827\left(k a_{eff}\right)^2\right) \quad (4)$$

where k is wave number and a_{eff} is effective scatterer size. By substitution (4) in (3), and (3) in (2), we have:

$$B(f) = B_0 f^4\, exp\left(-0.827\left(k a_{eff}\right)^2\right) \quad (5)$$

Consider the ratio of power spectra of echo signals of sample (s) and a reference (r) phantom:

$$\frac{S_s}{S_r} = \frac{B_s(f) A_s(f,z)}{B_r(f) A_r(f,z)} = \frac{B_{0_s} f^4\, exp(-0.827\,(k_s a_s)^2)\, exp(-4\alpha_s f z)}{B_{0_r} f^4\, exp(-0.827\,(k_r a_r)^2)\, exp(-4\alpha_r f z)} \quad (6)$$

In order to use RPM, reference and sample phantom must have the same sound speed, so $k_s = k_r$. After taking the natural logarithm from both sides of (6), and substituting $X_1 = \ln\frac{S_s}{S_r}, B = \ln\frac{B_{0_s}}{B_{0_r}}$, $a = a_s^2 - a_r^2,$, and $\alpha = \alpha_s - \alpha_r$ we have:

$$X_1 = B - 0.827 k^2 a - 4\alpha f z \quad (7)$$

The goal is to estimate $B, a,$ and α using DP.

In order to simulate data, we added Gaussian noise to $B, a,$ and α in (7). In the following equation, i refers to an instance of noise.

$$X = \log\frac{B_{0_s}}{B_{0_r}} + n_{B_i} - 0.827 k^2 \left((a_s^2 - a_r^2) + n_{a_i}\right) - 4\left((\alpha_s - \alpha_r) + n_{\alpha_i}\right) f z\,, \quad i = 1, \ldots 20 \quad (8)$$

Once B_{0_s} and a_s are estimated, acoustic concentration $(n\gamma^2)$ can be obtained using the following equation:

$$B_{0_s} = \left(\frac{2\pi}{c}\right)^4 a_s^6 \frac{n\gamma^2}{9} \quad (9)$$

Results and discussion: Figure 1 shows the estimations obtained by DP and LSQ. The estimation results of Fig. 1 (d) can be substantially improved if the frequency range is chosen such that $ka \sim 1$ is in the frequency range. In our simulations, this optimal frequency corresponds to 7.662 and 8.651 MHz for different layers of the phantom, whereas the frequency range of this work was set to 3.7 to 7 MHz.

Conclusions: Results show DP outperforms LSQ.

References:

[1] Vajihi, Z., et al., 2018, IEEE TUFFC, 65(11). 2042–2053.
[2] Nam, K., et al., 2011. Ultrasound Med. Biol. 37(12), 2096–2104.
[3] Insana MF, Hall TJ., 1990. Physics in Medicine & Biology. 35(10), 1373–1386.

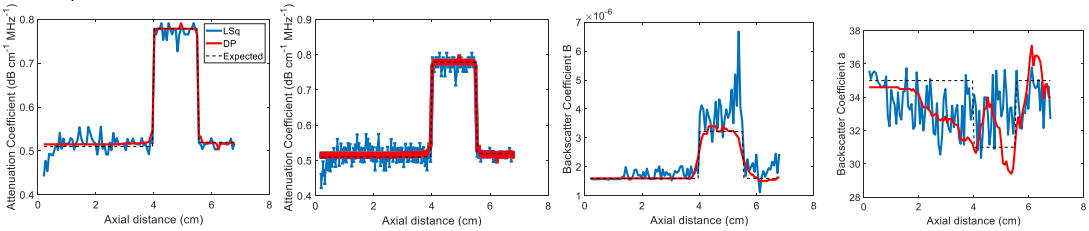

(a) Mean estimate (b) Error bar (c) Mean estimate (d) Mean estimate

Figure 1. The results of LSq and DP methods in a simulated phantom with three layers and 20 instances of added noise zero-mean Gaussian noise. The error bars in (b) show the standard deviation over the 20 instances of noise.

SS1-5 – WEDNESDAY October 28, 2020: 12:00-12:15

Application of dynamic-programing estimation of acoustic attenuation and backscatter coefficient of breast carcinoma

L. Castañeda-Martínez[1,a], J.P. Castillo[2], H. Galván[2,c], P. Pérez[2], L. Aguilar [2], F. Porras[2], Y. Villaseñor[2], Hassan Rivaz[3] and I. M. Rosado-Mendez[1,b],

[1]*Instituto de Física, Universidad Nacional Autónoma de México, Mexico City, MEX 04510;*
[2]*Instituto Nacional de Cancerología (INCAN), Mexico City, MEX 14080*
[3]*Department of Electrical and Computer Engineering, Concordia University, Montreal, CA*
[a]lcastaneda@ciencias.unam.mx, [b]irosado@fisica.unam.mx

Research area of interest: C
Keywords: Quantitative ultrasound, variability, breast cancer

Introduction: Quantitative ultrasound provides descriptors of tissue acoustic properties, reducing system- and operator-dependence of image interpretation. Two descriptors of interest for breast cancer are the acoustic attenuation (ATT, related to acoustic energy absorption) and the backscatter coefficient (BSC, related to tissue echogenicity). Applications of these parameters to *in vivo* tissue have been limited by the high variance of the estimated values. Recently, Vajihi *et al.* [1] proposed a new method based on dynamic programming (DP) that significantly improved precision of ATT and BSC estimates. In this study we applied DP to *in vivo* breast cancer data for the first time, and evaluated the level of inter-operator (InterOp) and intra-operator (IntraOp) variability of ATT and BSC.

Methods: The study included ten patients from INCAN with a suspicious breast mass (BIRADS 4 or 5) and scheduled for biopsy. Radiofrequency echo signals from breast lesions were acquired with a Siemens Acuson S2000 (Siemens Healthcare, Mountain View, CA, USA) using a 12L4 linear array transducer. Two radiologists with 10 and 15 years of experience acquired three data sets, allowing the patient to reposition between acquisitions.

ATT and BSC were quantified with the DP method, which provides α (the magnitude of ATT), b and n (the magnitude and frequency dependence of a power law model of the BSC). To evaluate the differences between the inter-operator (among radiologists) and intra-operator (among acquisitions from the same radiologists) variabilities of each parameter, the fractional absolute difference F_{var} between images i and j was defined as

$$F_{var}(i,j) = |p_i - p_j|/(p_i + p_j)/2$$

where the subscript *var*=IntraOp or InterOp and p is the intra-lesion average of α, b, or n. The statistical significance of differences between $F_{IntraOp}$ and $F_{InterOp}$ was assessed through a Wilcoxon rank sum test Matlab function.

Results and discussion: Table 1 shows mean and interquartile ranges of $F_{IntraOp}$ and $F_{InterOp}$ for all the lesions. No significant differences were found between $F_{IntraOp}$ and $F_{InterOp}$, which suggested operator-independence.

Conclusions: Results showed that the inter-operator and intra-operator variability of DP-based attenuation and backscatter coefficients are robust to operator variability.

References:
[1] Vajihi et al., IEEE TUFFC, 65(11), pp. 2042–2053 (2018).

Table 1: Magnitude and variability of each parameter estimated within the breast tissue mass.

Parameter	Mean [IQR]	F_{intra}- Mean [IQR]	F_{inter}- Mean [IQR]	p
α	0.9 [0.88, 0.96] dB/cm	0.04 [0.01,0.05]	0.03 [0.01,0.05]	0.54
b	3.4 [3.25, 3.80] $cm^{-1}sr^{-1}$	0.06 [0.02,0.08]	0.06 [0.01,0.09]	0.18
n	4.3 [4.07, 4.59]	0.07 [0.02,0.09]	0.05 [0.01,0.06]	0.15

SS2-1 – WEDNESDAY October 28, 2020: 15:30-15:45

Breast density quantification using dual-energy digital mammography

Gustavo Pacheco [a], Jorge P. Castillo [2,b] María Ester Brandan [1,c] and Yolanda Villaseñor[2]
[1]*Instituto de Física, Universidad Nacional Autónoma de México;* [2]*Instituto Nacional de Cancerología.*
[a]gustavo.p@ciencias.unam.mx, [b]jorge.castillo.mex@gmail.com, [c]brandan@fisica.unam.mx

Research area of interest: B.
Keywords: Breast imaging, dual energy digital mammography, breast density, image processing, mammography.

Introduction: Breast density, the percentage of glandular tissue within the mammary gland, is an indicator of breast cancer risk [1]. In this work, we propose a method to calculate breast density using dual-energy digital mammography.

Methods: Dual-energy imaging takes advantage of the energy dependence of photon attenuation by different materials to quantify their presence. The method used in this work is based upon the existence of an invertible mapping between material thickness and pixel value in images acquired with two energy spectra ("dual-energy"). To calibrate, variable thicknesses of aluminum (Al) and PMMA were imaged using a dual-energy technique. Rational mapping procedures, based on linear or 8-parameter mapping functions, were assessed in terms of error and noise. Following the basis material decomposition formalism [2], for a given glandular/adipose tissue thickness there exists an equivalent Al and PMMA thickness. Once the mapping function is determined, it is possible to generate glandular/adipose thickness images from Al/PMMA thickness images and use the former for breast density calculation. The material decomposition algorithm was evaluated on tissue-equivalent mammary phantoms, and breast density was calculated in 20 clinical images.

Results and discussion: Figure 1 shows the pixel value of dual-energy images as a function of Al and PMMA thickness. The fitted 8-parameter function offers an overall 30% decrease in error when compared to the linear function, at the cost of a 10% decrease in signal-to-noise-ratio, SNR. Errors in material thickness estimates are within 2%, and uncertainties below 5% when using this function. Because the method requires only pixel-by-pixel arithmetic operations using hard-coded fit parameters, it can be implemented on consumer-grade hardware with reasonable computation times.

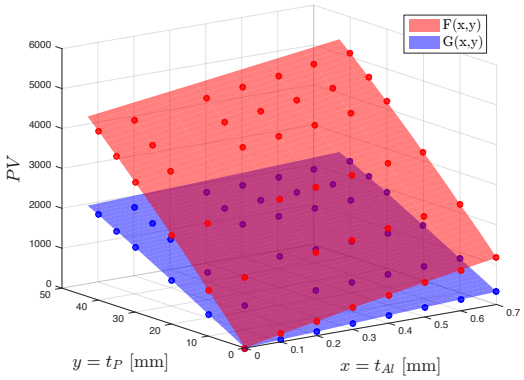

Figure 1. Pixel value (PV) of high- and low- energy images (in blue and red, respectively) as a function of Al and PMMA thickness. Dots represent the calibration points used to fit the mapping functions.

At the time of the Symposium, we plan to present glandular density measurements on tissue-equivalent breast phantoms and clinical images. Noise reduction techniques are currently being investigated.

Conclusions: The estimation of material thickness from dual-energy digital mammography images has been optimized and evaluated in terms of error and uncertainty. Breast density was calculated in 20 clinical images.

References:

[1] A.T. Wang et al. *Breast Density and Breast Cancer Risk. A Practical Review.* Mayo Clinic Proceedings 89(4), 2014.
[2] L.A. Lehmann, R.E. et al. *Generalized image combinations in dual KVP digital radiography*. Med. Phys. 8(5), 1981.

SS2-2 – WEDNESDAY October 28, 2020: 15:45-16:00

Use of Timepix detectors in preclinical CT/PET/SPECT imaging

Ludek Sefc[1a], Eliska Trojanova[1,2,b] ,Daniel Turecek[1,2,c], Karla Denaly Palma Alejandro[1d], Viktor Sykora[1e], Jan Jakubek[2f]

[1]*Center for Advanced Preclinical Imaging (CAPI), First Faculty of Medicine Charles University, Salmovska 3, Prague, Czech Republic* [2]*ADVACAM s.r.o., U Pergamenky 12, Prague, Czech Republic*
[a]sefc@cesnet.cz [b]eliska.trojanova@advacam.com [c]daniel.turecek@advacam.com
[d]kdpa27@gmail.com [e]viktor.ep@gmail.com [f]jan.jakubek@advacam.com

Research of interest: B. Physics and dosimetry of the images of medical diagnosis with ionizing radiation

Keywords: preclinical imaging, CT, PET, SPECT, Timepix detectors

Introduction: Current preclinical and clinical CT, PET, and/or SPECT imaging delivers a significant radiation dose to the scanned animal or human. It can interfere with viability, immune system and rapidly growing tissues. The new Timepix detectors developed by an international collaboration in CERN offer an alternative to the currently used detectors. Timepix3 detectors allow to measure simultaneously the exact time, position and energy of the interacting ionizing particle. We assessed a proof-of-principle of the use of these detectors for the preclinical CT, PET, and SPECT imaging.

Methods: Timepix3 detectors with 2 mm thick CdTe sensors were used. CT, PET, and SPECT imaging has been done on phantoms and laboratory mice.

Results and discussion: X-ray imaging with Timepix detectors allowed to achieve a "color" image with better resolution of soft tissues even without contrast. The high frame rate of the detector (1.7 kHz) was suitable for imaging very fast events. Excellent time and energy resolutions of the detectors were used for elimination of the Compton scattering and internal X-ray fluorescence of Cd and Te and led to a significant reduction of signal-to-background ratio. The Compton camera for SPECT was implemented in both two-layer (Fig. 1) and single-layer detector setting which allowed a major improvement in SPECT sensitivity.

Conclusions: The feasibility of the Timepix 3 detectors for CT/PET/SPECT preclinical imaging has been proofed. The unique properties of these detectors allowed effectively filtrate the unwanted events, which resulted in a significant increase in signal-to-background ratio and allowed to decrease scan times for CT and overall radioisotope activity needed for PET and SPECT imaging. Moreover, construction of Compton camera allowed non-collimated SPECT imaging which significantly increased its sensitivity.

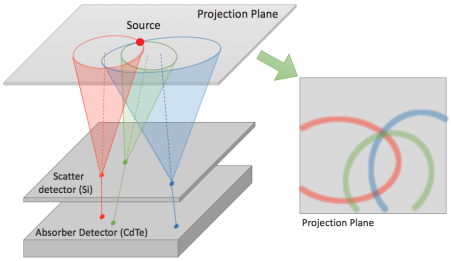

Figure 1. Reconstruction of the gamma source shape and position using a two-layer Compton camera.

References:

[1] Trojanova, E., et al., 2017. "Tissue sensitive imaging and tomography without contrast agents for small animals with Timepix based detectors". Journal of Instrumentation, Volume 12, Issue 01, pp. C01056.
[2] Turecek, D., et al., 2018. "Application of Timepix3 based CdTe spectral sensitive photon counting detector for PET imaging". Nuclear Inst. and Methods in Physics Research, A, Volume 895, p. 84-89.
[3] Trojanova, E., et al., 2018 "Evaluation of Timepix3 based CdTe photon counting detector for fully spectroscopic small animal SPECT imaging". Journal of Instrumentation, Volume 13, Issue 01, pp. C01001.
[4] Turecek, D., et al., 2018. "Compton camera based on Timepix3 technology". Journal of Instrumentation, Volume 13, Issue 11, pp. C11022.

SS2-3 – WEDNESDAY October 28, 2020: 16:00-16:15

Design of a bilateral filter for noise reduction in contrast-enhanced micro-CT

Lízbeth Ayala-Domínguez[1,a], Rubén Morales Oliver[2], Luis A Medina[3], María-Ester Brandan[1,b]
[1]*Instituto de Física, Universidad Nacional Autónoma de México, Mexico City, Mexico,* [2]*University of Calgary, Alberta, Canada,* [3]*Instituto Nacional de Cancerología, Mexico City, Mexico.*
[a]*ayalaliz@gmail.com,* [b]*brandan@fisica.unam.mx*

Research area of interest: B. Physics and dosimetry of medical images (ionizing radiation)
Keywords: micro-CT, noise reduction, bilateral filter, contrast-enhanced imaging.

Introduction: Noise amplification is an important concern in contrast-enhanced (CE) x-ray imaging, in which subtraction techniques are used with single or dual-energy (SE, DE) modalities [1, 2]. A common approach for noise reduction in DE micro-CT is bilateral filtering, which only averages pixels with similar intensities and preserves the edges [1, 3]. This work aimed at designing a bilateral filter (BF) for noise reduction in CE micro-CT for SE and DE imaging protocols. The performance of the BF was assessed with common image quality metrics and after the adequate filter parameters were chosen, it was validated in images of an animal model of tumor angiogenesis.

Methods: Images of a home-made iodinated phantom and a water phantom were acquired with the Albira ARS micro-CT system (Bruker), with SE and DE imaging protocols. All images were reconstructed with the filtered back-projection (FBP) method. The BF was implemented in Matlab®. The animal model of tumor angiogenesis consisted of male Wistar rats inoculated with C6 glioma cells that were injected in two contralateral sites of their dorsum. All animal procedures were under the approval of the Research Ethics Committee of the Instituto Nacional de Cancerología, Mexico (018/051/1B1/CE1/1294/18).

Results and discussion. The BF parameters were chosen according to the image quality characteristics of each imaging protocol, such as the noise of the CT number for water (in Hounsfield units, HU) and the spatial resolution (in mm), which was measured from the modulation transfer function obtained with the edge method in images of the water phantom. Figure 1 shows a transversal view of the iodinated phantom for original and filtered images in the case of an inadequate or adequate selection of the BF parameters. CNR improved for all the evaluated iodine concentrations in the filtered images pre and post SE and DE subtraction, which could translate into an increment of lesion visibility. The filtered image of the animal model showed an adequate level of smoothing within homogeneous tissues, as well as the preservation of vascular structures, indicating the preservation of the edges (not shown).

(a) (b) (c)

Figure 1. (a) Original SE image (pre-subtraction), and filtered images with (b) an inadequate and (c) adequate selection of the BF parameters. CNR = 12, 65, and 26, respectively.

Conclusions. The BF implemented in this work for SE and DE imaging improved the image quality of CE micro-CT images, which could improve the usefulness of these images in the study of tumor vascularization in cancer.

Acknowledgments. This work was partially supported by CONACyT grant CB-251497 and PAPIIT-UNAM IN103219.

References.

[1] Clark DP, Ghaghada K, Moding EJ, Kirsch DG, Badea CT (2013) In vivo characterization of tumor vasculature using iodine and gold nanoparticles and dual energy micro-CT. *Phys Med Biol* **58**:l1683-1704
[2] Ayala-Domínguez L, Brandan ME (2018) Quantification of tumor angiogenesis with contrast-enhanced x-ray imaging in preclinical studies: a review. *Biomed Phys Eng Express* **4**:062001
[3] Tomasi C, Manduchi R (1998) Bilateral filtering of gray and color images. *Sixth Int Conf on Computer Vision*. pp 839-46

SS2-4 – WEDNESDAY October 28, 2020: 16:15-16:30

Characterization of a Fricke-gel solution as a potential low-dose dosimeter

M. A. Ochoa[1,a], D. Ramírez,[1,2,b], L. A. Medina[1,3,c]

[1]*Instituto de Física, Universidad Nacional Autónoma de México,* [2]*Facultad de Química, Universidad Nacional Autónoma de México, ,* [3]*Unidad de Investigación Biomédica en Cáncer INCan/UNAM, Instituto Nacional de Cancerología.*

[a]ochoa.m.mario@gmail.com, [b]350davidramirez@gmail.com , [c]medina@fisica.unam.mx

Research area of interest: Physics and dosimetry of medical images with ionizing radiation.

Keywords: dosimetry, Fricke-gel solution, FXG, low-dose dosimetry

Introduction: The Fricke ferrous sulphate solution is a chemical high-dose dosimeter, commonly used to measure doses between 40 – 400 Gy, [1]. An important limitation of this dosimeter is the time constraints between irradiation and measurement caused by the ion diffusion which eventually eliminates the spatial dose information [2], as well as its impossibility to measure low-range doses (< 10 Gy) commonly used in preclinical studies. The dosimetric basis of Fricke solutions is the dose dependant transformation of ferrous ions (Fe^{2+}) into ferric ions (Fe^{3+}) caused by a reduction-oxidation reaction with free radicals in the aqueous medium of the solution, that were created by its interaction with ionizing radiation, [2,3]. In recent years, research has focused on the development of Fricke-gel solutions able to perform dosimetric measurements under 10 Gy and to give information about the spatial dose distribution on three dimensions (3D) using magnetic resonance imaging (MRI), [2,3]. Here we present a first characterization of a Fricke-gel developed in our laboratory.

Methods: We evaluate the effect of multiple reagents to promote the generation of free radicals and the reduction-oxidation of the ferrous ions in Fricke-gel solutions. The characteristic absorption-wavelengths of the ferrous and ferric ions in their pure form and complex form, with chelators like EDTA and Xylenol Orange (XO), were evaluated. The dose-response relationship and the sensitivity of the solutions to ionizing radiation were also measured.

Results and discussion: The ferric ion and its complex form with EDTA (Fe^{3+} and Fe^{3+}EDTA respectively) showed a preferential absorption at 304 nm, while the Fe^{3+}XO complex absorbs preferentially at 585 nm, which cause changes in the color of the solution after the irradiation. This change of color was proportional to the absorbed dose.

The EDTA complex showed higher absorbance variability at 304 nm as compared to XO complex at 585 nm; the absorbance is also highly influenced by the initial concentration of the ferrous ions in the solution. It was observed that at low concentrations there are not enough ferrous ions to react, while at high concentrations the solution saturates so quickly, showing no significant differences between the pre-irradiation and post-irradiation absorbance values.

Conclusions: Fricke solutions using XO and 0.4 mM Fe^{2+} ions show the highest accuracy and sensibility in absorbance response to ionizing radiation.

References:

[1] Attix FH. (2004). Introduction to Radiological Physics and Radiation Dosimetry. 2nd Ed. Wiley-VCH.

[2] Schreiner, L. J. (2004). Review of Fricke gel dosimeters. Journal of Physics: Conference Series, 3, 9–21.

[3] Marini A, et.al. (2017). Fricke gel dosimeters with low-diffusion and high-sensitivity based on a chemically cross-linked PVA matrix. Radiation Measurements 106, 618-621.

SS3-1 – THURSDAY October 29, 2020: 11:00-11:15

A Three-Dimensional Electronic Detector Array Readout Configuration for Radiotherapy based on Active Matrices

Roger Challco Chalco*[,1,1], D. Roa[2,2], Zintia Arqque [3,3], Oliver Paucar[4,4], Sandra Guzman[1,5], Jose Valladolid[1,6], Alberto Gonzales[1,7], Andres Gonzales[5,8], Modesto Montoya[1,9]

[1]*Department of Physics, Universidad Nacional de Ingenieria (UNI), Peru*
[2]*Department of Radiation Oncology, Chao Family Comprehensive Cancer Center, University of California, Irvine-Medical Center, USA*
[3]*Department of Electronic Engineering, Universidad Nacional San Antonio Abad, Peru´*
[4]*Department of Electronic Engineering, Universidad Nacional de Ingenieria (UNI), Peru´*
[5]*Clinica Aliada Contra el Cancer, Peru*

[1]*rogerchallco@gmail.com*, [2]*dante_roa@yahoo.com*, [3]*zintiamilagrosmeza@gmail.com*, [4]*oliwpaucar11@mail.com*, [5]*fis_guzman@yahoo.com*, [6]*zeka.vidal@gmail.com*, [7]*betoagc@hotmail.com*, [8]*gonzales@aliada.com.pe*, [9]*modesto_montoya @yahoo.com*

Research area of interest:
A: Physics and dosimetry of radiotherapy.
Key words: Active Matrix, Radiotherapy, three-dimensional electronic array, PBW34 diode.

Introduction: Due to the importance of 3D dosimetry in radiotherapy. [1] A three-dimensional electronic array based on an active matrix concept has been designed. [2][3] The array will consist of 31,560 submillimeter size diode detectors distributed within a 20 cm diameter semi-spherical volume of water equivalent material. Each active matrix (AM) would read from 27 to 972 detectors and 80 active matrices with 4200 channels connected to a data acquisition unit (DAQ) would be used for readout.

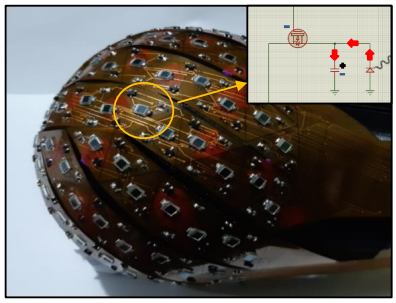

Figure1. Layer of semi-spherical electronic detector

Methods: For initial testing, a low resolution semi-spherical electronic detector was constructed. The semi-spherical phantom has 20 cm in diameter, consists of 135 BPW34 photodiodes in a layer of 12 cm diameter and one ionization chamber mounted in the center of the volume. A simulated quality assurance intracranial treatment plan involving a 6 MV photon beam was generated in the treatment planning system using the semi-spherical phantom volume. Subsequently, the semi-spherical phantom was irradiated using a 6 MV photon beam from a Varian 2100 C/D linear accelerator and using the planning treatment. Finally, the dose measured by each diode has been compared with the dose calculated by the planning software.

Results and discussions:
The percentage difference of the dose calculated by planning software and the experimental measurement by the electronic detector array was less than 4%. This result was showed us a good detector response

Conclusion:
A three-dimensional configuration of electronic detector has been established using active matrix technology. The experimental tests provided the first results of the three-dimensional electronic array.

References

[1] Low, D. The importance of 3D dosimetry. Journal of Physics: Conference Series, 573(1), 0–7. (2005)
[2] Zhao W, Rowlands JA. Digital radiology using active matrix readout of amorphous selenium: Theoretical analysis of detective quantum efficiency. Med. Phys. 24, 1819–1833 (1997).
[3] Mendis SK, Kemeny SE, Gee RC, Pain B, Staller CO, Kim Q, Fossum ER. CMOS active pixel image sensors for highly integrated imaging systems. IEEE J. of Solid-State Circuits. 32, 187-197 (1997).

SS3-2 – THURSDAY October 29, 2020: 11:15-11:30

Monte Carlo modelling of kV and MV imaging systems of the Varian TrueBeam STx Linac

Zapien-Campos B.[1,a)], Martínez-Dávalos A.[1,b)], Alva-Sánchez H.[1], Rodríguez-Villafuerte M.[1], Herrera-Martínez F.P.[2]

[1]*Instituto de Física, Universidad Nacional Autónoma de México, CDMX, México.* [2]*Instituto Nacional de Cancerología, CDMX, México.*

[a)]*brianzapien@ciencias.unam.mx,* [b)]*arnulfo@fisica.unam.mx*

Research area of interest: A. Physics and dosimetry of radiotherapy.

Keyword: Monte Carlo simulation, cone-beam CT, MV portal imaging,

Introduction: Image-guided radiation therapy (IGRT) consists on the use of medical images to improve precision and accuracy of radiation therapy treatments. Images are necessary for treatment planning, patient positioning verification, and, most recently, adaptative radiation therapy. Dosimetry and image quality assessment are important because there is always a compromise between image quality and patient dose. State of the art LINACs, such as the Varian TrueBeam STx, incorporate both an electronic portal imaging device, which uses an FFF 2.5 MV beam, and a 40-140 kV cone-beam CT. The aim of this work has been to develop Monte Carlo models of the TrueBeam STx on-board imaging systems, and to validate these models using relative transmission measurements, PDD curves and off-axis profiles.

Methods: Monte Carlo simulations were performed in two stages. First, the LINAC head and the X-ray tube were simulated using BEAMnrc [1] to obtain phase-spaces in a plane located at SSD=100 cm. In the second stage, we used the phase-space to perform dosimetric calculations in a water phantom and to obtain PDD curves and off-axis profiles using the DOSXYZ code.

The validation method consisted on acquiring images of two step wedge phantoms (aluminum and copper) and applying an exponential transform (eq. 1) to the images to obtain transmission values $T(x_m)$ for each thickness x_m. The normalized transmission values were compared with theoretical detector signal values $S(x_m)$, which were obtained from the MC calculated photon energy spectrum $\phi(E)$ using eq. 2.

$$T(x_m) = e^{-\frac{\bar{v}_p - \bar{v}_{bkg}}{k}} \quad (1)$$

$$S(x_m) = \int_0^{E_{max}} \phi(E) E (1 - e^{-\mu_{CsI} D}) \left(\frac{\mu_{en}}{\rho}\right)_{CsI,E} e^{-\mu_m x_m} dE \quad (2)$$

Results:

Figure 1 shows the transmission values obtained from the Al step wedge phantom image (red symbols) and the theoretical detector signal curve (blue). Comparison of MC dosimetric data of both imaging systems have also been compared with previously reported data [2,3], obtaining very good agreement.

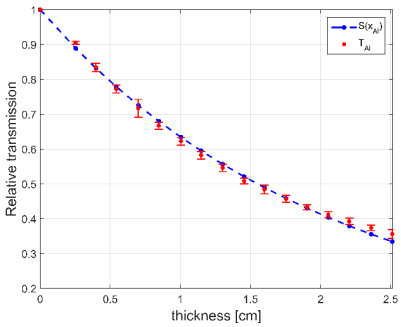

Figure 1. Measured (red) and calculated (blue) transmission curves for Al.

Conclusions: The MC models of the on-board imaging systems of the TrueBeam STx developed in this work show very good agreement with experimental measurements and with previous results reported in the literature. A novel technique, based on transmission measurements, proved to be an excellent and fast method for the validation of MC calculated photon energy spectra using experimental measurements.

References:

[1] Rogers D.W.O. et al. (1995) *Med. Phys.* **22**, 503-524.
[2] Ding G.X. (2017) *Radiat. Oncol.* **125**, 541-547.
[3] Ding G.X. and Coffey C.W (2010) *Phys. Med. Biol.* **55** 5231-5248.

SS3-3 – THURSDAY October 29, 2020: 11:30-11:45

Optical transport studies in monolithic LYSO crystals for PEM detectors

Víctor M. Lara-Camacho[1,a], Edgar M. Hernández-Acevedo[2,b], Héctor Alva-Sánchez[2,c], Tirso Murrieta-Rodríguez[2,d], Arnulfo Martínez-Dávalos[2,e] and Mercedes Rodríguez-Villafuerte[2,f]
[1]*Escuela Superior de Física y Matemáticas, IPN, Cd. Mx., México,* [2]*Laboratorio de Imágenes Biomédicas, Instituto de Física, UNAM, Cd. Mx., México.*

[a]*victormlc13@gmail.com,* [b]*marcial@fisica.unam.mx,* [c]*halva@fisica.unam.mx,* [d]*tmurrieta@fisica.unam.mx,* [e]*arnulfo@fisica.unam.mx,* [f]*mercedes@fisica.unam.mx*

Research area of interest: B. Physics and dosimetry of the images of medical diagnosis with ionizing radiation.

Keywords: Scintillator crystal, LYSO, PET.

Introduction: One of the most commonly used scintillators in Positron Emission Tomography (PET) is the LYSO/LSO crystal, which transforms the energy deposited by 511 keV annihilation photons into optical scintillation light. However, this scintillator contains natural lutetium, of which 2.6% is ^{176}Lu, a β^- emitter, responsible for the LYSO/LSO intrinsic radioactive background. Interestingly, the structure of the background energy spectrum depends on crystal size, as recently demonstrated by Alva-Sánchez *et al*. [1].

The aim of this work has been to experimentally assess the intrinsic energy spectrum of LYSO monolithic crystals in terms of its dependence with the optical properties of the crystal surface wrapping. These measurements have also been used to validate detailed Monte Carlo simulations of optical transport in LYSO crystals carried out with the ANTS2 code [2].

Methods: Two LYSO crystals of different sizes (57.4×57.4×10 mm^3 and 10×10×10 mm^3) were wrapped on five of their faces (top and lateral) with different optical interfaces (reflective or absorbent). The crystals were coupled to a large area (57.4×57.4 mm^2) 8×8 elements SiPM array (SensL ArrayC-60035-64P) using a 7 mm thick optical interface. MC simulations of optical photon transport were performed with the public domain code ANTS2 v4.14 [2] considering a realistic geometry based on the experimental detector assemblies.

Results and discussion: The LYSO intrinsic energy spectra obtained by MC simulation were compared to the experimental data (figure 1). All the spectra were normalized to the area under the curve in order to facilitate the comparison.

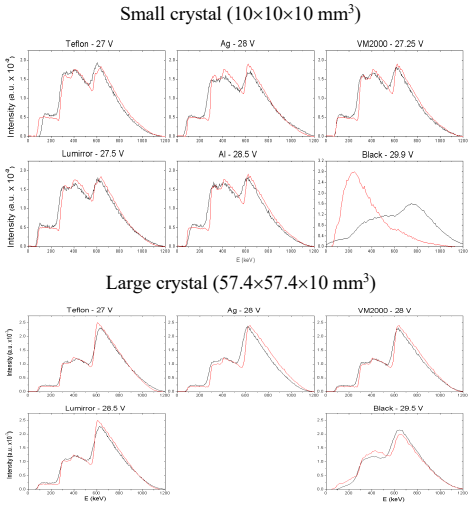

Fig 1. LYSO intrinsic energy spectra. MC simulation (red lines) and experimental data (black lines).

Conclusions: The total intensity of the scintillation light reaching the SiPM strongly depends on the optical properties of the crystal wrapping materials. Teflon, a diffuse-reflective material, produces the most luminous signals. In all cases, the MC results have very good agreement with the experimental data, except for the small crystal covered with absorbing black paint, in which the systematics of both, measurements and simulations, disappear.

References:

[1] H. Alva-Sánchez *et al*., "Understanding the intrinsic radioactivity energy spectrum from ^{176}Lu in LYSO/LSO scintillation crystals". *Sci. Rep.* 8 (2018) 17310.
[2] A. Morozov *et al.*, "ANTS2 package: simulation and experimental data processing for Anger camera type detectors". *J. Instrum.* 11 (2016) 04022.

SS3-4 – THURSDAY October 29, 2020: 12:00-12:45

Lipomics: a coloidal system with potential as a hydrophilic-lipophilic drugs carrier

David Ramírez Hernández[1*], Carlos Juárez-Osornio[2,3] Luis Alberto Medina Vlazquez[2,3]

[1]Facultad de Química, Universidad Nacional Autónoma de México, Ciudad de México, 04510, México. [2]Instituto de Física, Universidad Nacional Autónoma de México, Ciudad de México, 04510, México. [3]Unidad de Investigación Biomédica en Cáncer INCan-UNAM, Instituto Nacional de Cancerología, Ciudad de México, 14080, México.
350davidramirez@gmail.com

Research area of interest: Physics and dosimetry of the images of medical diagnosis with ionizing radiation

Keywords: Drug carriers, Lipomics, Radiopharmacology, microSPECT/CT imaging.

Introduction: Lipomic is a new drug carrier approach, which is defined as a colloidal system based in micelles incorporated into a liposome. This system shows potential as a hydrophilic-lipophilic drugs carrier that does not requires the use of organic solvents in its manufacture [1]. In this work we present the pharmacokinetic behavior of radiolabeled ^{99m}Tc-lipomics in experimental rats using microSPECT/CT imaging.

Methods: A methodology based on the use of ternary diagrams and Taguchi´s approach was implemented in the manufacturing of the lipomics. Particle Size and zeta potential were measured to evaluate the physicochemical stability of this colloidal system. Different electron microscopy techniques (SEM, TEM, STEM) were used to evaluate particle size and morphology, and to confirm the presence of micelles inside the structures. A plasmatic pharmacokinetic study in healthy rats was performed by radiolabeling of the lipomics with the ^{99m}Tc-2BMEDA complex and the in vivo biodistribution to evaluate the distribution of the lipomics in real time was evaluated by microSPECT/CT imaging.

Results and discussion: The physicochemical evaluation of lipomics showed a stable system with particle size and Zeta-potential of 80 nm and -40 mV, respectively. Radiochemical purity was grater than 95% with radiolabeling efficiency over 80%. The microSPECT/CT results show the capacity of this system as a carrier of hydrophilic-lipophilic drugs, with pharmacokinetics parameters: $T_{1/2}$=3.5 h, $T_{1/2}$=0.04 h, AUC=2.8 mCi*h/mL and Cl=126 ml/h. High uptake in the liver was observed during 6 h after injection.

Conclusions: The method of Taguchi and ternary diagrams allowed the development of a reproducible technique for manufacturing of lipomic. The physicochemical evaluation shows evidence of the Lipomic´s potential to transport lipophilic as hydrophilic molecules, while the pharmacokinetic evaluation shows its capacity as a pharmaceutical carrier.

References:

[1] Osornio, C. J. (16 may 2016). Structure similar to lipid emulsions and liposomes. Dipalmitoylphosphatidylcholine, colesterol, Tween 20-Span 20 or Tween 80-Span 80 in aqueus media. Journal of liposome research, 1-12.

SS3-5– THURSDAY October 29, 2020: 12:00-12:15

Preparation and Preclinical Evaluation of ^{64}Cu-NOTA-iPSMA as a Theranostic Radiopharmaceutical for Prostate Cancer

B. Góngora-Servín[1,a] and M. A. Ávila-Rodríguez[1,b]
[1]*Unidad Radiofarmacia-Ciclotrón, Facultad de Medicina, UNAM*
[a]*benny_alucard@ciencias.unam.mx,* [b]*avilarod@uwalumni.com*

Research area of interest:
A: Physics and Dosimetry of the images of medical diagnosis with ionizing radiation.

Keywords: Internal dosimetry, positron emission tomography, radiopharmaceutical, theranostic.

Introduction.
In Mexico, prostate cancer (PCa) is the second leading cause of death from malignant tumors in men 65 years of age or older, with about 5,000 deaths annually. Unfortunately, 75% of patients with PCa are diagnosed when the disease is already very advanced, and consequently it is much more difficult to treat it. So, there is no doubt about the importance of having techniques that allow not only to diagnose the disease at an early stage, but also to monitor the therapy in order to evaluate the effectiveness of the treatments.
Nowadays, radiopharmaceuticals based in the Prostate-Specific Membrane Antigen (PSMA) are the gold standard for the diagnosis of PCa via PET molecular imaging. In 2014 The Cyclotron-Radiopharmacy Unit introduced in the country the use of ^{68}Ga-labeled PSMA and given its high demand, and the exponential rise in the cost of the ^{68}Ge/^{68}Ga generators, it was recently decided to move to ^{18}F-labelled PSMA. Currently, a research project is under way to evaluate the clinical use of ^{64}Cu-labeled PSMA, a better imaging option when considering theranostic applications. The aim of this work was to prepare the radiopharmaceutical ^{64}Cu-NOTA-iPSMA, and to perform the preclinical evaluation of this radiotracer as a potential agent for the diagnosis of PCa.

Methods.
High specific activity ^{64}Cu was produced via the ^{64}Ni(p,n)^{64}Cu nuclear reaction with 11 MeV protons [1]. Radiochemical purification of ^{64}Cu was performed in a Trasis All-In-One module. For the preparation of ^{64}Cu-NOTA-Benzoil-NCS-HYNIC-iPSMA (^{64}Cu-NOTA-iPSMA), the iPSMA-conjugate was synthetized as a single vial kit formulation at the National Laboratory of Research and Development of Radiopharmaceuticals (LANIDER). For radiolabeling, the lyophilized conjugate (0.1 mg) was reconstituted with 1.5 ml of 1M NaOAc buffer, and after adding 0.2 ml of $^{64}CuCl_2$ (0.1M HCl) was incubated for 20 min at 90 °C. Preclinical evaluation was performed in mouse tumor xenograft model of PCa (LNCap) acquiring microPET images at several time points after the administration of the radiotracer. This protocol was approved by the ethics and research committee of the Research Division, Faculty of Medicine, under research project number 2018-131.

Results and Discussion.
The labeling yield of ^{64}Cu-NOTA-iPSMA was almost quantitative with a radiochemical purity greater than 97% (n=5), without the need of purification. MicroPET images showed a contrasted tumor as early as 60 min after administration of the radiopharmaceutical, and remained stable up to 24 h, suggesting a high and specific uptake of ^{64}Cu-NOTA-iPSMA in this PSMA+ cell line.

Conclusions.
The use of ^{64}Cu labelled PSMA in PET molecular imaging will be a great option for the diagnosis and treatment planning for PCa patients, allowing the acquisition of late images that better suits theranostic applications.

References.
[1] Manrique-Arias, J. C., & Avila-Rodriguez, M. A. (2014). *A simple and efficient method of nickel electrodeposition for the cyclotron production of 64Cu*. Appl Radiat Isot. 89, 37–41.

SS4-1 – THURSDAY October 29, 2020: 15:30-15:45

OSL nanoDot Response at High Dose Gradient Regions: Validation with phantom and *in vivo* tests

Agüero H [1,a], Rojas-López J A [1,2,b], Mancuzo A [1,c], and Binia S [1,d]

1 Fundación Escuela de Medicina Nuclear, 5500 Mendoza, Argentina
2 Instituto Balseiro, Universidad Nacional de Cuyo, 8400 San Carlos de Bariloche, Argentina
a haguero2626@gmail.com b alexrojas@ciencias.unam.mx, c arielmancuzo@gmail.com,
d sergiobinia@gmail.com

Research area of interest:
A: Physics and dosimetry of radiotherapy

Keywords: OSL, IMRT, *in vivo* dosimetry, geometrical uncertainty, high dose gradient.

Introduction: Due to IMRT technique deals with high dose gradient regions, it is necessary to evaluate geometrical uncertainties and its dosimetric impact [1]. For this reason, *in vivo* intracavitary dosimetry is a useful tool to measure dose variations in gradient regions.

Methods: Commissioning test. OSL nanoDot response in a high dose gradient at penumbra region of an open field was evaluated. Five dosimeters were placed at field edge and they were exposed (SSD 100 cm, depth 5 cm, field size 10x10cm2, 100 cGy) in acrylic phantom. Values were compared with ionization chamber (IC) Semiflex 3D (0.07 cc) dose profile measured in a PTW ScanLift automatic phantom. Clinical test: *In vivo* intracavitary dosimetry system was commissioned in prostate treatments in IMRT technique with compensator filters. The protocol allowed measuring doses at rectum such as organ at risk (OAR) in 23 patients (2 dosimeters per patient). Measurements were compared with doses calculated by TPS MIRS v.5.1 (semi-empirical scatter integrator algorithm). Uncertainty test. Geometrical uncertainties of IMRT technique carried out in a Varian Clinac iX (6 MV) were evaluated: i) dosimeters placement at planar digital images (for *in vivo* dosimetry) as shown in figure 1, ii) internal anatomical movements, iii) construction and placement of compensator filters and iv) mechanical indicators of the linear accelerator (linac), such as gantry, telemeter, laser, among others.

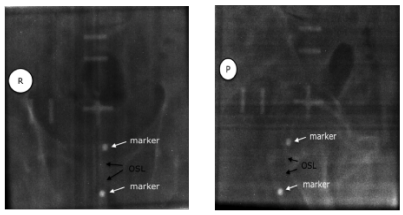

Figure 1. Placement of OSL at planar digital images (antero-posterior and lateral-right) in rectum in prostate treatments.

Results and discussion: Commissioning test. OSL relative doses followed with good agreement IC response in high dose gradient at penumbra region. Comparisons were carried out by DTA (distance to agreement). At maximum, DTA was 1.2 mm (figure 2). Clinical test. Mean difference between measured and calculated doses was 1.5% and the standard deviation was 18.7%. In order to define an action level as AL = |mean| + 1.96*standard deviation [2], action level was evaluated in 38% in rectum as OAR in a high dose gradient region. Third test. Geometrical uncertainties were calculated: i) 3 mm corresponding to dosimeters position at planar digital images, ii) 3 mm corresponding to internal anatomical movements, iii) 2 mm corresponding to construction and placement of compensator filters and iv) 2 mm corresponding to mechanical indicators of the linac. Total geometrical uncertainty was 5 mm. This value was associated a dosimetric impact of 37% in rectum as OAR in prostate IMRT treatments.

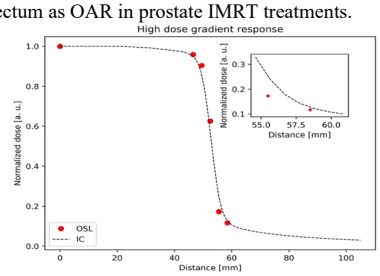

Figure 2. OSL an IC normalized dose at penumbra region of an open field.

Conclusions: *In vivo* tests had shown to be reliable to accurately measure dosimetric variations in high dose gradient regions. Action level for rectum as OAR in prostate IMRT treatments corresponded to 5 mm global geometrical uncertainty.

References:
[1] The Royal College of Radiologist. Institute of Physics and Engineering in Medicine. 11 (2008).
[2] Ezzell GA, Buermeister J, Dogan N, Losasso TJ, et al. (2009). Medical Physics 36(11):5359-5373.

SS4-2 – THURSDAY October 29, 2020: 15:45-16:00

Image Guided Radiotherapy Protocols and Doses: A CEMENER Experience

Eddie Palacios[1, a)] Nicolás Larragueta[1 b),] Federico Bregains[1, c)]
[1]CEMENER (Entre Ríos Nuclear and Molecular Medicine Center Foundation), Camino de la Cuchilla 595, Oro Verde, Entre Ríos, Argentina - PC 3100.
[a]palacios.ne@gmail.com, [b]nicolas.larragueta@cemener.ar, [c]federico.bregains@cemener.ar

Research area of interest: B. Physics and dosimetry of radiotherapy.
Keywords: IGRT protocols, head and neck and prostate cancer, CTV-PTV margins extension, dosimetry of volumetric and planar setup imaging.

Introduction: IGRT provides an efficient way of delimitation, planning and patient positioning. However, we must consider the cost-benefit relationship and the ALARA philosophy in case ionizing radiation in medical imaging is recommended. Although the delivered imaging doses are smaller than those for therapy, radiosensitive organs and large portions of the body are irradiated. The IGRT protocols provide a safe way to achieve high accuracy in the treatment, reducing geometric and variations, also providing an evaluation of appropriated CTV-PTV margins extension.

Methods: We sought to obtain specific IGRT protocols and establishing reference levels for IGRT exposures. A retrospective analysis has been performed on 37 prostate cancer (PCa) patients, and 31 head and neck (H&N) patients treated at CEMENER. We proposed IGRT positioning protocols for PCa and H&N patients in order to reduce systematic positioning errors. Additionally, we measured and compared the associated doses with the acquisition of planar and CBCT (CBDIw method) images; PTW solutions for low energy x-ray were required for such purpose: the Nomex system and the CTDI phantom. We calculated the effective doses using the w_T factors suggested by the ICRP 103 and by Hyer et al. [1]. Finally, we reevaluated our CTV-PTV margins using the van Herk Formula [2].

Results and discussion: We have implemented two protocols for H&N, when the tumor had had variation (CBCT) and when it was required to irradiate a surgical bed; the effective doses imparted by were 0.90 mSv and 0.43 mSv, respectively. The effective dose for PCa patients was 48.90 mSv. Couch displacements were restricted to 3mm for H&N and 5mm for PCa, and used as action levels.

Conclusions: After the evaluation of 23 patients in H&N and Prostate regions, the actual margins considered as safe are 6mm for both regions, which represented a reduction of 1 – 3 mm. However, these margins are still being evaluated as more data is collected.

References:

[1] Hyer, D.E., 2010. “Imaging doses in radiation therapy from kilovoltage cone-beam computed tomography”, Gainesville, Fla.: University of Florida.
[2] Bel A., van Herk, M., et al., 1993. ”A verification procedure to improve patient set-up accuracy using portal images”, *Radiotherapy and Oncology,* vol. 29, nº 2, pp. 253-260.

SS4-3 – THURSDAY October 29, 2020: 16:00-16:15

A Proposed Method to Assure the Efficiency of Thermotherapy Treatments

José Agustín Pérez Ahumada[1a], J. Fabian Vázquez de la Rosa[1b], Rodrigo Alfonso Martin Salas[1c], and Lucia Medina[1d]

[1] *Facultad de Ciencias, Universidad Nacional Autónoma de México, CD.MX. 04510, México*
[a]jagustinpa@ciencias.unam.mx, [b]jfuv@ciencias.unam.mx, ,
[c]r.martin@ciencias.unam.mx,[d]luciamedina@ciencias.unam.mx

Research area of interest: Biological Physics, Physiological Measurements and Mathematical Methods in Medical Physics

Keywords: Thermotherapy, Blood oxygen saturation, Muscular injuries, Sports treatment.

Introduction: Thermotherapy is a method indicated for rehabilitation in different conditions such as osteoarthritis, hypertonia, muscle contractures, osteoarthritis, rheumatoid arthritis, injuries of skeletal muscle, edema, among others, even in cases of patients with ischemic stroke [1]. Thermotherapy is widely indicated in muscular lesions on athletes due to approximately 55% of injuries are muscular, and 90% are bruises, contractures or muscle strains [1]; but there is not a method to quantify the efficiency of the treatment or to obtain quantitative evidence of the number of sessions and time that the subject should be submitted to the treatment. In this paper we propose a method for ensuring the effectivity of the thermotherapy treatments, based on the measure of the blood oxygenation when the therapy is applied to a superior extremity.

Methods: Thermotherapy treatment with a thermal conduction agent for surface thermotherapy was applied to 40 volunteers who met the following characteristics: male from 18 to 25 years old who did not perform physical gym activity (more than 3 times a week) or were high-profile athletes. Oxygen saturation was measured as an indicator of the vasodilation effect by thermotherapy.

The subjects were divided into two groups of 20 patients: experimental group who received a treatment by thermotherapy at 40°C by 15 minutes, and a control group, which doesn't received thermotherapy.

The thermal agent was an armband that had the property of maintaining its constant temperature throughout the treatment.

Regardless of the subject's group, all of participants remained at rest for 15 minutes and their blood oxygen saturation was monitored, registering three measurements in the first minute and three measurements after 15 minutes.

Results and discussion: Blood oxygen saturation measurements were used for a statistical test of difference in means, this to prove that there is a significative difference between measurements of oxygen saturation in users due the thermal agent.

After analyzing the statistical test, it was found that there was an increase in blood oxygen saturation of the users who received the treatment by thermotherapy, compared to those who didn't.

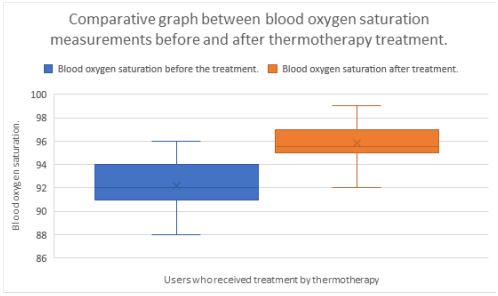

Fig. 1. Comparative graph between oxygen saturation measurements before and after thermotherapy treatment.

Conclusions: It was found that the use of a thermal agent can increase the blood oxygen saturation of users. This increase could be caused by the vasodilatation effect caused by thermotherapy in the area of interest.

SS5-1 –FRIDAY October 30, 2020: 12:00-12:15

Parallels Between Homeostatic Regulation and a Balance Robot Toy Model

Juan Uriel Legaria Peña[1,a] Félix Sánchez Morales[1,b] Jorge Chávez Carlos[2,c] Ruben Fossion[2,3,d]

[1]*Departamento de física, Facultad de Ciencias UNAM* [2]*Centro de Ciencias de la Complejidad (C3)* [3]*Instituto de Ciencias Nucleares UNAM*

[a]*walup@ciencias.unam.mx,* [b]*felixsm@ciencias.unam.mx,* [c]*jorge.chavez@correo.nucleares.unam.mx,* [d]*ruben.fossion@gmail.com,*

Research of interest: D. Biological physics, physiological measures and mathematical methods.

Keywords: Homeostasis, time series, control theory.

Introduction: Medical Physics tackles the problems of prevention, diagnosis and treatment of human diseases [1]. While diagnosis and treatment are covered by areas such as medical imaging and radiotherapy, the question of prevention remains largely unexplored. One approach focuses on detecting changes in homeostatic regulation that could arise before the onset of symptoms. This can be done by studying the variability of time series of regulated and regulating variables. In optimal conditions of youth and health, regulating variables such as breathing amplitude (BA) allow to adapt to external conditions such that corresponding regulated variables such as blood oxygen saturation (SpO2) may remain relatively constant [2]. The identification of toy control systems that can emulate this behavior would be a crucial first step in establishing a framework within control theory to study homeostasis.

Methods: Time series of SpO2, and BA where registered simultaneously in resting state and while walking at a steady pace. The study was part of a research protocol approved by the ethics committee of the General Hospital of Mexico with registry number DI/14/110-B/03/002 and all participants signed a letter of informed consent. Variation of the data was visualized through box and whisker plots to assess the differences between the regulated variable (SpO2) and regulating variable (BA). A 2-wheeled self-balancing robot which can be interpreted as an inverted pendulum was built using the Lego Mindstorms EV3 kit. The objective of the control in this system is to maintain the robot in the upright position by moving the wheels in order to maintain the center of mass above the base of support. A rotating rod was attached to the robot and time series of both the angle of the robot to the vertical and angle of its wheels were recorded for different frequencies of rotation of the rod, to investigate their role as regulated and regulating variables.

Results and discussion: Physiological results are shown for a representative young healthy student (Figures 1a and 1b). In the walking experiment, average value and variability of BA change drastically and reflect different physiological strategies to adapt to different external conditions (Fig. 1b); as a result, variations in SpO2 are restricted to few percent and the internal environment remains relatively constant (Fig. 1a). In the case of the robot, the movement of the wheels absorbs most of the perturbations (Fig. 1d) such that the angle with the vertical is almost independent from the external conditions (Fig. 1c).

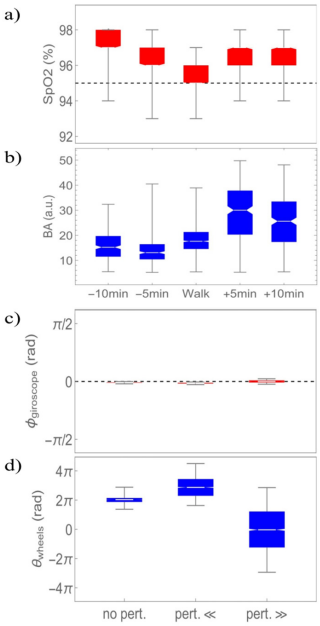

Fig. 1. Average values and variability of regulated (red) vs regulating (blue) variables in resting and stressed conditions. (a) SpO2 and (b) BA during 20 min walk and 5 min rest periods before and after walk. (c) Gyroscope angle of the robot from the vertical and (d) angle of the wheels, under different levels of perturbation.

Conclusions: In both cases, physiological and technological, time series analysis allows to quantify in a non-invasive way the dynamics of the underlying regulatory processes.Applications from control theory such as the 2-wheeled self-balancing robot will be helpful to identify statistical biomarkers in regulatory dynamics to detect advancing pathologies before symptoms arise.

References:

[1] Brandan, M.E., et al. (2017). Red Física Médica: http://fisicamedica.mx

[2] Fossion, R., et al. (2019). *AIP* Conf. Proc. 2090 (2019) 050007.

SS5-2 –FRIDAY October 30, 2020: 12:15-12:30

Design of a Faraday Cage for Biomedical Measurements Based on Site Electromagnetic Field Mapping

Alfredo Cruz Valenzuela[1a], Jaime Fabian Vázquez de la Rosa[1b], Rodrigo Martin Salas[1c], Sergio Enrique Solís Nájera[1] and Lucia Medina[1]

[1] *Facultad de Ciencias, Universidad Nacional Autónoma de México, CD.MX. 04510, México*
[a]alfredocruzvalenzuela@ciencias.unam.mx, [b]jfuv@ciencias.unam.mx, , [c]r.martin@ciencias.unam.mx
[d]solisnajera@ciencias.unam.mx,[e]luciamedina@ciencias.unam.mx

Research area of interest: Biological Physics, Physiological Measurements and Mathematical Methods in Medical Physics

Keywords: Biomedical signals, Electromagnetic Interference, Faraday Cage, Field Mapping.

Introduction: One of the principal problems in the measurement of biomedical signals is the inherent noise produced by the environment, mainly by the induction phenomenon in metallic parts of the electrical supply, the noise originated by electromechanical devices, air conditioners or the lighting installations, and also from wireless communications. All of these factors contribute to distorting the acquisition of biopotentials. To overcome these problems, a Faraday cage could be employed in the acquisition of biomedical signals and in the process of testing biomedical instrumentation. In this work, we present a method based on an Electromagnetic Field Mapping (EFM) to identify the potential sources of Electromagnetic Interference (EMI), their wavelength and therefore, physical dimensions of the enclosure.

Methods: An EFM was performed in a destined site for a Faraday cage installation. The area was divided into 9 quadrants in which electric field was measured using a Biconical type antenna, located on a non-conductive tripod, and a Spectrum Analyzer (Anritsu MS2711D). A frequency spam from 30 MHz to 1000 MHz was employed for the measurement of EMI. The frequencies detected in the electromagnetic spectrum were used for determining the physical dimensions of the enclosure.

A computational simulation on Finite Element Method (FEM) was executed for the designed enclosure, the distribution of EM field was computed with the Faraday cage containing EM absorbents and without them.

Results and discussion: The EFM acquired in the site showed that the frequency with the major levels of emissions is 206 MHz. In order to avoid resonant effects in the enclosure, the physical dimensions were determined as 4m x 4m x 3m. The biconical antenna was excited at the frequency with the major intensity, and the radiation pattern was computed, there is no distortion on the pattern (Fig. 1) which implies that there are no reflections of consideration, so the area of interest for experimentation presents a homogeneous field. Some areas of accumulation can be found in the walls of the enclosure, but they are maintained in values that do not represent a problematic field.

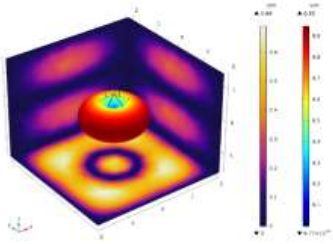

Conclusions: The design of an EM enclosure for biomedical experiments based on the exploration of the EM environment of the site provides a tool for minimizing the EMI, and therefore the distortion of the field in the enclosure that could improve the results of the biomedical acquisitions. A more efficient use of the physical spaces for dedicated laboratories can be achieved considering the real EM conditions.

References:

[1] Purcell, 1988. "Electricity and magnetism" Berkeley Physics Course. Editorial Reverté. Segunda edición.
[2] Balanis, C., 2005. "Antenna Theory. Analysis and Design" -John Wiley and Sons. Tercera Edición.

SS5-3 –FRIDAY October 30, 2020: 12:30-12:45

Spectral and Statistical analysis of actigraphic recordings of acute insomnia patients

Arlex Marín-García[1,a], Rubén Fossión[1,2], Ana Leonor Rivera[1,2]
[1] *Centro de Ciencias de la Complejidad, Universidad Nacional Autónoma de México,México*
[2] *Instituto de Ciencias Nucleares, Universidad Nacional Autónoma de México, México*
[a] arlex.marin@c3.unam.mx

Research Area of Interest: D. Biological Physics, physiological measures, and mathematical methods.
Keywords: Actigraphy, insomnia, circadian and ultradian rhythms.

Introduction: Circadian, ultradian and infradian rhythms are physical, mental and behavioural patterns of activity that exhibit stable periodicities at several time scales. A large body of evidence has accumulated establishing a direct link between physiological systems and central and peripheral biological clocks, as well as their disturbances in disease[1]. Actigraphy, the monitoring of physical activity, is a non-invasive and ecologically valid method to study behavioural patterns in humans[2]. Through the study of actigraphic recordings it has been observed that perturbations from the healthy condition of circadian rhythmicity is present in a number of illnesses, such as acute insomnia, depression, anxiety, post–traumatic stress disorder, among others[3]; and while a wide variety of parametric methods for the analysis of actigraphic recordings exist, non-parametric, model free analyses have shown greater sensitivity to subtle differences between healthy controls and patients with different diseases [4]. This work proposes the use of fully data–driven and non–parametric methods which can both reproduce previous results and reveal new insights into the disturbances of ultradian, circadian and infradian rhythms in disease.

Methods: We performed spectral and statistical analyses of experimental actigraphic recordings for the publicly available data of the publication of [4]. The data collection for the original analysis was approved by the University of Glasgow Ethics Committee and was recorded with an Actiwatch device, worn at all times throughout day and night, for a period of 2 weeks at most and 1 at least. It consists of time series of activity counts summed at P = 1min epochs taken from 21 asymptomatic controls (28yo ± 6, 7 males and 14 females) and 18 acute insomnia subjects (25yo ± 6, 5 males and 13 females). Each time series is divided into segments of Td = 1440 and Tw = 10080 minutes, corresponding to daily and weekly time scales, thus creating ensembles of time series at both time resolutions, allowing for individual– and group–wise definitions of probability density functions (PDFs) of motor activity as a function of time. In the first place, spectral analysis consist in statistical comparisons of both Fourier amplitudes and phases using the Kolmogorov—Smirnoff test for infradian, circadian, and ultradian spectral bands. Second, a non—parametric measure of distance between PDFs, the Jaccard distance[5], is used to quantify the degree of dissimilarity between controls and insomniac subjects. Third, Shannon Entropy is used to estimate the dissimilarity of information content between both individual— and group—wise PDFs. Fourth, intra—group and inter—subject similarities are estimated through the use of the zero—lag correlation coefficient between PDFs.

Results and Discussion: For spectral characteristics, non—parametric statistical differences on the amplitudes can be found at the ultradian rhythmicities, specifically, at the BRAC time scales[6]; while differences on the phases are observed only on the circadian rhythmicities. For the case of statistical properties, the measured statistical distance metric shows a clear time-lag between group-wise activity profiles as well as differences in information content. Equally important, the group-wise similarity profiles exhibit significant differences in both the average and dispersion of similarities. These results indicate not only a perturbation on the expression of ultradian, circadian, and infradian rhythmicities (meaning their *amplitude*) but also on their *phases*.

Conclusions: Simple and straightforward methods of analysis can be used to obtain novel results from continuous actigraphic recordings, this time-series analysis approach yields not only confirmation of previously obtained results, but new directions for future research.

References:

[1] Halberg et al. Journal of circadian rhythms 1.1 (2003): 2.
[2] Sadeh, Avi. Sleep medicine reviews 15.4 (2011): 259-267.
[3] McClung, C.A. European Neuropsychopharmacology 21 (2011): S683-S693.
[4] Fossion et al. PloS one 12.7 (2017): e0181762.
[5] Levandowsky & Winter. Nature 234.5323 (1971): 34-35.
[6] Kleitman, N. Sleep 5.4 (1982): 311-317.

SS5-4 –FRIDAY October 30, 2020: 12:45-13:00

Analysis of the exponent Hurst in RR series of healthy subjects and congestive patients in sleep and wake state and in healthy subjects during physical activity

A. Salcedo-Martínez[1], J. A. Zamora-Justo[2], A.Muñoz-Diosdado[3]
Basic Sciences Department, UPIBI-Instituto Politécnico Nacional, Mexico City, Mexico
E-mail: amparo-mtez@hotmail.com[1], zamora.justo@outlook.com[2], amunozdiosdado@gmail.com[3],

Research area of interest:
D. Biological physics, physiological measures and mathematical methods.
Keywords: Hurst exponent, cardiac stress, physical condition, stress test, congestive heart failure

Introduction

It has been observed that the correlation analysis in a complex system, like the heart, allows to detect certain heart diseases [1], which are the leading cause of death in the world [2], such as congestive heart failure (CHF).

The main objective is to use Hurst exponent estimates for the study of the complexity in physiological signals of the cardiac interbeat, in order to find information that allows us to evaluate the sleep-wake phases in healthy subjects and patients with insufficiency in its different New York Heart Association (NYHA) classifications, as well as qualitatively determine the cardiac stress and physical condition applied in the stress tests of healthy young subjects with a sedentary lifestyle and healthy subjects who practice some physical sport.

Methods

-RR series, healthy subjects and CHF patients: We analyzed records of 54 healthy subjects and 44 patients with CHF from PhysioNet databases. These RR series were separated by hours, and RR series of 6 hours were obtained for each of the mentioned phases.

-Stress tests: Tacograms of 23 healthy young subjects and 11 adults, both with a sedentary lifestyle and 5 active healthy young subjects were analyzed, these groups without any apparent cardiovascular disease. The protocol to obtain the ECG signals consisted of 4 phases: two stress tests at different speeds (3.5 and 4 miles per hour (MPH) for healthy subjects; 3 and 3.5 MPH for adults), both lasting 30 minutes and two resting states between each test. The obtained tachograms were segmented into subseries for the rest section and for the first and second stress tests. Finally, each subseries were analyzed by using the Hurst exponent estimations.

-Hurst exponent. The meaning of the values of the Hurst exponent (H) indicates the persistence level of a time series [3]:

- $0 < H < 0.5$, corresponds to anti-persistence or anti-correlational behavior in time series.
- $0.5 < H < 1$ corresponds to persistence or correlated processes.

We used the estimates of H exponent: the discrete second order derivative (DSOD) and its Wavelet-based adaptation (WDSOD), which are provided in the MATLAB software; and both approximations give consistent results for all cases, so we decided to report only one H-value that is the average of the two values.

Results and discussion

The results obtained indicate that, if the tachograms are persistent they correspond to healthy subjects at rest, but if the RR series involves antipersistence, these correspond to subjects with heart failure and when a healthy young subject is in physical activity. Also, in subjects who perform some physical activity the exercise tolerance was proven, due to the fact that their RR subseries are characterized by long-term memory effects. On the other hand, we corroborated that in patients with CHF, their symptoms are maintained both in wakefulness and in the sleep phase.

Conclusions

This method is considerably acceptable to show changes in the dynamics of the cardiovascular system that are not present in people who are at rest. In addition, with this parameter is possible to verify the health state and at least qualitatively to determine the stress to which the heart is subjected during a certain physical activity.

Acknowledgments

The authors thank to the Secretaría de Investigación y Posgrado of the Instituto Politécnico Nacional (SIP-IPN) from grant number: 20196318 for economic support and for the scholarships gotten by means of the BEIFI program. And to all the study subjects.

References

[1] Muñoz Diosdado, A., Reyes Cruz, H., Bueno Hernández, D., Gálvez Coyt, G., Arellanes González, J. New Results in Magnitude and Sign Correlations in Heartbeat Fluctuations for Healthy Persons and Congestive Heart Failure (CHF) Patients. AIP Conference Proceedings 1032 (2008), 255-258.
[2] G. Fruchter and S. Ben-Haim, "Dynamic properties of cardiovascular systems", Mathematical Biosciences 110 (Elsevier Co., Inc., New York, 1992) pp.103-117.
[3] Flandrin, P. (1992), "Wavelet analysis and synthesis of fractional Brownian motion," IEEE Trans. on Inf. Th. 38, pp. 910–917.

SS6-1 –FRIDAY October 30, 2020: 16:00-16:15

2D Radiotherapy in Mexico Today

García-Zúñiga, N.[1,a], Armengol-Cruz, V. E.[2,b], Barrientos-Luna, H. G.[1,c] and Mercado-Hernández, I.[1,d]

[1]*Hospital Central "Ignacio Morones Prieto", S.L.P.,* [2] *Hospital General de México "Dr. Eduardo Liceaga"., Cd. Mx.*

[a]nancygz@ciencias.unam.mx, [b]armengolcruz@gmail.com, [c]titobarrientos1@gmail.com, [d]imercado72@gmail.com

Research area of interest: E: Education and profession.

Keywords: 2D Radiotherapy, 2D Simulator, Radiographic film.

Introduction:

2D Radiotherapy is a treatment option that uses generally parallel and opposite fields. Fields are conformed to the treatment area by Multileaf Collimator (MLC) or Cerrobend® blocks. This radiotherapy allows simple and palliative treatments. [1]

The *Centro Potosino Contra el Cancer* in *San Luis Potosí* has a radiotherapy unit that see anyone 60 mean patients per day with the 2D technique. The unit has a LINAC with integrated MLC, a 2D Simulator, a radiographic film Digitizer and dosimetric equipment.

Methods: Stages of 2D radiotherapy are:

Patient evaluation: The Radiation Oncologist to execute screening clinically that includes the pathology report. Determine if the patient is candidate for radiotherapy, and then he can schedule the simulation session.

Simulation: The treatment region is located with fluoroscopy. When the region of interest is defined, the radiographic film is obtained. Treatment depths and field designed are established in the simulation. Next, films are revealed and labeled, they are transferred to Medical Physicist with the treatment sheet and the clinical history [1,2].

Treatment Planning: It consists of the manual calculation of the Monitor Units to be imparted. The data for the calculation are provided by the Physician on the treatment sheet. For this process two tools were created for the calculation of the MU, a spreadsheet and an algorithm in Matlab, with the purpose of being able to perform the calculation in two different ways [1, 3].

Design of the fields is performed with an optical digitizer according to the delimitation of the treatment area made by the Physician on the radiographic film.

Treatment delivery: The patient is positioned according to the tattoos made in the simulation. The MLC is formed based on the information generated by the *Shaper MLC* software and the monitor units that will be supplied by each field are introduced manually.

Dosimetry of the LINAC: This is done periodically to verify that the parameters of the LINAC are kept within the permitted values.

Results and discussion: 2D radiotherapy has associated inherent limitations, some of the critical points that have been observed are the following: It is very important that the pathological report contains the correct diagnostic. The exposure of the simulation radiographic films must be appropriated so that the should be able to correctly define the treatment area. A double verification system to calculate the monitor units allows to reduce the human errors and the planning process has become more efficient. In the absence of a patient verification imaging system, it is important to raise awareness among technical staff.

Conclusions: The treatment of cancer in Mexico faces great challenges, one of them is the development and modernization of the public sector health infrastructure, however, with the implementation of tools that minimize possible human errors in 2D Radiotherapy Treatments It can be administered safely. It is important to generate quality policies to assure optimal treatment in RT 2d to continue saving lives.

References:

[1] Besa, P. (2013). Radioterapia externa: lo que el médico general debe saber. Rev Med Clin Condes, 24(4), 705-15.

[2] Khan, F. M., Gibbons, J. P., & Sperduto, P. W. (2016). Khan's Treatment Planning in Radiation Oncology. Lippincott Williams & Wilkins.

[3] Burns, J. E. (1996). BJR Supplement 25: Central axis depth dose data for use in radiotherapy. British Institute of Radiology, London: England

SS6-2 –FRIDAY October 30, 2020: 16:15-16:30

Professional and academic follow up of 100+ graduates of the UAEM-ININ masters and doctorate program in medical physics in Mexico

Eleni Mitsoura[1,a], Keila Isaac-Olive[1,b], Liliana Aranda-Lara[1,c], Miguel Angel Camacho-Lopez[1,d], Eugenio Torres-Garcia[1,e], Alberto Ernesto Hardy-Perez[1,f]

[1] *Universidad Autónoma del Estado de México (UAEMex)*

[a]meleni@uaemex.mx [b]kisaaco@uaemex.mx [c]larandal@uaemex.mx [d]macamachol@uaemex.mx

[e]etorresg@uaemex.mx [f]aehardyp@uaemex.mx

Research area of interest: E. Educational and professional issues.

Keywords: Medical physics, education, graduate program, UAEM-ININ, follow up.

Introduction: At the beginning of the 90´s the reduced number of medical physicists in Mexico was concerning. In 1994, the National Institute of Nuclear Research (ININ), sponsored by the International Atomic Energy Agency (IAEA), promoted the creation of a teaching and training program in Medical Physics. In 1996, the Autonomous University of the State of Mexico (UAEM) and the ININ started the first formal Graduate Program in Science (Masters and Doctorate degree) specialized in Medical Physics in Mexico. In 2012, the Master program was restructured and is still in force. In 2009, the Doctorate program joined the Doctorate in Health Sciences, from the same University. Both programs have been recognized for their quality by the National Council of Science and Technology in Mexico (CONACyT). Mexico only has 2 programs in Medical Physics, the (UAEM-ININ) and the one from the National Autonomous University of the Mexico (UNAM) opened since 1997. Still, the need of medical physics in Mexico is an issue today. The objective of this work is to present the professional and academic follow up of 100+ graduates of the UAEM-ININ program after 24 year experience.

Methods: From the current student files, alumni records and the alumni tracking program, a retrospective analysis was carried out, based on: a. Professional and social matters (geographical origin of the students, academic background, number of graduated students per year, ratio of graduated students currently working as medical physicists and related areas, etc.). b. Academic impact (scientific publications produced by the M.Sc. and D.Sc. programs, number of thesis by the study areas of the Medical Physics field, etc.).

Results and discussion: Twenty four years after its creation, a comprehensive professional and academic follow up of the UAEM-ININ program is presented in this work, based on the achievements attained, regarding the number of graduated Medical Physicists, their geographic and academic origin, their current professional activities and the number of scientific publications produced as a result of their thesis. For example, as of December 2019, 79% of our 105 graduated students are working in areas related to medical physics, and 21% in different ones.

Conclusions: The indicators presented in this work demonstrate that, in the last 24 years, the UAEM-ININ M.Sc. and D.Sc. Medical Physics Graduate Program has achieved its goals, in forming clinical medical physicists and researchers. We are working now to strengthen collaboration with the clinical sector, to impact in the national normativity, to support the establishment of clinical residency, to promote international collaboration and to lead our graduated to obtain recognized certifications in the medical physics areas.

References:

http://web.uaemex.mx/fmedicina/fisica-medica.html

SS6-3 –FRIDAY October 30, 2020: 16:30-16:45

Academic offer in the UNAM M. Sc. (Medical Physics) program

María-Ester Brandan [1,a]
[1]*Instituto de Física, Universidad Nacional Autónoma de México, Mexico City, Mexico.*
[a]*brandan@fisica.unam.mx*

Research area of interest: E
Keywords: Medical physics education, Mexico, academic offer, professors, thesis, students

Introduction: The M.Sc. (Medical Physics) program offered by UNAM, the National Autonomous University of Mexico, has graduated about 150 medical physicists since the year 2000. This presentation analyses the academic offer, the preferences when choosing a thesis subject, and the job opportunities after graduation. A recent reform of the UNAM Physics Graduate program (PCF) has defined a new academic structure and this will be analyzed in terms of the past and current offer.

Methods: The analysis is based on data recorded over the 22 years of the program. The subjects of the thesis as well as the present occupation of the graduates are available at the program´s web page [1].

Results and discussion: The traditional areas for medical physics, physics of radiotherapy and diagnostic imaging, are those with the stronger academic offer as well as those preferred by students in the program. However, less-traditional options such as medical applications of optics and non-ionizing radiation, as well as biophysics, physiological measurements and mathematical models in medicine and biology also interest tutors and students. After graduation, medical physicists have clinical jobs, follow doctoral studies and do research, or work in companies associated with medical equipment and services.

Conclusions: The areas of thesis specialization of the UNAM students not only include those considered traditional in medical physics, but also others where a wide academic offer exists. Clinical jobs only exist in the traditional services.

Reference:
[1] Posgrado en Física Médica, UNAM, http://www.fisica.unam.mx/fismed. Accessed on November 25, 2019.

SS6-4 –FRIDAY October 30, 2020: 16:45-17:00

International experiences on a budget: the role of online technologies in the training of young scientists in developing countries

Mariela A. Porras-Chaverri[1],Laura Padilla[2], Diane Alvarez[3] and Iván M. Rosado-Méndez[4],
[1]*Escuela de Física, Universidad de Costa Rica, San José, Costa Rica, mariela.porras@ucr.ac.cr*
[2]*Department of Radiation Oncology, Virginia Commonwealth University, Richmond, Virginia, United States of*
[3]*Miami Cancer Institute, Florida International University, Miami, Florida United States of America,* [4]*Instituto de Física, Universidad Nacional Autónoma de México, Ciudad de México, México*

Research area of interest:
E. Education and professional issues
Keywords: scientific training, developing world, online technologies
Introduction: Limited financial resources available for science research and training in Latin America preclude most young scientists from having international experiences. This limitation has an impact on their development as scientists, because it restricts the opportunities to interact with cutting-edge researchers and receive mentoring from such scientists. The lack of international forums in which to present their work may limit their development of soft skills such as English and communication proficiency. [1] The popularity of online technologies, even in developing countries, allows for new methods in which students can have international experiences without extensive costs. [2,3]
Methods: The International Academic Virtual Exchange network (IAVE) was created as a way to provide students in the developing world with international experiences. The student members of this network include graduate students in Medical Physics and Physics undergraduate students. The network currently has members from 10 different countries in the Americas and Europe. Activities such as weekly journal clubs, scientific conferences, workshops and a peer-reviewed annual congress are organized online using free software and allow for real-time audience interaction via chat or video. Most activities are conducted in English, with occasional activities in Spanish, to allow participation of students with all levels of English command.
The annual IAVE Congress accepts abstracts in two modalities, original research and literature review. This allows students with limited access to research opportunities the chance to hone their literature research and presentation skills using their available resources. Both modalities undergo the same peer-review process and students present through videoconference to an international audience.
Results and discussion: Since 2017, IAVE has hosted over 60 webinars, including weekly sessions, covering subjects from clinical applications of radiation to professional development topics, such as scientific communication. These webinars include presentations of both graduate and undergraduate students in Latin America and the United States. Webinars with professional speakers are organized at each site institution and broadcast to the IAVE network, taking advantage of visits from experts. Two IAVE Congresses have been organized, with participation of 11 students in 2018 and another 11 in 2019, for a total of 18 different students from Latin America (graduate and undergraduate level) and 4 students from the United States (graduate level). Mentoring activities and research opportunities are organized at each site institution and across-sites.
Conclusions: It is possible to establish a beneficial, fruitful, international relationship between initially un-affiliated institutions with limited resources, through the efforts and commitment of participating members. IAVE has been able to plan and execute several types of activities that increase the opportunities of interaction between members regardless of geographical limitations, providing students the opportunity to participate in international scientific activities, even without access to research or travel funding.
References:
[1] Sánchez-Tarragó et al., 2015. “La producción científica latinoamericana desde una mirada poscolonial,” XVI Encontro Nacional de Pesquisa en Ciência da Informação, João Pessoa, Brasil.
[2] Amador et al., 2016. Estadísticas del sector de comunicaciones, Superintendencia de Telecomunicaciones, San José, Costa Rica.
[3] Valk et al.,2010. “Using mobile phones to improve educational outcomes: an analysis of evidence from Asia” Int. rev. res. open dist. learn., 11,1.

Abstracts: Best Student Paper Competition

SC1–THURSDAY October 29, 2020: 18:00-18:15

Cardio-respiratory Variability of Healthy Young Subjects

Antonio Barajas-Martínez[1,2,3,a], Geraldine Tello-Santoyo[1,2,b], Pablo Berumen-Cano[1,2], Adriana Robles-Cabrera[1,2,3], Juan Antonio López-Rivera[1,4], Ruben Fossion[1,5], Juan Claudio Toledo-Roy[1,5], Alejandro Frank[1,5,6], Bruno Estañol[1,7], Ana Leonor Rivera[1,5,c]

[1]*Centro de Ciencias de la Complejidad, UNAM.* [2] *Facultad de Medicina, UNAM.*
[3]*Programa de Doctorado en Ciencias Biomédicas, UNAM.* [4]*Facultad de Ciencias,UNAM.* [5]*Instituto de Ciencias Nucleares, UNAM.* [6]*El Colegio Nacional, México.*
[7]*Instituto Nacional de Ciencias Médicas y Nutrición "Salvador Zubirán".*
[a] anbama16@gmail.com, [b]ageraldine.10@gmail.com, [c]ana.rivera@nucleares.unam.mx.

Research area of interest: D. Physiological measures and mathematical methods.
Keywords: Time series analysis, menstrual cycle, heart rate variability, respiration.

Introduction: Human health is characterized by robustness, supported by systems that allow it to maintain homeostasis and survive in a wide range of conditions, but also by its ability to rapidly and effectively adapt to a changing external environment [1,2]. This balance between robustness and adaptability can be measured by biomarkers in the time [3] and frequency domains [4] reflecting distinctive physiological responses [5,6]. Alterations in these biomarkers may appear before symptoms arise and opens up promising possibilities for applications in preventive medicine [7]. One of the unsolved paradoxes in medicine is that women have a longer life expectancy than men yet they exhibit a more fragile health. Unfortunately, the effect of the menstrual cycle in women in physiology has been largely neglected in research. Here, our goal is to study the effect of female hormones on physiological time series and their relation to health.

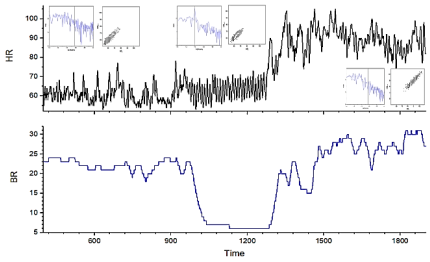

Fig. 1. Respiratory and heart rate of a 19-year old, male control subject. Insets are the power spectral density (PSD or amplitude of the Fourier transform) and Poincaré plots of the 3 maneuvers: supine resting, breathing rhytmically at 0.1 Hz, and standing up.

Methods: Over the course of 5 successive weeks, we carried out daily 5min cardio-respiratory monitoring of 4 female and 4 male young adults on different positions and we also collected data on the circadian rhythm of physical activity and skin temperature. Female's menstrual cycle phase is found from a personal record, urine and blood samples. All subjects sign an informed consent. The protocol was approved by the Ethics Committee of Facultad de Medicina, UNAM, FM/DI/023/2014.

Results and discussion: A typical time-series record of cardio-respiratory response from a young healthy man is shown in Fig. 1. Physiological time series of heart rate and breathing dynamics are less variable in women than in men. It is possible that in women hormones play a larger role in physiological regulation than in men.

Conclusion: Our study of respiratory and heart rate variability exhibit scale-invariant random fluctuations in all the subjects. Reliable non-invasive biomarkers are statistical moments, entropy, Poincaré plots, and spectral parameters. Female hormones should be taken into account in medical prognosis in women.

References:

[1] Toledo-Roy, J., et al., 2019. *AIP Conf Proc* 2150.1: 020014.
[2] Fossion R., et al., 2018. *Physiol Meas* 39.8: 084007.
[3] Rivera A.L., et al., 2016. *Plos one* 11.2: e0148378.
[4] Rivera AL., et al., 2016. *Plos one* 11.11: e0165904.
[5] Estañol B., et al., 2016. *Physiol Rep* 4.24: e13053.
[6] Rivera AL., et al., 2018. in *Quantitative Models*, Springer, p. 111-131.
[7] Fossion R., et al. 2019. *AIP Conf Proc* 2090, 050007.

SC2 –THURSDAY October 29, 2020: 18:15-18:30

A preclinical model for radio-osteoporosis induction

Efrén Hernández Ramírez[1,2,a], Flor Herrera Martínez[3], Janeth Serrano Bello[4], Luis Alberto Medina[2,5,b]

[1]Posgrado en Ciencias Físicas, UNAM, [2]Instituto de Física, UNAM, [3]Departamento de Radioterapia, Instituto Nacional de Cancerología, [4]Laboratorio de Bioingeniería de Tejidos, Facultad de Odontología UNAM, [5]Unidad de Investigación Biomédica en Cáncer, INCan/UNAM.
[a]efrenhr25@gmail.com [b]medina@fisica.unam.mx

Research area of interest: Physics and dosimetry of radiotherapy.
Keywords: radiation induced osteoporosis, animal model, microCT images.

Introduction: Radiation therapy has proven to be an effective treatment option of cancer. Approximately two thirds of patients with malignant neoplasms receive radiotherapy as part of their treatment [1,2]. Bone tissue is one of the most affected by radiation therapy treatments. In postmenopausal women, the risk of a hip and femoral head fracture increases from 65% to 216% after receiving treatment for cervical, anal or rectal cancer [2,3]. To date, there is no preventive or curative treatment for this damage; this situation promotes the need to explore preclinical models in order to assess the radiobiological parameter (α/β) associated with the radiosensitivity of bone tissues.

Methods: The pelvic region of adult (male and female) *Wistar* rats was irradiated with a 6 MV photon beam. Four schemes of two fractions and one scheme of four fractions, all with different fractional doses, were evaluated. microCT images were acquired two and four months after irradiations to evaluate changes in the hydroxyapatite concentration [HA] in the hip and femoral head. After imaging, animals were sacrificed and the femurs were removed to perform histological and scanning electron microscopy studies to evaluate changes in trabecular bone microarchitecture.

Results and discussion: Low [HA] in femoral head (25% lower that the control) was observed in male rats (30 weeks old) after two months post-irradiations. In the hip, a 30% reduction of [HA] was observed after four months.

No significant changes were detected in the bone microarchitecture.

In female rats, no significant differences (experimental vs. control) in [HA] were observed. This result was associated with the age of rats (12 week old) at the time of irradiations; it is known that the repair of radiation damage in bone tissue is more efficient in younger rats than in older rats. Visual inspection in the shape of the microarchitecture shows structural differences in the irradiated group; however, quantitative differences in the parameters of evaluation (trabecular space and trabecular separation) were not detected.

Conclusions: The fractionation schemes of irradiation implemented in this work results in bone damage that could promote radio-osteoporosis

Work is in progress with different image analysis techniques to quantify the damage in the microarchitecture.

References:
[1] Willey, J. (2008). Radiation-induced osteoporosis: Bone quantity, architecture, and increased resorption following exposure to ionizing radiation.
[2] Chandra, A., Lan, S., Zhu, J., Lin, T., Zhang, X., Siclari, V. A., \& Qin, L. (2013). PTH prevents the adverse effects of focal radiation on bone architecture in young rats. Bone, 55(2), 449-457.
[3] Podgorsak, E. B. (2003). Review of radiation oncology physics: a handbook for teachers and students. Vienna, Austria: IAE Agency.

SC3 –THURSDAY October 29, 2020: 18:30-18:45

Sleep staging with a hyperdimensional specialized dense network

Leonardo Hernández-Cano[1], Alejandro Hernández-Cano[1], and Ana Leonor Rivera [2]
[1]*Facultad de Ciencias, UNAM*
[2]*Instituto de Ciencias Nucleares, UNAM*
leonardohernandezcano@ciencias.unam.mx, ale.hdz333@ciencias.unam.mx, ana.rivera@nucleares.unam.mx,

Research area of interest: Physiological measures and mathematical methods.

Keywords: Sleep staging, hyperdimensional-computing, convolutional neural networks, classification

Introduction: The scoring of sleep into various stages is used to diagnose sleep related disorders. It is generally done following R&K or AASM rules using a polysomnographic (PSG) recording which usually includes electroencephalogram (EEG), electrooculogram (EOG), electromyogram (EMG) and electrocardiogram (ECG) signals [6]. Advances on computer hardware and machine-learning have allowed the research community to introduce new scoring methods and challenge limitations of multisignal recordings, with attention shifting towards using few or a single channel and techniques, such as Support Vector Machines and Random Forests [6, 1, 3, 7].

We focus on two brain-inspired state-of-the-art machine-learning techniques with available specialized hardware proposed by the AI community: hyperdimensional-computing (HD) and convolutional artificial neural networks (CNNs). HD is a computing model based on projecting data to sparse high-dimensional spaces that has been applied to EEG-based gesture recognition [5]. Dense Convolutional Networks are a novel approach to CNNs that takle the vanishing-gradient problem using a sequence of *denseblocks*: sequences of convolutional layers which connect each layer to every other layer in a feed-forward fashion [2].

We embrace these technological advances and introduce *Hyperdimensional Specialized Dense Networks.*

Methods: We propose a novel branching architecture that uses *denseblocks* as structural blocks with the motivation of allowing separate branches to learn specialized representations of the input data, which are then used as an encoder for a HD-model. We used `numpy` and `tensorflow` with Python for the implementation. We present an extensible open-source HD framework along with all of our source code. To challenge the curse of dimensionality we train on very limited data from a balanced dataset [4], which complied with ethical standards.

Results: The effectiveness of the proposed learning process is shown by attaining results comparable to state-of-the-art CNNs with a fraction of the data (99.05% of the best reported performance of [7], and less than 4.6% of the data in [8] and 88% of their best reported performance).

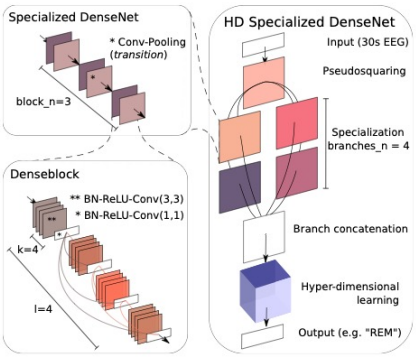

Figure 1: A Hyperdimensional Specialized Dense Network

Conclusions: We present state-of-the art-results on sleep staging, introduce a flexible architecture based on two novel machine-learning techniques and present an open source hyperdimensional-computing framework.

References

[1] Peyman Ghasemzadeh et al. "Sleep stages classification from EEG signal based on Stockwell transform." In: *IET Signal Processing* (2019).
[2] Gao Huang et al. "Densely Connected Convolutional Networks." In: *2017 IEEE Conference on Computer Vision and Pattern Recognition (CVPR)* (2017).
[3] Dihong Jiang et al. "Robust sleep stage classification with single-channel EEG signals using multimodal decomposition and HMM-based refinement." In: *Expert Systems With Applications* (2019).
[4] Sirvan Khalighi et al. "ISRUC-Sleep: A comprehensive public dataset for sleep researchers." In: *Computer Methods and Programs in Biomedicine* (2016).
[5] Abbas Rahimi et al. "A Robust and Energy-Efficient Classifier Using Brain-Inspired Hyperdimensional Computing." In: *International Symposium on Low Power Electronics & Design* (2016), p. 64.
[6] Md Mosheyur Rahman et al. "Sleep stage classification using single-channel EOG." In: *Computers in Biology and Medicine* (2018).
[7] Orestis Tsinalis et al. "Automatic Sleep Stage Scoring with Single-Channel EEG Using Convolutional Neural Networks." In: *Annals of Biomedical Engineering* (2016).
[8] Cui Zhihong et al. "Automatic Sleep Stage Classification Based on Convolutional Neural Network and Fine-Grained Segments." In: *Complexity* (2018).

Abstracts: Poster Contributions

Relative efficiency of TLD-100 glow peaks induced by low photon energy beams

E Arzaga-Barajas[1, a] and G Massillon-JL[1, b]

[1] *Instituto de Física, Universidad Nacional Autónoma de México, 04510 Coyoacan Mexico City, Mexico*

[a] arzaga@ciencias.unam.mx [b] massillon@fisica.unam.mx

Research area of interest:
Physics and dosimetry of medical images (ionizing radiation)

Keywords: low-energy X-rays, TLD-100, relative efficiency, glow curve deconvolution, dose from diagnostic.

Introduction:
LiF:Mg,Ti (known commercially as TLD-100) is considered as a "gold standard" dosimeter in multiple fields of dosimetry, including diagnosis radiology and brachytherapy. Because of this, it is relevant to understand the basic phenomena that occur during the interaction of low-energy X-rays with such a material and the subsequent thermoluminescent (TL) process leading to the light emission from the heated irradiated crystal. This can be done through a systematic analysis of the glow curves (see figure 1) obtained from the LiF:Mg,Ti after exposure to several radiation beams commonly used in clinical dosimetry.

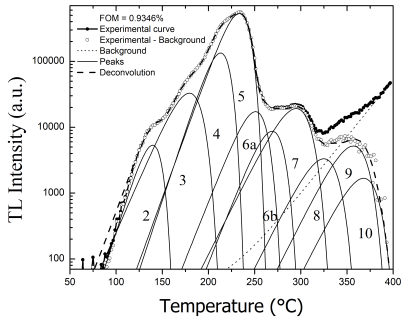

Figure 1 Deconvoluted TLD-100 glow curve. Graph is displayed in semi-log in order to show the high temperature (HT) peaks.

Methods
TLD-100 were exposed to 10 X-ray beams between 20 kV and 300 kV, whose effective energies vary from 15 keV to 270 keV; ^{137}Cs and ^{60}Co gamma [1]. The dosimeters were irradiated in different phantom materials, having 4 dosimeters irradiated individually on a beam-phantom combination at dose values between 50 mGy and 150 mGy where the TL response is linear [2]. The experimental glow curves were deconvoluted into individual glow peaks by using an algorithm developed in MATLAB considering the deconvolution parameters established before [2]. The algorithm is based on the first-order kinetics according to the Podgorsak approximation [3]. The glow peak areas were thus obtained. The relative efficiency (RE) of the peaks was compared as a function of effective energy for each phantom material.

Results and discussion
Agreement is observed in the RE behavior between the "dosimetric" peak (peak 5) and the total TL signal response reported previously [1]. RE of the HT peaks (peaks 6a to 10) are higher compared to the RE of low temperature (LT) peaks (peaks 3 to 5). The influence of phantom material on the RE magnitude is also observed: RE for the irradiation in air is lower compared to that obtained for the other phantom materials. This can be seen as a consequence of the backscatter effect presented in the materials with higher effective atomic number compared to air.

Conclusions
With the information collected in this work, it is clear that the components of the glow curve (and, therefore, the glow curve shape as a whole) is affected by the effective energy of the X-ray beams and the phantom materials.

Acknowledgments
This project is partially supported by Royal Society- Newton Advanced Fellowship grant NA150212 and PAPIIT- UNAM grant IN115117

References
[1] Massillon-JL G., Cabrera-Santiago A., Minniti R., O'Brien M. and Soares C. G. 2014 Influence of phantom materials on the energy dependence of LiF:Mg,Ti thermoluminescent dosimeters exposed to 20–300 kV narrow x-ray spectra, ^{137}Cs and ^{60}Co photons. *Phys. Med. and Biol.* **59** 4149–4166.
[2] Massillon-JL G., Gamboa-deBuen I., and Brandan M.E. 2006 Onset of supralinear response in TLD-100 exposed to ^{60}Co gamma rays, *J. Phys. D: Appl. Phys.* **39** 262-268.
[3] E.B. Podgorsak, P.R. Moran and J.R. Cameron, Proc. (1971) 3rd Int. Conf. on Luminescence Dosimetry, Riso Report 249 p. 1. (AEC, Rise, Denmark).

Assessment of ^{99m}Tc-Octreotide through a hybrid quantification method

Gerardo J. Ramírez Nava[1,2,a], Clara L. Santos Cuevas[2],
Isaac Chairez-Oria[1], Eurídice Rioja-Guerrero[3], Eleazar Ignacio-Alvarez[3]
[1] *UPIBI-Instituto Politécnico Nacional,* [2] *Instituto Nacional de Investigaciones Nucleares,*
[3] *Instituto Nacional de Ciencias Médicas y Nutrición Salvador Zubirán*
[a] *gramirezn1700@alumno.ipn.mx*

Research area of interest: Physics and dosimetry of the images of medical diagnosis with ionizing radiation.

Keywords: Nuclear imaging, quantitative SPECT, SPECT/CT, conjugate-view.

Introduction: Conjugate-view method is the most commonly 2D imaging technique employed for radiopharmaceuticals assessment [1]. Advances in medical technology and the development of sophisticated imaging equipment, such as the Single-photon emission computed tomography/Computed tomography (SPECT/CT), has led to the appearance of more accurate techniques based on 3D images. In recent years, the hybrid (2D/3D) quantification methods have been proposed as an interesting alternative to obtain biokinetic and dosimetric data of radiopharmaceuticals [1,2].

Methods: In this study, we assessed the biodistribution and dosimetry of ^{99m}Tc-Octreotide through a hybrid quantification method. For this purpose, anterior and posterior whole-body planar images (at 0.5, 2, 6 and 24 h, Fig.1A), and SPECT/CT images (2.5 h, Fig.1B) were acquired after ^{99m}Tc-Octreotide administration (37 MBq) in 2 patients. All images were corrected for attenuation, scattering, partial volume effect and radioactive decay. 2D and SPECT/CT images were quantified with the conjugate-view method and the 3D method, respectively [1,2].

Correction factors (CF_H) between imaging modalities were calculated to scale the activity obtained from planar imaging, according to equation 1.

$$CF_H = \frac{A_{\ organ\ of\ interest\ in\ SPECT}}{A_{\ organ\ of\ interest\ in\ planar}} \qquad (1)$$

The CF_H were applied in the quantifications of the 2D method (A_P) to obtain the volumetric activity quantification (A_V), according to equation 2.

$$A_V = CF_H A_P \qquad (2)$$

The fraction of the injected activity of each organ were fitted to three-exponential models and the absorbed doses were obtained using OLINDA/EXM.

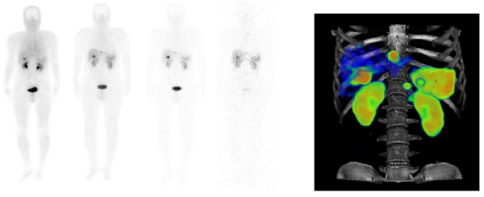

A B

Fig. 1 A) 2D images at 0.5, 2, 6 and 24 h B) SPECT/CT at 2.5 h

Results and discussion: In the first patient, the 2D method underestimated the activity in liver, spleen and the tumoral lesion, while kidneys activity was overestimated. In the second patient, the 2D method underestimated the activity in liver and two tumoral lesions. The activity in the spleen and kidneys was overestimated.
Hybrid dosimetric calculations obtained in this research were more accurate than those assessed with the traditional 2D conjugate-view method.

Conclusions: The quantification processes based on 2D images and conjugate-view method tend to overestimate or underestimate the activity in regions and organs of interest, leading to inaccuracies in dosimetric calculations. Following the hybrid approach, these inaccuracies were reduced.

References:
[1] Siegel J a, Thomas SR, Stubbs JB, Stabin MG, Hays MT, Koral KF, et al. MIRD pamphlet no. 16: Techniques for quantitative radiopharmaceutical biodistribution data acquisition and analysis for use in human radiation dose estimates. J Nucl Med 1999;40:37S-61S.
[2] Bailey DL, Willowson KP. Quantitative SPECT / CT : SPECT joins PET as a quantitative imaging modality 2014;41. doi:10.1007/s00259-013-2542-4.

Scatter and attenuation corrections for a PEM system: A thesis protocol

Jaime Morón Fernández[1,2,a] , Hector Alva-Sánchez[2,b], Arnulfo Martínez-Dávalos[2,c], Tirso Murrieta-Rodríguez[2,d], Mercedes Rodríguez-Villafuerte[2,e]

[1]*Posgrado en Ciencias Físicas, UNAM,* [2]*Instituto de Física, UNAM, Cd. Mx., México.*

[a] *jmoron@estudiantes.fisica.unam.mx,* [b]*halva@fisica.unam.mx,* [c]*tmurrieta@fisica.unam.mx,* [d]*arnulfo@fisica.unam.mx,* [e]*mercedes@fisica.unam.mx*

Research area of interest: Physics and dosimetry of medical images.

Keywords: PEM; Scatter correction; Attenuation correction; Positron Emission Mammography; Monte Carlo.

Introduction: Positron Emission Mammography (PEM) is a nuclear medicine imaging modality used as a complementary technique for the diagnosis and staging of breast cancer. Imaging techniques that use positron emitting isotopes are known for their potential to quantify biologic processes. The latter can only be achieved if appropriate corrections are applied pre- or post-image reconstruction to account for deleterious physical mechanisms such as absorption and scattering of the annihilation photons in the breast [1]. Scatter, which arises from the detection of coincidence events where at least one photon has undergone Compton scattering, results in a loss of contrast in reconstructed PEM images [2]. Absorption, on the other hand, produces a loss in image intensity values thus, activity concentrations, due to photon interactions.

This thesis project has two main objectives: a) To study the effects of photon attenuation and scatter in PEM and b) to establish a methodology to correct for these physical effects. These corrections will allow to reduce the number of events produced by photon scattering and to compensate the loss of events produced by attenuation in the reconstructed PEM images.

Methods: Monte Carlo simulations of photon interactions with matter will be performed using the public domain code Geant4 Application for Tomographic Emission (GATE) [3]. The simulations will consider two breast geometries: a) simple geometrical bodies and b) realistic voxel phantoms obtained from computed tomography (CT) or magnetic resonance (MRI) data from real patients. Several sizes and breast compositions will be considered. The detector system will also be simulated according to technical characteristics of a PEM prototype being developed by the Biomedical Imaging Laboratory group of the Institute of Physics, UNAM. The Monte Carlo results using geometrical phantoms will be validated with experimental data using the IFUNAM´s PEM prototype.

Corrections for photon scatter and attenuation effects will be investigated and implemented during image reconstruction using list-mode iterative methods. The importance of performing these corrections during reconstruction relies in the fact that the acquired PEM data are typically characterized by having low signal-to-noise ratios; iterative reconstruction methods are ideal to handle noise while preserving good image quality. Simple analytical methods will also be implemented for comparison purposes.

In this work, the thesis protocol will be presented with partial results from the Monte Carlo simulations using geometric phantoms. Several sizes (breast thicknesses between 8 – 12 cm) and breast compositions (common ranges between 70% fat – 30% glandular tissues and 50% fat – 50% gland [4]) will be considered.

References:

[1] Ferreira CS, *et al.*, IEEE NSS/MIC Conf Rec (2013) 1-4.
[2] Martins L, *et al.*, Procedia Tech 5 (2012) 903–911.
[3] Jan S., *et al.*, 2004, Phys Med Biol 49 (2004) 4543-61.
[4] Nelson TR, *et al.*, 2008, Med Phys 35-3 (2008) 1078-86.

Acknowledgments:
JMF acknowledges funding to PAEP-UNAM and a scholarship from Conacyt.

M3D: Mammography phantom to assess mean glandular dose using thermoluminescent dosimetry

Eduardo López-Pineda[1,a], Jesús Emmanuel Morales-Nolasco[2,b], Miguel Angel Nava-Cabrera[2,c] and María-Ester Brandan[1,d]
[1]Instituto de Física, UNAM, [2]Facutad de Ciencias, UNAM
[a]edlope@fisica.unam.mx, [b]emanuelmoralesnolasco@gmail.com, [c]A40893@hotmail.com, [d]brandan@fisica.unam.mx

Research area of interest:
B. Physics and dosimetry of the images of medical diagnosis with ionizing radiation

Keywords: Mammography, Dosis, Phantom

Introduction: Mammography requires quality control tests to ensure the best results for the patient, and one of these tests is the estimation of absorbed dose.

We have developed a phantom (called M3D) to determine Mean Glandular Dose (MGD) using thermoluminescent (TL) dosimeters and aluminum foils [1]. The original version of M3D was designed for one breast thickness and the conventional anode/ filter combinations. This report presents updates that enable the use of M3D to evaluate different compressed breast thicknesses and a variety of anode/filter combinations. We have also evaluated the possible addition of TLD-300 as indicator of beam quality [2].

Methods: M3D is composed by 19 cm diameter semicircular PMMA plates of different thicknesses. The whole system is divided in two phantoms: A determines the automatic radiological technique and B determines entrance air kerma and half value layer (HVL). Phantom A varies its thickness from 2 to 7 cm, B is 4.5 cm thick and contains cavities to carry TL dosimeters under a 0.5 cm plate. A group of 3 TLD-100 dosimeters evaluate kerma. Two options were tested to determine HVL: Al foil and 12 TLD-100 (original design) and 3 TLD-300. Calibrations were made using a Senographe 2000D, a Selenia Dimensions and a YXLON Y.SMART 160E/1.5 units, with Mo/Mo, Mo/Rh, Rh/Rh, W/Rh, W/Ag and W/Al anode/ filter combinations and 24 - 40 kV. TL dosimeters were annealed at 400°C for 1 hour (TLD-100/TLD-300), followed by rapid cooling to room temperature and a second annealing at 100°C for 2 hours (TLD-100). Dosimeters were read in a Harshaw 3500, under N_2 flux from room temperature to 320°C (TLD-100) and 400°C (TLD-300), at 8°C/s rate. Al least 24 hours passed between each process (annealing, irradiation and reading). Comparisons were made with an ionization chamber (IC) in 5 systems.

Results and discussion: The combination of TLD-100 and Al foils enabled to determine MGD with 11% uncertainty after only 4 irradiations (~5 min). The results were comparable with those with an IC (obtained in ~30 min), and we have determined that both methods were equivalent ($p>0.05$). Calibration of TLD-300 showed a poor performance (no difference in response), probably due to similar beam qualities and intense scattered radiation inside the phantom. Currently, the TLD-300 calibration is being extended to get better performance.

Conclusions: The M3D phantom has proven to be a flexible option to evaluate MGD in cases when IC are not available, or if availability of beam time is a limiting factor.

References:

[1] López-Pineda, E., C. Ruiz-Trejo, and M. E. Brandan. "A mammographic phantom to measure mean glandular dose by thermoluminescent dosimetry." Radiation Measurements 71 (2014): 297-299.

[2] Muñoz, I. D., et al. "Evolution of the CaF_2: Tm (TLD-300) glow curve as an indicator of beam quality for low-energy photon beams." Physics in Medicine & Biology 60.6 (2015): 2135.

Development of the CMC for air kerma for X-Ray reference beams in the RQR-M qualities of the IEC 61267:2005 in the SSDL-ININ

Mario Raymundo Cabrera Vertti, María de los Ángeles Montes Rodríguez, José Trinidad Álvarez-Romero[1]

[1]*SSDL, ININ Carretera México-Toluca s/n, C.P. 52750, La Marquesa, Méx., Mexico*

Research area of interest: Physics and Dosimetry of Medical Images (Ionizing Radiation)

Keywords: CMC, mammography, Mo/Mo, PPV, HVL, IEC 61267, beam quality

Introduction: In the population of Mexican women, as of 2006, the breast cancer is the main cause of cancer death [1]; in fact, the Mexican standard NOM 041-SSA2-2011 establishes strategies and protocols for the prevention, diagnosis, treatment, control and surveillance of the breast cancer [2]; and the NOM-229-SSA1-2002 is more specific in the area of diagnosis and establishes the technical requirements for the operation, attainment and quality of X-ray facilities, per section 13 for mammography equipment [3].

Furthermore, in the Mexican Republic there are 642 mammography equipment that must be calibrated radiologically [1]; therefore the SSDL-ININ, as Designated Institute by CENAM, has to develop the Calibration and Measurement Capabilities (CMC) for air kerma to mammographs, for several beam qualities.

Methods: The characterization of the reference X-ray beams for the RQR-M beam qualities is carried out according to IEC 61267:2005 [4]:

a) For the determination of the Practical Peak Voltage (PPV) by invasive method with a Radcal Dynalyzer III U voltage divider, calibrated at NIST, and non-invasive method using a PPV meter PTW, Diavolt Universal, calibrated at the PTB (Germany).

b) To determine the first half-value layer (HVL_1); and additionally, the second half-value layer (HVL_2). The HVL values were determined by least squares fitting with a 4th degree polynomial from the attenuation measurements of the ionization currents, obtained with the ionization chambers Radcal 0X6-6M, s/n 30502 and Keithley 96035, s/n 63373.

The validation of these results was done by Monte Carlo simulations (MC) using the PENELOPE 2008 code.

Results and discussion:

IEC 61267 qualities	Nominal[4] PPV /kV	PPV SSDL-ININ /kV		$\bar{E}$ calculated by MC /keV
		Non invasive	Invasive	
RQR-M 1	25	24.9±0.7	24.81±0.60	16.13±2.72
RQR-M 2	28	27.7±0.7	27.84±1.74	16.71±2.93
RQR-M 3	30	29.7±0.7	29.80±0.98	17.04±3.15
RQR-M 4	35	34.5±0.7	34.50±1.03	17.73±3.77

Table 1. Mean energy ($\bar{E}$) and PPV for the SSDL-ININ reference beams.

IEC 61267 qualities	Nominal[4] HVL_1 /mm	HVL_1 LSCD-ININ /mm	
		Experimental	Monte Carlo
RQR-M 1	0.28 ± 0.02	0.29 ± 0.02	0.26
RQR-M 2	0.31 ± 0.02	0.32 ± 0.01	0.29
RQR-M 3	0.33 ± 0.02	0.34 ± 0.01	0.30
RQR-M 4	0.36 ± 0.02	0.37 ± 0.02	0.33

Table 2. HVL values of aluminum for the SSDL-ININ reference beams.

As observed in both tables, the values obtained meet the specifications of IEC 61267: 2005 [4].

Conclusions: The SSDL-ININ realized the reference beams (Mo/Mo) for the IEC 61267 RQR-M qualities in order to provide calibration services for ionization chambers in terms of air kerma.

References:

[1] ME-ININ, "Reporte Técnico ININ.GANS-2019-01: Desarrollo de las CMCs de Ka para haces de referencia de RX en las calidades de mamografía RQR-M de la norma IEC 61267:2005 en las instalaciones del LSCD-ININ", Agosto 2019.
[2] Secretaría de Salud, "NOM-041-SSA2-2011", DOF, 2011-06-09
[3] Secretaría de Salud, "NOM-229-SSA1-2002", DOF, 2006-09-15.
[4] IEC, "IEC 61267, Medical diagnostic X-ray equipment – Radiation conditions for use in the determination of characteristics", 2nd edition (2005)

Determination of image features in cone beam computerized tomography used in lung stereotactic radiotherapy: a phantom study

David Valdes-Corona[1,a], Mariana Hernández-Bojórquez[2,b], Alberto E. Hardy-Pérez[1,c], Eleni Mitsoura[1,d]

[1]*Universidad Autónoma del Estado de México,* [2]*Centro Médico ABC*

[a]corona@ciencias.unam.mx [b]mariana.hernandez.b@gmail.com [c]aehardyp@uaemex.mx

[d]meleni@uaemex.mx

Research area of interest: B: Physics and dosimetry of the images medical diagnosis with ionizing radiation.

Keywords: Image features, Stereotactic Body Radiotherapy, lung cancer, cone beam computed tomography.

Introduction: The extraction of features from medical images can provide information about the induced changes in tumor tissue when patients undergo radiotherapy treatments [1]. One of the imaging modalities for everyday use to assure accurate positioning in patients with lung cancer who undergo stereotactic body radiotherapy (SBRT) is cone beam computed tomography (CBCT). In this study we propose a method to extract potentially useful quantitative features from CBCT images in a thorax phantom, which will be used to analyze the changes that may appear during treatment in tumor tissue after SBRT.

Methods: After implementation of a CBCT quality control protocol [2] to the On-Board Imager System (OBI) of a Novalis Tx medical linear accelerator (Varian Medical Systems), at the American British Cowdray Medical Center in Mexico City, CBCT images of a thorax phantom with simulated tumor tissue were acquired. Using an open access software, features such as intensity histograms, morphology, local intensity and texture were extracted.

Results and discussion: From the CBCT images analyzed, a total of 130 features were extracted. Methodology was selected according to semi-automatic segmentation procedures to reduce user dependent results, starting with threshold Hounsfield unit values in a window range for lung tissue. Shape (voxel volume, sphericity, surface area, etc.) and first order (uniformity, median, energy, etc.) features were mainly analized. Additionally, features that represent a temporary behavior of the tumor during an SBRT treatment such as profiles and histograms, are reported. In the same way, the degree of reproducibility and repeatability of the extracted features and the possible viability of CBCT images for possible radiomics studies in patients with lung cancer and undergoing radiosurgery are analyzed.

Conclusions: This work describes a methodology for the extraction of reproducible and repeatable features in CBCT images that provide information on lung tumors behavior during SBRT treatments and that can potentially be used for making treatment decisions related to adaptive radiotherapy. However, the prognostic value of reported features should be investigated in subsequent studies.

References:

[1] Zwanenburg, A., Leger, S., Vallières, M., and Löck, S. (2016). Image biomarker standardisation initiative. arXiv:1612.07003v10

[2] Quality control in cone-beam computed tomography (CBCT), EFOMP-ESTRO-IAEA protocol (2017). https://www.efomp.org/uploads/2017-06-02-CBCT_EFOMP-ESTRO-IAEA_protocol.pdf

Does Cone Beam Computed Tomography image have the potential to monitor response to lung stereotactic body radiotherapy? Initial analysis

Alejandro Zepeda-Barrios[1,a], Mariana Hernández-Bojórquez[2,b], Eleni Mitsoura[1,c]
[1]*Universidad Autónoma del Estado de México,* [2]*Centro Médico ABC*
[a]alejandro.zepeda@ciencias.unam.mx [b]mariana.hernandez.b@gmail.com [c]meleni@uaemex.mx

Research area of interest: B: Physics and dosimetry of the images medical diagnosis with ionizing radiation.
Keywords: CBCT, feature analysis, non-small cell lung cancer, 3D slicer.

Introduction: Non-small cell lung cancer (NSCLC) is the most common type of lung cancer, with 85% of all cases. It is characterized by a poor prognosis and a low survival rate (1). Several studies have performed quantitative analysis of different features after a treatment of body stereotactic radiotherapy (SBRT) in lung cancer, using computed tomography studies (2), more specifically, with the cone beam computed tomography (CBCT) technique which is used to assess the patient positioning before every treatment session. These studies have suggested that from these features it is possible to study the evolution of the patient's treatment outcome. In this retrospective work we propose several CBCT features evaluated in actual patient lung tumor tissue.

Methods: Segmentation of the region of interest was performed to analyze the different features that can be extracted using the free software 3D Slicer 4.10.2. Once the features to be used have been defined, the images obtained by CBCT related to lung tumors of actual patients who underwent lung SBRT were analyzed at the beginning, middle and end of the treatment. Intensity features were of particular interest in this work.

Results and discussion: In thorax CBCT images, the tumor volume intensity features that showed a pattern of change, were chosen to assess the influence of the treatment. First, the technique was applied to a thorax phantom and then to a series of images corresponding to actual clinical cases of lung cancer SBRT, though the CBCT images acquired prior to every SBRT session. Energy, mean absolute deviation and total energy are examples of the intensity features that reflect in some degree the influence of the treatment.

Conclusions: In this retrospective work we propose several CBCT imaging features that reflect in some degree the influence of lung SBRT treatment in tumor tissue.

References:

[1] Bernchou U., Hansen O., Schytte T., Bertelsen A., Hope A., Moseley D., Brink C. (2015). "Prediction of lung density changes after radiotherapy by cone beam computed tomography response markers and pre-treatment factors for non-small cell lung cancer patients". Radiotherapy and Oncology, 117 (1), pp. 17-22.

[2] Moran A., Daly M., Yip S., Yamamoto T. (2017). "Radiomics-Based Assessment of Radiation-Induced Lung Injury after Stereotactic Body Radiotherapy". Clinical Lung Cancer. 18 (6), pp. 425-431.

Depth of Interaction in Monolithic Scintillators for Positron Emission Tomography

Víctor D. Díaz-Martínez[1,a], Natalia I. Ambrosio-Macías[1,b], Tirso Murrieta-Rodríguez[2,c], Arnulfo Martínez-Dávalos[2,d], Mercedes Rodríguez-Villafuerte[2,e] and Héctor Alva-Sánchez[2,f],

[1] *Facultad de Ciencias, UNAM, MEXICO,* [2] *Instituto de Física, UNAM, MEXICO.*

[a]*victordiaz@ciencias.unam.mx,* [b]*natambros@ciencias.unam.mx,* [c]*tmurrieta@fisica.unam.mx,* [d]*arnulfo@fisica.unam.mx,* [e]*mercedes@fisica.unam.mx,* [f]*halva@fisica.unam.mx*

Research area of interest: B. Physics and dosimetry of the images of medical diagnosis with ionizing radiation.

Keywords: PET, scintillation crystal, spatial resolution, parallax error, Depth of Interaction (DOI).

Introduction: Positron emission tomography (PET) scanners use scintillation crystals coupled to position-sensitive photomultiplier tubes (PMTs) or silicon photomultipliers (SiPMs) for the detection of 511 keV annihilation photons. Parallax error due to lines of response assigned incorrectly for photon interactions inside thick crystals is one of the limiting factors for spatial resolution. In order to correct for this problem, it is necessary to determine the photon depth of interaction (DOI) in the scintillation crystal.

Previous works have studied DOI in lutetium yttrium oxyorthosilicate (LYSO) monolithic scintillation crystals, coupled to a 12×12 array SiPM by means of the scintillation light distribution in the photodetector [1]. In this work DOI was determined in two different monolithic scintillator materials coupled to an 8×8 SiPM array.

Methods: DOI was determined by analyzing the light distribution inside two monolithic scintillator materials: i) a 60×60×30 mm^3 plastic scintillator (Eljen Technology EJ-232) and ii) a 57.4×57.4×10 mm^3 monolithic scintillator LYSO crystal. These were coupled to an 8×8 silicon photomultiplier array (SensL ArrayC-60035-64P). The position interaction identification was performed with an 8 column + 8 row symmetric charge division read-out circuit and a center-of-mass algorithm [2]. Collimated gamma-ray sources of ^{22}Na (511 and 1275 keV) and ^{137}Cs (662 keV) were used to perform the measurements. *N/I* ratios were calculated to estimate the depth of interaction, where *N* represents the sum of the light distribution and *I* is the maximum intensity registered long the sums of rows or columns [1]. In a calibration stage, measurements of a collimated beam at different *z* positions of the scintillator and an analysis considering the different regions in the *x-y* plane (central, edges and corners) were performed.

Due to its intrinsic radioactivity (~300 cps cm^{-3}), the LYSO scintillation crystal required a more complex setup. Two detectors with a LYSO crystal were used in coincidence mode for the positron emitter Na-22 source: one detector was used to perform the DOI measurements and the other for coincidence triggering, thus eliminating most of the background counts. The calibration allowed assigning the complete (*x, y, z*) coordinates to each detected event.

Results and discussion: Figure 1 shows an example of a histogram of the light distribution in the plastic scintillator registered by the row (Ri) and column (Ci) elements of the SiPM array for a central region of the photodetector for (a) deep and (b) shallow events. The differences in the distributions enabled DOI calibration.

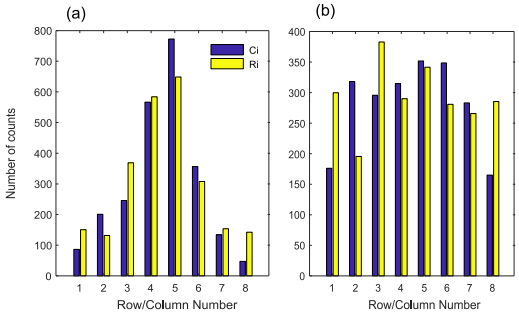

Fig. 1. Projected light distribution in the plastic scintillator for events (a) deep in the crystal and (b) closer to the crystal surface.

Conclusions: Our results are similar to the ones reported by González A.J. *et al.* [1] for the plastic scintillator obtaining a z-resolution of approximately 5 mm despite of working with an 8×8 SiPM array. DOI calibration in the 10 mm thick LYSO crystal is more challenging and preliminary results will be shown.

References

[1] González, A.J., *et al*., "A PET Design Based on SiPM and Monolithic LYSO Crystals: Performance Evaluation". *IEEE Trans. Nucl. Sci.* 63 (2016) 2471.

[2] Calva-Coraza E. *et al*., "Optimization of a large-area detector-block based on SiPM and pixelated LYSO crystal arrays", *Phys. Medica* 42 (2017) 19.

Subsurface laser engraving to pixelate scintillation crystals used in PET/PEM detectors

Hernández-Cordero Lourdes Lizet[1, a], Vásquez-Arzola Alejandro[1, b], Murrieta-Rodríguez Tirso[1, c], Alva-Sánchez Héctor[1, d]

[1]*Instituto de Física, Universidad Nacional Autónoma de México*

[a]lulu.hc@ciencias.unam.mx, , [b]alejandro@fisica.unam.mx, [c]tmurrieta@fisica.unam.mx, [d]halva@fisica.unam.mx

Research area of interest:

B. Physics and dosimetry of the images of medical diagnosis with ionizing radiation.

Keywords: subsurface laser engraving, scintillation crystal, LYSO, Depth of interaction, phoswitch detector.

Introduction: Most modern positron emission tomography (PET) scanners and dedicated imaging system, like positron emission mammography (PEM) scanners, use pixelated scintillation crystal arrays in their detectors to determine the interaction position of the 511 keV annihilation photons. The detector spatial resolution is directly related to the crystal pixel size. In addition, the reconstructed image quality is affected by a parallax error introduced by the incorrect line of response assignment when the photon annihilation interaction occurs inside thick crystals, a problem that can be reduced if the depth of interaction (DOI) is known [1]. One way to obtain such information is using a stack of different scintillator materials as a phoswitch detector [2].

In 2010 Moriya *et al.* [3] proposed the use of the subsurface laser engraving technique to process monolithic crystal blocks as an alternative to pixelate scintillators used in PET scanners. In this method microstructures are formed inside the crystal as a result of focusing an intense pulsed laser beam in a very small region in the bulk material. By producing a pattern of equidistant microstructures the crystal can be pixelated.

In this work we show the results of pixelating a cerium-doped lutetium yttrium oxyorthosilicate (LYSO:Ce) monolithic crystal by SSLE and we propose to it to create two or more pixel patterns along the crystal depth to develop a scintillator with DOI capabilities.

Methods: At the Institute of Physics, UNAM a new laser engraving laboratory has been created to process scintillation crystals and for other laser applications. A Q-switched, diode-pulsed Nd:YAG laser with 180 µJ/pulse, 500 ps and λ=532 nm (Standa STA-01SH-5) and a 3-axis motorized stage system with computer numeric control (CNC) are used to engrave the crystals in 3D.

We have evaluated the microstructure shape and size in LYSO crystals. The optimized engraving parameters were used to process a 1 cm length LYSO cube to produce a square array of 6×6 pixels with 1.67 mm pixel pitch. The pixel quality was evaluated by coupling the cube to an array of silicon photomultipliers detector (SensL ArrayC-60035-64P). The evaluation included the assessment of the crystal maps, in terms of uniformity and geometric distortions, using the crystal intrinsic radioactivity and a Na-22 external sealed source.

Results and discussion: Figure 1(left) shows a photograph of the 1 cm LYSO pixelated cube using the SSLE technique. In figure 1(right) the crystal map of the processed crystal is shown; typical peak-to-valley ratios of 4:1 were measured. During pixilation parameter optimization some interesting phenomena were found, including a birefringence of the crystal depending on the direction of the incident laser beam, results which will also be shown.

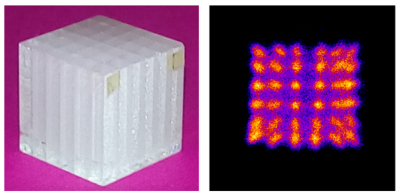

Figure 1. Photograph of a 6×6 pixilated crystal using the SSLE technique (left) and the corresponding crystal map obtained with a SiPM array detector (right).

Conclusions: The SSLE has been correctly implemented to produce 3D patterns LYSO scintillation crystal pixilation for PET/PEM detectors. A research project to extend the method to develop a phoswitch detector using SSLE is currently underway.

References:

[1] Cherry S., Sorenson J., Phelps M. 2012. "Physics in Nuclear Medicine". 4th Ed. Elsevier Inc., pp. 316-318.
[2] Berg E. & Cherry S. 2018. "Innovation in instrumentation for positron emission tomography", Seminars in Nuclear Medicine **48**(4):311-331.
[3] Moriya T., et al., 2010. "Development of PET detectors using monolithic scintillation crystals processed with Sub-Surface Laser Engraving technique", IEEE Transactions on Nuclear Science **57**(5):2455-2459.

Comparison between NEMA NU-2 and the new report of AAPM TG 126 for PET-CT Image Quality.

Eugenio Galicia Larios [1,a], Carlos Alberto Reynoso-Mejía [2,b]

[1] *Department of Physics, School of Sciences, Universidad Nacional Autónoma de México, Ciudad Universitaria, 04320, Mexico City, Mexico.*
[2] *Unidad de Imagen Molecular PET-CT, Instituto Nacional de Neurología y Neurocirugía Manuel Velasco Suarez, La Fama, 14269, Mexico City, Mexico.*
[a] *eugenio98@ciencias.unam.mx,* [b] *betoven@ciencias.unam.mx*

Research area of interest
B: Physics and Dosimetry of Medical Images (Ionizing Radiation)

Keywords
PET-CT, Image quality, NEMA NU-2, Acceptance testing, AAPM.

Introduction
Since the early 1990s, the most widely implemented and cited reference for testing PET-CT systems has been the NEMA Standards Publication NU 2-2007 Standard Performance Measurements of PET. However, the NEMA NU-2 and other standards can be challenging to follow given their requirements for specialized software, equipment, and phantoms [1].
Recently the report of AAPM Task Group 126 PET/CT "Acceptance Testing and Quality Assurance" was published with the purpose to provide a standardized set of acceptance and periodic tests that can be easily implemented in a QA program for various Positron Emission Tomographs and Computed Tomography system platforms from different manufacturers [2].
The TG 126 intent to develop procedures that adhere to the spirit of the NEMA document but do not require the purchase of specialized equipment to perform the experiments (beyond standard, inexpensive, and easily obtainable phantoms and those supplied by the manufacturer) or specific software to analyze the acquired data.
The aim of this work was comparing the new AAPM report TG 126 with the reference NEMA NU-2 Standard Performance for PET image quality.

Methods
The NEMA and ACR phantom were used to assess image quality. 18F was used as a radioactive source (radiopharmaceutical) for the acquisition test. The NEMA and ACR protocols for image quality were carried out follow guidelines. Additional variations in reconstruction algorithms and parameters were varied to assume various realistic clinical scenarios.

Results and discussions
Parameters such as contrast, noise and scatter were evaluated. Different results with different algorithms image reconstruction with the two methods were obtained. With both protocols it is possible to obtain relevant information on the image quality of PET-CT equipment. However, the NEMA phantom provides the possibility of obtaining recovery coefficients which may be of clinical relevance due to the correction of the partial effect of volume.

Conclusions
Our data suggest a difference between both methods for PET-CT image quality, but each one provides useful and important information to perform tests necessary to monitor the image quality acquired by the PET scan.

References
[1] NEMA Standard Publication NU 2-2007, Performance Measurements of PET.
[2] The Report of AAPM, Task Group 126, PET/CT Acceptance Testing and Quality Assurance, October 2019.

Tumor Sphericity as Predictor of Tumor Changes In Patients With HPV-Positive Oropharyngeal Carcinoma

Paulina Galavis[1], PhD, Moses Tam[1], MD, Gene Kim[2], PhD, Elcin Zan[2], MD, Wei Wang,[1] CMD, Ken Hu[1] MD

[1] *Department of Radiation Oncology, NYU Langone Health, New York, NY*
[2] *Department of Radiology, NYU Langone Health, New York, NY*

Paulina.galavis@nyumc.org *(corresponding author)*

Research area of interest

D. Biological physics, physiological measures and mathematical methods

Keywords: Radiomics, treatment assessment, HPV-positive oropharyngeal carcinoma,

Introduction: Tumor volume shrinkage is currently used as a tool to predict treatment response for patients under radiation or chemo-radiation treatments of head and neck cancers [1-3]. However, cut off values for volumetric changes vary widely among published studies. Our work evaluates retrospectively the tumor sphericity as a tool to predict of tumor changes.

Methods: Fifteen patients from an institutional phase II clinical trial were CE-CT (Contrast-Enhanced-CT) simulated prior to starting radiotherapy treatment and at week-four as part of the protocol. A radiation oncologist manually contoured the GTVn (primary nodal disease) on both scans. Based on GTVn volume variation (≥ 40%) patients were eligible/ineligible for dose de-escalation. CE-CT scans and contours were transferred to IBEX [4] for texture-feature calculation. The relative net change of shaped-based texture-features was calculated. Particular attention was given to sphericity (Sp) since it is independent on tumor volume. The sphericity is a measure of the roundness of the shape of the tumor relative to a sphere, with value between 0 and 1, where a value of 1 means a perfect sphere. Comparison between the groups of patients that were eligible/ineligible is presented and its significance level was evaluated using the t-test ($p<0.05$).

Results and discussion: Ten patients met criteria for mid-treatment nodal response and were deescalated, the rest of the patients continued with standard radiotherapy treatment. The mean pre-tx GTV_n volume and Sp across all patients were 16.4cc (SD 11.3) and 0.63 (SD 0.08) respectively. Sphericity comparison between the groups of patients that were eligible/ineligible showed 0.61±0.08 and 0.67±0.08, this difference was statistically significant ($p<0.05$). We observed small sphericity changes (≤ 10% difference) for patients that showed high Sp values (>0.7) before starting radiation treatment.

Conclusions: Evaluation of tumor volume changes has shown to be useful for treatment evaluation; however, there is no definite cut off value. The sphericity showed to be a potential candidate for treatment prognosis of HPV positive oropharyngeal carcinoma. Future work includes evaluating solid vs cystic tumor and their correlation with sphericity for the cases that were not deescalated.

References:

[1] Hu et al. ASTRO Arizona 2016; [2] Hermans R. Staging of laryngeal and hypopharyngeal cancer: value of imaging studies. 2006. [3] Doweck et al. Tumor volume predicts outcome for advance head and neck cancer treated with targeted chemoradiotherapy. [4] Zhang L, et al. IBEX: an open infrastructure software platform to facilitate collaborative work in radiomics. Med Phys 2015.

Designed of a free-air ionization chamber to medium energy X-ray for operation at the SSDL-ININ atmospheric conditions

Daniel De la Cruz-Hernández[1], José Trinidad Álvarez-Romero[2]

[1,2] *PhD student of the ESFM, Instituto Politécnico Nacional,* [2] *SSDL, ININ*

Research area of interest: Physics and Dosimetry of Medical Images (Ionizing Radiation)

Keywords:
Air kerma rate, primary standard, free air chamber (FAC), Charged Particle Equilibrium (CPE), fail of air density correction, Monte Carlo (MC) simulation

Introduction. Due to the air density correction in the operation of secondary standards with no equivalent air walls, there is a difference of 1% to 2.5% in the realization of air kerma rate $\dot{K}_a$ at the atmospheric conditions of the Mexican highlands (3000 meters above sea level) [1]. For this reason, The SSDL-ININ-MEXICO has chosen to design and build the FAC, for medium energy X-ray dosimetry.

Methods. The $\dot{K}_a$ primary standard for X-ray photons is based on parallel-plate FAC. With a volume V, where the rate $\dot{K}_a$ is determined in CPE conditions, by [2]:

$$\dot{K}_a = \frac{I}{\rho_{air} \cdot V} \cdot \frac{W_{air}}{e} \cdot \frac{1}{1 - g_{air}} \cdot \prod_i k_i$$

Where:
$\boldsymbol{I}$, is the ionization current measured on V by the standard.
$\boldsymbol{W_{air}}$ is the mean energy expended by an electron charge e to produce a pair of ions in dry air.
$\boldsymbol{g_{air}}$ is the fraction of energy lost from the initial electron as bremsstrahlung in air.
$\boldsymbol{\rho_{air} V}$ is the mass of the effective volume (V) of the standard.
$\prod_i \boldsymbol{k_i}$ is the product of a set of correction factors that are applied to the ionization currents measured with the standard chamber to ensure compliance with CPE, where these are determinate experimentally or by MC simulation. In fact, to fulfill the CPE condition, one of the main correction factors is the attenuation factor k_{att}; therefore, the attenuation length L_{at} must enough for to realize the CPE, where this L_{at} is obtained by MC simulation.

Results and discussion. Figure 1 shows the deposited energy of 300 keV monoenergetic photons as a function of the distance from the reference plane, simulated with the PENELOPE 2008 code.

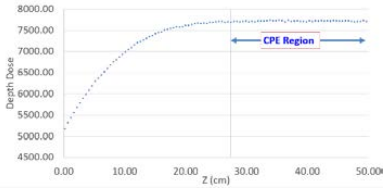

FIGURE 1. Energy deposited from monoenergetic photons of 300 keV as a function of distance from the reference plate

The working region suitable for the operation of an ionization chamber is the CPE region. Therefore, according to the MC simulation, the value of attenuation length L_{at} must be calculated for the point: 44.0 ± 0.5 cm, where the width of the collector electrode is chosen 20 cm, within the CPE region of [34,54] cm.

Conclusions. In this first stage of the design of a FAC, the MC simulation determines that the range to achieve the CPE condition is from 34 cm for a P ≈ 710 hPa, therefore for a collector electrode width of 20 cm, in the operating region it is CPE: 34 to 54 cm.

References

[1] O'Brien M. *et al*. Metrologia 52 (2015) Tech. Suppl. 06015
[2] D. T. Burns and et al. Free-air ionization chambers, Metrologia 46(2), S9-S23 (2009)

On the stability of asymmetry of thermal emission in diabetic foot disease

R. Ortiz-Sosa[1, a], E. I. Fuentes-Oliver,[1, b], C. García-Segundo[1, c],
R. Solalinde-Vargas[2, d] and R. Serrano-Loyola[2, e]

[1]*Instituto de Ciencias Aplicadas y Tecnología, Universidad Nacional Autónoma de México, Circuito Exterior S/N, Ciudad Universitaria, Coyoacán, CDMX, Mexico, 04510.*
[2]*Hospital General de México "Dr. Eduardo Liceaga", Dr. Balmis 148, Doctores, Cuauhtémoc, CDMX, Mexico, 06720.*
[a]r.ortizsosa@gmail.com, [b]edgarfuentes@ciencias.unam.mx, [c]crescencio.garcia@icat.unam.mx, [d]serranoraul48@yahoo.com.mx, [e]rebeca.solv@gmail.com.

Research area of interest: C. Use of non-ionizing radiation in medicine

Keywords: Biomedical Infrared Imaging, Type 2 Diabetes Mellitus, Diabetic Foot Disease, non-destructive testing.

Introduction: Infrared Imaging (IRI) is a non-invasive tool, useful in clinical diagnosis. Because the nature of the images, it is used to analyze metabolic pathologies [1, 2]. We report findings when IRI is applied for type 2 Diabetes Mellitus (DM2) diagnosis. DM2 implies alterations of the metabolic heat emission that are pictured with IRI [3]. These alterations include oxidative stress, degradation of neural and vascular networks, inflammatory processes, among other factors [4,5]. Viability of IRI as aiding tool for DM2 and its evolution to diabetic foot disease (DFD) depend on how well one can establish the truth or certainty degree of the information contained in the IR-images. We present preliminary results, where we discuss noise and fluctuations of information contained in IR-images.

Methods: We analyze IR-images of the lower limbs for a control group and a set of subjects diagnosed with DM2 and possible prognosis to DFD. Image analysis is made over a defined region of interest (ROI), split in: (R1) tibiofibular trunk region; (R2) calf-shin region; and (R3) the region above the ankle. The corresponding dimension of each region is: $n/4$, $n/2$ and $n/4$; being n the total number of rows in the ROI. For each one of these regions we analyze thermal asymmetry between left and right legs using a statistical asymmetry test (AT), as indicated in Fig. 1. We setup the reference natural asymmetry from the AT of the control group. Then we repeat this analysis for patients.

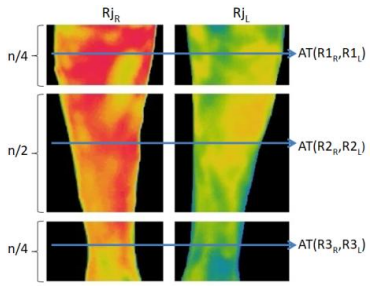

Fig. 1. Statistical asymmetry test (AT) applied to IR-images

Results and discussion: According to the analysis of the temperatures' distribution, significant differences between controls and patients can be distinguished in the three regions. Values of sensitivity and specificity achieved are, respectively: 77.7% and 86.11% for the three regions in the frontal view and 83.3% and 83.3% for the three regions in the posterior view. The AT indicates that the largest record of asymmetry is found in the calf-shin region.

Conclusions: Calf-shin region is expected to exhibit larger thermal asymmetry due to its vascular density. However, in presence of stenosis at R2 or R3, these regions would display a larger drift in thermal asymmetry.

References:

[1] M. Diakides, J.D. Bronzino and D.R. Peterson. (CRC Press 2012, FL-USA).
[2] R. Usamentiaga et al., 2014.Sensors. 12305–12348.
[3] E. I. Fuentes-Oliver, et al., 2019. Biomedical Physics and Engineering Express. 065015-1–065015-113.
[4] J.E. Hall. (Elsevier 2016, PA-USA). 911-924.
[5] L. Walloe, 2016. Temperature. 92–103.

Synthesis and Characterization of Au@SiO_2 Nanoparticles

Gutiérrez-Velásquez, A[1,a] , Melendrez, R[2,b], Santacruz-Gómez, K[3,c]

[1]*Departamento de Ciencias Químico-Biológicas Universidad de Sonora,* [2]*Departamento de Investigación en Física Universidad de Sonora,* [3]*Departamento de Física Universidad de Sonora*

[a] andresgtz96@hotmail.com, [b] rodrigo.melendrez@unison.com, [c]karla.santacruz@unison.com

Research area of interest

C. Use Of Non-Ionizing Radiation In Medicine

Keywords: Surface plasmon resonance, composite nanostructure, metallic nanoparticle.

Introduction: Nanotechnology is an emergent science, which includes the generation of both organic and inorganic materials at nanoscale. The importance of these materials came to light when researchers realized that small alteration in size at nanoscale can influence their physicochemical properties, allowing novel applications in Nanomedicine; such is the case of the plasmonic photothermal therapy (PPTT). The PPTT consist in the use of metallic nanoparticles (MNPs) to induce local heating, in order to damage cancer cells [1]. MNPs such as gold and silver nanomaterials in different shapes are the most frequently used nanomaterials in biomedicine [2], particularly for PPTT.

In the present work, we have synthesized a silica nanosphere embedded with gold (Au@SiO_2) nanoparticles, and their optical properties are reported.

Methods: Hollow nanoparticles of Au@SiO_2 were synthesized using a layer-by-layer method with polystyrene template, a 200 nm sphere was covered with a Polydiallyldimethylammonium chloride (PDDA) layer then was attached a polystyrene 50 nm spheres and Gold seeds finally was covered with a silica shell and the polystyrene templates were removed. The Au@SiO_2 were PEGylated with polyethene glycol (PEG) by standard thiol PEGylation using 5000 M.W. mPEG-SH to a final concentration of 10 mM. The PEGylated Au@SiO_2 were centrifuged at 2000 x g for 10 minutes, sterile filtered, and re-dispersed in PBS. The hydrodynamic size was determined using a dynamic light scattering (DLS) Zetasizer Nano ZS90; size and shape were observed using a TEM. Localized plasmon was obtain from the absorption spectra of the nanoparticles using a Thermo Scientific Multiskan Go UV-VIS spectrophotometer.

Results and discussion: Hydrodynamic size of nanoparticles with nominal size of 149 nm was obtained by DLS (Fig. 1A). TEM micrography shows a homogeneous spherical nanoparticles population (Fig. 1A, inset).

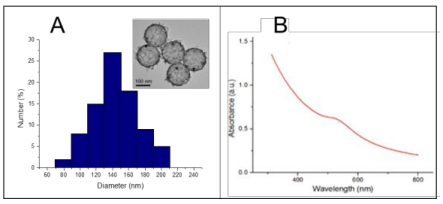

Figure 1. (A) Hydrodynamic size of Au@SiO2 nanospheres obtained by DLS. The inset shows TEM micrograph. (B) UV-Vis absorption spectra.

The presence of a localized plasmon resonance was confirm by absorbance. Figure 1B present the SPR with a maximum of absorbance localized at 550 nm, as well as a good absorption at 750-800 nm as reported by Janetanakit et al. [3]. NIR wavelength absorption indicates that the SPR of our nanostructure corresponds with the first biological window

Conclusions: The synthesized Au@SiO_2 nanostructures exhibit promising characteristics for application in PPTT.

References

[1] Huang, X., Jain, P. K., El-Sayed, I. H., & El-Sayed, M. A. (2008). Plasmonic photothermal therapy (PPTT) using gold nanoparticles. Lasers in Medical Science, 23(3), 217–228.

[2] Dreaden, E. C., Alkilany, A. M., Huang, X., Murphy, C. J., & El-Sayed, M. A. (2012). The golden age: gold nanoparticles for biomedicine. Chemical Society Reviews, 41(7).

[3] Janetanakit, W., Wang, L., Santacruz-Gomez, K. et al. (2017) Gold-Embedded Hollow Silica Nanogolf Balls for Imaging and Photothermal Therapy. ACS Appl. Mater. Interfaces 2017.9:27533-2754

Design and Building of a Phantom for the Recording of Internal Temperature, in an Ultra-Low Magnetic Field MR System

Juan Alberto Martínez Martínez[1a], Jaime Fabian Vázquez de la Rosa[1b], Rodrigo Alfonso Martin Salas[1c] Alfredo Rodríguez Gonzalez[2d] and Sergio Enrique Solís Nájera[1e],

[1] *Facultad de Ciencias, Universidad Nacional Autónoma de México, CD.MX. 04510, México*
[2] *Departamento de Ing. Eléctrica, Universidad Autónoma Metropolitana, CD.MX. 09340, México*
[a] j.alberto_mtz100@ciencias.unam.mx, [b] jfuv@ciencias.unam.mx, [c] rmartin@ciencias.unam.mx, [c] arog@xanum.uam.mx
[d] solisnajera@ciencias.unam.mx

Research area of interest: Use of non-ionizing in medicine

Keywords: Ultra low magnetic field MRI, Phantom, temperature measurement.

Introduction: In Mexico, at the beginning of the year 2000, there was the registry of only sixty Magnetic Resonance Systems, of which the mayor percentage correspond to Low-Field Systems [1]. An important issue with MRI systems is testing the energy deposition, known as Specific Absorption Rate (SAR) and the effects on the rise of the temperature inside MRI probes. It has been demonstrated that this can produce biological effects, or changes in the structure and function in human cells due this effect [2]. We develop a temperature monitoring system, which consisted of an arrangement of five thermistors, to measure changes in temperature in an Ultra-Low Field MRI system.

Methods: We designed and develop a container that was filled with a synthetic tissue model. Five thermistors were calibrated individually to ensure correct measurement of temperature. The phantom was filled with an organic tissue model, and the temperature measurement device was inserted, so we can measurement the possible increases in temperature using a ULMF MRI system, during long periods of time, while image acquisition was performed. All data was recorded and stored into a micro SD card. Spin Echo (SE) and Gradient Echo (GE) sequences were used in a Terranova System. We used the following imaging protocols: T1Bp (T1 relaxation time with a magnetic field produced by a pre-polarizing coil, T1Be (T1 relaxation time with Earth's Magnetic Field produced by a pre-polarizing coil) and T2 (spin-spin relaxation time). For all studies, the duration of the acquisition was at least 909 minutes.

Results and discussion: The designed temperature recording system allow us to obtain the temperature in low-field magnetic resonance imaging studies, different regions of the phantom with different imaging sequences.

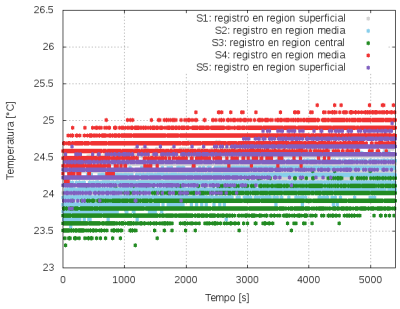

Fig. 1. Changes in temperature vs time inside the phantom.

Conclusions: It was possible to design an automatic temperature recording system for five thermistors with a phantom for the ULMF-MRI system. It was observed that an increment in temperature was mainly observed when gradient-echo studies were performed than in spin echo studies, this because of the power dissipation in the gradient coils. The temperature increased in a range of two degrees Celsius approximately from the beginning of the gradient-echo studies until they finished. The data can give us an idea for the temperature distribution along an organic sample during long periods of time, which can help to propose another alternative method to quantify the energy deposition in tissues and avoid biological effects due to RF energy exposure from the MR coils.

References:

[1] A. Rodriguez, R. Rojas, and F.A. Barrios, 2001. "Year 2000 Status of MRI in Mexico", Journal of Magnetic Resonance Imaging, 13:813-817.
[2] Tobias R. Kiebling et al 2013 New J. Thermorheology of living cells—impact of temperature variations on cell mechanics". Phys.15 045026.

Development of Anatomical Phantoms for an Ultra-Low Field Magnetic Resonance Imaging System

Steve Alejandro Avendaño García[1a], Rodrigo Alfonso Martín Salas[1b], Jaime Fabian Vázquez de la Rosa [1c], and Sergio Enrique Solís Nájera[1d]

[1] *Facultad de Ciencias, Universidad Nacional Autónoma de México, CD.MX. 04510, México*
[a] steveavendano97@ciencias.unam.mx , [b] r.martin@ciencias.unam.mx, [c] jfuv@ciencias.unam.mx
[d] solisnajera@ciencias.unam.mx

Research area of interest: Education and Profession, Use of Non-Ionizing radiation in Medicine.
Keywords: Magnetic Resonance Imaging, ultra-low field system, image phantom.

Introduction: The emerging of new Magnetic Resonance Imaging (MRI) systems of Ultra-Low Field as a new alternative to substitute systems that are based on superconductive properties, have a great contribution in research and educational purposes, even though they operate in a range of few micro Tesla[1]. The field inhomogeneities are one of the main limitations with systems that use local Earth's magnetic field resulting in a poor image quality and low signal to noise ratio (SNR). So, there is a need to improve image assessment, using phantoms in which we can appreciate at least good borders in the acquired image.

In this work, we present the development of phantoms made out by anatomical models printed with a 3D printer and adequate them to fit our Ultra-Low Field system, in order to obtain 2D images and verify that contours from structure can be appreciated.

Methods: Anatomical images were selected from different images databases; mainly from CT and MRI images (lungs, liver, and kidneys). The steps followed for organs isolation were: a) delimitation of organs of interest from Dicom images; b) creation of a mask for organs isolation; and c) rendering of all images segmented; these procedures were carried out using Amira Software.

Once the organs were segmented and reconstructed, we used a 3D printer in order to build hollow structures, which were filled with a cupric sulfate solution with a concentration of 2mM. After that, we placed them in an acrylic cylinder which diameter was of 5 cm. The rest of the cylinder's area was filled with a compound similar to ballistic gel, so the structures were fixed into the cylinders.

For image acquisition, we used Spin Echo and Gradient Echo sequences in a Terranova-MRI System (Magritek Limited, Wellington, NZ)

Results and discussion: In Figure 1, we show some examples of the masks for segmentation, the result of 3D images, and finally some images acquired with our Earth's Magnetic Field MRI System.

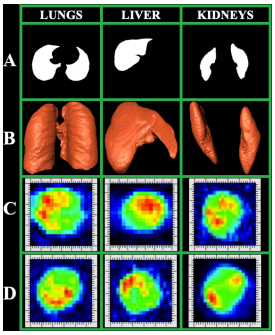

Figure 1. Example of the masks obtained for image segmentation (row A), rendered images (row B), Gradient Echo images (row C), and Spin Echo images acquired (row D)

From Figure 1, we can appreciate some contours limiting the different structures. In each image acquired, we can distinguish points in red which correspond to the cupric sulfate solution concentrated more in those areas, but we can still appreciate the boundaries from the entire structures.

Conclusions: We were able to develop phantoms for MRI Ultra Low field system that help us detect at least differences between signals from different compounds, and also we can see boundaries from structures; even though the poor spatial resolution from image acquisition. These results lead us to develop other methods to increase spatial resolution from our system, as for example treating raw data for developing of a mathematical method for image reconstruction.

References:

[1] P.T. Callaghan, et. al., 2007. "New Zealand Developments in Earth's Field NMR", Appl Magn Reson 32:63.

[2] G. Liney. 2006. "Quality Assurance". Chap. 4 in "MRI Clinical Practice". Ed. Springer. pp. 53-59.

Modified Petal Resonator Surface Coil for UHF-MRI

Sergio Enrique Solís Nájera[1e], Estibaliz Margarita Ramírez Vázquez[1a], Jaime Fabian Vázquez de la Rosa[1b], Lucia Medina[1c] and Alfredo Rodríguez Gonzalez[2d],

[1] *Facultad de Ciencias, Universidad Nacional Autónoma de México, CD.MX. 04510, México*
[2] *Departamento de Ing. Eléctrica, Universidad Autónoma Metropolitana, CD.MX. 09340, México*
[a] estibalizrv@ciencias.unam.mx, [b] jfuv@ciencias.unam.mx, [c] luciamedina@ciencias.unam.mx, [c] arog@xanum.uam.mx [d] solisnajera@ciencias.unam.mx

Research area of interest: Use of non-ionizing in medicine

Keywords: Ultra High Field MRI, Surface Coil, Numerical Simulations

Introduction: Ultra High Field Magnetic Resonance Imaging (UHF-MRI) has become a wide spread commodity since increase the signal-to-noise ratio (SNR) over the volume of interest. UHF-MRI systems up to 11T are in development as the Ekosi 20Tesla human scanner and 21T small animal MRI system located at the MagLab's Tallahassee NMR-MRI/S Facility in Florida, USA. [1]. The use of appropriate RF coils for UHF to achieve the SNR desirable and low Specific Absorption Ratio (SAR) made imperative the development of new coils. The purpose of this study is to develop and evaluate a custom-designed 21.1T RF coil and explore its use for rat brain applications.

Methods: The design of radiofrequency coils for magnetic resonance imaging still been a challenge. The geometry is an important concern due to affects considerably the magnetic field distribution. It is important the design of new geometries and it is important that the electric field distribution not produce hot spots that can burn the sample. The propose RF coil is shown in Figure 1. To predict image quality, the spatial distribution of the magnetic field, B1 and the electric field produced by the petal resonator surface coil was numerically simulated using a finite integral technique (FIT) with a three-dimensional electromagnetic model. This numerical approach uses the electromagnetic field voltages and fluxes defined on an arranged grid doublet are combined with the cell-averaged dielectric properties of materials. All numerical computations were carried out with the commercial software tool, CST Microwave Studio.

Results and discussion: Numerical simulations were performed using a spherical phantom as sample. The numerically computed electric and magnetic field is shown in Figure 2 and for the case of the magnetic field displays the contribution from the externals loops that are attached to the main loop from the coil. The electric field distribution is enclosure in the capacitor. This implies that the coil will produce a lower specific absorption ratio (SAR).

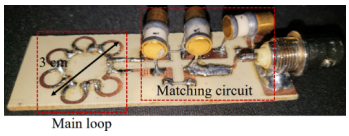

Fig. 1. Photo of the experimental petal resonator surface coil at 900 MHz.

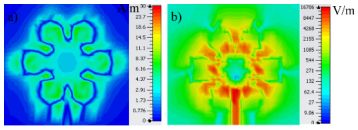

Fig. 2. a) Magnetic Field and b) Electric Field produced by the numerical simulation.

Conclusions: The propose RF coil, shows good magnetic field distribution that the standard RF coils used and shows that the electric field can be contained in the capacitors and over the surface of the coil.

References:

[1] Gor'kov PL, et al., 2009, A modular MRI probe for large rodent neuroimaging at 21.1 T (900 MHz). Proceeding, 17th Annual Meeting, ISMRM; Honolulu, Hawai'i, USA. p. 2952.

Ultrasound-Sensitive Prophylaxis for Prevention of Post-Operative Infection in Spinal Fusion Surgery

Lauren J Delaney[1], Selin Isguven [1,2], John R Eisenbrey[1], Keith Fitzgerald[2], Christopher K Kepler[2,3], Taolin Fang[2,3], Samantha L Knott[2], Priscilla Machado[1], Steven M Kurtz[4,5], Noreen J Hickok[2], Flemming Forsberg[1]

[1]Department of Radiology, Thomas Jefferson University, Philadelphia, PA, USA, [2]Department of Orthopaedic Surgery, Thomas Jefferson University, Philadelphia, PA, USA, [3]Rothman Institute, Philadelphia, PA, USA, [4]School of Biomedical Engineering, Drexel University, Philadelphia, PA, USA, [5]Exponent, Inc., Philadelphia, PA, USA

Email: *flemming.forsberg@jefferson.edu*

Research Area of Interest: C. Use of non-ionizing radiation in medicine

Keywords: ultrasound triggered delivery, spine, infection

Introduction: Bacterial infection following spinal fusion surgery is a major clinical concern, with up to 10% of patients developing infection despite aggressive peri-operative antibiotic treatments [1]. The current clinical standard of prophylactic care is to sterilize the surgical site with 1-2 g of powered vancomycin (VAN) during wound closure [2]. However, this method has variable outcomes due to several factors, including wound drainage, patient health, and the presence of persistent bacteria. To combat this problem, we have designed an ultrasound (US)-activated drug release system to deliver prophylactic antibiotics to combat post-surgical bacterial survival [3]. Our hypothesis is that maintaining supra-therapeutic concentrations of prophylactic antibiotics at the wound site following spinal fusion surgery will lower infection rates. The goal of this study was to quantify antibiotic release from these devices and to evaluate their efficacy against bacterial infection in an *ex vivo* model.

Methods: Polylactic acid (PLA)-coated, VAN-loaded polyether ether ketone clips (1 cm^3) with a drug-loading reservoir (0.785 cm^3) were created in our lab. Two clip designs were evaluated: 1 hole for drug release vs 2 holes. *In vitro* US-triggered release was quantified following insonation with a GE Logiq E9 ultrasound scanner equipped with a C1-6 curvilinear probe, using power Doppler imaging (1.7 MHz frequency, 6.4 kHz PRF, 100% acoustic output power). For *ex vivo* evaluation, clips were implanted medial to the midline of the spine in mature (~6 months, 3 kg) female White New Zealand cadaveric rabbits (n = 4). Two of the 4 sites were insonated for 20 minutes as previously described to induce cavitation and rupture of the PLA coating, and 10^4 cfu *S. aureus* were added to 2 of the 4 sites, while 2 sites were left as was. In parallel, positive and negative bacterial controls were evaluated. All implanted devices were incubated for 2 hours post-insonation, and then retrieved for analysis. Results were collected in duplicate (n=2 for each evaluated device and condition; n=16 total) and compared with a two-way ANOVA.

Results and Discussion: The two device designs released VAN levels sufficient to prevent adhesion of *S. aureus* to implant materials. *In vitro*, background VAN release from the PLA-coated, uninsonated 1-hole clip was 169.41 ± 2.89 µg vs. 452.84 ± 2.89 µg for the 2-hole clip ($p < 0.0001$). Additionally, the 1-hole clip exhibited markedly increased VAN release with time ($p < 0.0001$). At 1 hour post-insonation, 74.66 ± 5.77 µg of VAN was released ($p = 0.0023$ compared to no US). The total cumulative VAN release from the insonated 1-hole clips was 527.50 ± 32.27 µg ($p < 0.0001$ compared to uninsonated). Interestingly, there was no significant difference in cumulative US-triggered VAN release between the 1-hole and the 2-hole design (527.50 ± 32.27 µg for 1-hole vs. 485.75 ± 107.04 µg for 2-hole, $p = 0.28$). In the *ex vivo* study, infected sites showed up to 10-fold reduction in bacterial colonization following US-triggered VAN release, while uninsonated sites exhibited at most a 2-fold reduction in bacterial colonization. Negative controls indicated no surgical site contamination, and positive controls confirmed that the added *S. aureus* survived in the wound environment. VAN release in the rabbit model was dependent on both design and time. There was significantly greater US-triggered total VAN release from the 1-hole clip design than from the 2-hole design (7420 ± 2992 µg vs. 3500 ± 954 µg, $p < 0.0001$). We identified a viable prototype (i.e., the 1-hole clip) for US-mediated localized prophylactic delivery to the spinal surgical site.

Conclusions: Existing methods for preventing infection following spinal fusion surgery are only partially successful. The feasibility of our US-sensitive antimicrobial platform for delivering a bolus of antibiotics to a spinal wound site has been demonstrated both *in vitro* and in tissue *ex vivo*, representing an important proof of principle for continued development of this system.

References:

[1] S.M. Kurtz et al., J. Neurosurg. Spine, vol. 17(4), pp. 342–347, October 2012.
[2] K.R. O'Neill et al., Spine J., vol. 11(7), pp. 641-646, July 2011.
[3] L.J. Delaney et al., Acta Biomaterialia, vol. 93, pp. 12-24, July 2019

Initial experience on the application of quantitative tests for ultrasound quality control in Mexican hospitals

Mauricio Manríquez-Padilla and Iván M. Rosado-Méndez
Instituto de Física, Universidad Nacional Autónoma de México (IFUNAM), Mexico City, MEX
[a]*mauman@ciencias.unam.mx,* [b]*irosado@fisica.unam.mx*

C. Use of non- ionizing radiation in medicine.

Keywords: Ultrasound, quality control, quantitative tests, uniformity, depth of penetration, resolution, linearity.

Introduction: Ultrasound (US) is a highly used imaging modality due to its relatively low cost, practicality and safety. Despite these advantages, its efficacy can be significantly affected by poor image quality. Several international organizations have developed guidelines for establishing quality US control programs. Currently there is no regulation in Mexico on US quality control. Therefore, the goal of this project is to generate a manual of US quality control with special focus on quantitative tests that are less observer dependent.

Methods: The quality control manual is based on guidelines form the American College of Radiology[1], the American Institute of Ultrasound in Medicine,[2] and the International Electrotechnical Commission,[3] among others. It incorporates tests on hardware integrity, image uniformity, depth of penetration, spatial resolution, and system linearity. These tests require the use of a tissue-mimicking phantom, and we have used a Gammex Sono410 (Gammex Sun Nuclear, Middleton, WI). Quantitative versions of some of these tests were prioritized as this avoids subjectivity in each evaluation.

Results: So far, we have applied the manual to five transducers in three different equipments from different vendors: System A (5-11MHz linear transducer), System B (5-10MHz linear transducer), and System C (2-5MHz curvilinear, 4-9 MHz endocavitary, 2-8MHz convex probe transducers). Figure 1 shows an example of the linearity tests from one system. The system behaved nonlinearly at high gains. All transducers passed the other QC tests.

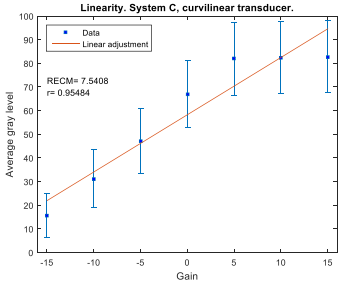

Figure 1. Example of linearity test.

Discussion and Conclusions: None of the participant institutions applied periodic quantitative QC tests before our application. All transducers passed all tests, with the exception of system linearity. This test is important because nonlinearity between tissue echogenicity and image brightness can affect the interpretation of variations of echogenicity from tissue to tissue. Thus, we suggest users to identify ranges of pulse power and gain in which the system behaves linearly. We are currently completing the manual with display performance tests and expanding its use in hospitals in Mexico City.

References

[1] American College of Radiology, ACR–AAPM technical standard for diagnostic medical physics performance monitoring of real time ultrasound equipment www.acr.org
[2] American Institute of Ultrasound in Medicine, Routine Quality Assurance for Diagnostic Ultrasound Equipment, http://aium.s3.amazonaws.com/resourceLibrary/rqa.pdf
[3] IEC-International Electrotechnical Commission et al. IEC ts 62736. 2016.

Multiple Scattering and Scattering Cross-Section Models in Ultrasound

Fatima Fonseca-Rodriguez[a] and J. Hector Morales-Barcenas[b]
Departamento de Matematicas, UAM-Iztapalapa
fonsecafr93@gmail.com [a], jhmb@xanum.uam.mx [b]

Research Area of Interest: C. Use of non-ionized radiation in medicine.

Keywords: inverse scattering, scattering cross-section, biological tissue, ultrasound.

Introduction: One of the main tasks in the inverse scattering problems in tissue is to quantify cell distribution and density using probing waves. To accomplish this task, we assume that the ultrasound pulse-echoes recorded in the transducers carry out valuable information about the tissue's structure and functionality, even in a random environment. Before to solve this inverse problem, we need to fully understand the associated forward problem, which consists of characterizing the scatterer wave-field u_{sc} and the scattering cross-section σ_{sc} of the known scatterer configurations. In this work, *our objective is to present the scattering cross-section models derived from clusters of ``small'' scatterers.* We are focusing on the ability to identify the geometrical distribution of the scatterers in the scattering pattern [1, 2].

Methods: Let the Helmholtz equation be the model for the scalar acoustic wave-field u(x,k), defined in a bounded domain D in R^3: $(\nabla^2+k^2)u(x,k)=0$, where $k=\omega/c > 0$ is the wavenumber, ω is the angular frequency, and c is the wave speed. Consider a cluster of N scatterers labeled by b_j, j=1, 2, ..., N. Let s_j be the boundary of each b_j's and define S = the union of all s_j. We enclose the cluster by a sphere of radius R, namely S_R, such that the domain of the solution of the Helmholtz equation in the region $D = S_R\backslash S$. In spherical coordinates (r,θ,φ), r=R is the sphere S_R. The scattering cross-sections models are derived from an integral formulation of the Helmholtz equation in D as follows. From the Helmholtz First Theorem [3], where u is assumed to be regular (non-singular), we have:

$$\frac{1}{2i}\int_S \left(\bar{u}\frac{\partial u}{\partial n}-u\frac{\partial \bar{u}}{\partial n}\right)dS=\Im\int_S \bar{u}\frac{\partial u}{\partial n}\,dS=0, \quad (1)$$

where $\Im$ means the imaginary part of the expression, and $\bar{u}$ is the complex conjugate of u. In scattering theory, we separate the total wave-field as $u = u_{inc} + u_{sc}$, where $u_{inc}(r,k)$ is the incident wave-field, and $u_{sc}(r,k)$ is the scattered field that satisfies the Sommerfeld's radiation condition. The energy that has been taken from the incident wave by the scattering process is called the *extinction* cross-section $\sigma_{ex}= \sigma_{sc}+\sigma_{ab}$, where σ_{sc} is a measure of the scattered energy by the obstacle and σ_{ab} represents the scattering energy absorbed. After substituting the total field u in the Equation (1), we obtain the scattering cross-sections:

$$\sigma_{sc} = k\,\Im\int_{S_R}\bar{u}_{sc}\left(\partial u_{sc}/\partial r\right)\mathrm{dS},$$

and

$$\sigma_{ab} = -k\,\Im\int_S \bar{u}\left(\partial u/\partial n\right)dS.$$

There are many limits of interest in ultrasound that we want to show from these scattering cross-section models. In the one scatterer case, it is well known their formulation in terms of the spherical harmonic wave-functions [4], the far-field pattern [5], the Waterman's T-matrix [1], the optical theorem [1], etc. In the multiple scattering case, it is worthwhile to mention the Foldy's method for small scatterers or the Mitri's cross-section model [1]. However, to solve the scattering problem in the former case, the superposition principle continues to be a remarkable tool.

Results and Discussion: Interesting situations of applicability to biological tissue of this theory relies on the boundary conditions that we can consider for the scatterers: cells and extracellular matrix. They can be soft-soft or sound-hard scatterers, or they can be regarded as lossy or lossless.

Conclusion: The full comprehension of the scattering cross-section over different situations is the first step to tackle the inverse scattering problem in real cases.

References:

[1] P.A. Martin, ``Multiple scattering and scattering cross-sections", J. Acoust. Soc. Am. 143 (2), Feb 2018.
[2] M.F. Insana, et al., ``Describing small-scale structure in random media using pulse-echo ultrasound", J. Acoust. Soc. Am. 87 (1), January 1990.
[3] B.B. Baker, and E.T. Copson, The Mathematical Theory of Huygens' Principle, Oxford, 1939.
[4] A. Ishimaru, Wave propagation and Scattering in Random Media, Vol. 1 & 2, Academic Press, 1978.
[5] D. Colton and R. Kress, Inverse Acoustic and Electromagnetic Scattering Theory, 2nd Ed., Springer, 1998.

Ultrasound image segmentation methods

Vivian Bass[1,3,4,a], Julieta Mateos[1,2,4,b], Jorge Márquez[1,2,4,c], Iván M. Rosado[3,4,d]
[1]*Instituto de Investigaciones en Matemáticas Aplicadas y en Sistemas,* [2]*Instituto de Ciencias Aplicadas y Tecnología,* [3]*Instituto de Física,* [4]*Universidad Nacional Autónoma de México*
[a]*vivbass4@gmail.com,* [b]*julieta8a3@gmail.com,* [c]*jorge.marquez@icat.unam.mx,* [d]*irosado@fisica.unam.mx*

C. Use of non- ionizing radiation in medicine.

Keywords: Segmentation, breast ultrasound images, breast cancer, ultrasound.

Introduction: Breast cancer is one of the leading causes of death in México and among the world. This is mainly due to late diagnosis and the price of cancer treatment.
Ultrasound (US) is one of the most used tools for the diagnosis of this disease, since it has been detected the use of these images can discriminate between benign or malignant masses [1], but it depends largely on the radiologists experience. A detection that does not depend on the radiologists experience should produce better diagnoses [2], therefore, it is necessary to develop automatic detection systems for US images. These systems are based on the image segmentation, which is an image processing technique used to analyze and group pixels by their features. US image segmentation represents challenging problem due to the very nature of the image, since it has a speckle pattern, low contrast, blurred boundaries, etc. [3]. This is why different segmentation methods have been tested and compared [2] [3] [4], in order to develop computer-aided diagnostic systems that help radiologists to do better diagnoses.

Methods: We present a review of different segmentation methods (e.g. thresholding, clustering, watershed, active contours, neural networks), with the pros and cons of each them, based on different papers that have worked with breast ultrasound image segmentation and papers that have already made comparisons of some of these methods.

Results and discussion: There are methods that are not convenient to use in US images. They have been used some methods such as the clustering-based model, active contours, random Markov field and NN, which deliver very good results and some of them are very fast computationally. Figure 1d shows a very defined active contour segmentation of the region of interest (ROI). Others, such as thresholding-based and watershed-based methods, although they are widely used and deliver good results in the analysis of other types of images, are not good if used in US images, as it is shown in image 1d, where it is used the thresholding-based method and it is not a good segmentation of the ROI.

a	b
c	d

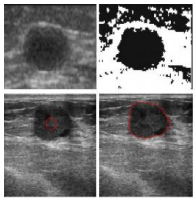

Figure 1. [3] a) Original image, b) Thresholding-based method, c) Original image, d) Active contours method.

Conclusions: Due to all the artifacts presented in US images, not all methods work for them. The best results are obtained, mostly, with the active contour model and random Markov field, but these methods are semi-automatic, since they require radiologist intervention. Neural networks deliver very good results, but their disadvantage is that thousands of images are needed to train them at the beginning, the advantage is that they are automatic and very fast when analyzing the image.

References

[1] Sahiner, B., Chan, H. P., Roubidoux, M. A., Hadjiiski, L. M., Helvie, M. A., Paramagul, C., & Blane, C. (2007). Malignant and benign breast masses on 3D US volumetric images: effect of computer-aided diagnosis on radiologist accuracy. *Radiology*, *242*(3), 716-724.
[2] Cheng, H. D., Shan, J., Ju, W., Guo, Y., & Zhang, L. (2010). Automated breast cancer detection and classification using ultrasound images: A survey. *Pattern recognition*, *43*(1), 299-317.
[3] Huang, Q., Luo, Y., & Zhang, Q. (2017). Breast ultrasound image segmentation: a survey. International journal of computer assisted radiology and surgery, 12(3), 493-507.
[4] Xian, M., Zhang, Y., Cheng, H. D., Xu, F., Zhang, B., & Ding, J. (2018). Automatic breast ultrasound image segmentation: A survey. Pattern Recognition, 79, 340-355.

On the graphic representation of clinical data: the metabolic syndrome case

E.I. Fuentes-Oliver[1, a], C. García-Segundo[1, b], A. Ruiz-Margáin[2, c], R.U. Macías-Rodríguez[2, d]
[1]*Instituto de Ciencias Aplicadas y Tecnología, Universidad Nacional Autónoma de México, Circuito Exterior S/N, Ciudad Universitaria, Coyoacán, CDMX, Mexico, 04510.*
[2]*Instituto Nacional de ciencias Médicas y Nutrición "Salvador Zubirán" (INCMNSZ), Vasco de Quiroga 15, Belisario Domínguez Secc 16, Tlalpan, CDMX, Mexico, 14080.*
[a]edgarfuentes@ciencias.unam.mx, [b]crescencio.garcia@icat.unam.mx,
[c]ruizm.astrid@gmail.com, [d]ricardomacro@yahoo.com.mx

Research area of interest: C. Use of non-ionizing radiation in medicine

Keywords: metabolic syndrome, infrared imaging, bioelectric impedance analysis

Introduction: Metabolic syndrome (MetS) comprises a group of entities strongly related to cardiovascular risk disorders. Currently it is one of the major non-contagious health threats worldwide. Its definition includes the presence of at least three of the following characteristics: high values of triglycerides, abnormal waist/hip ratio, high blood pressure, insulin resistance and low values of HDL cholesterol [1].
MetS is associated to endothelial dysfunction and systemic inflammation, evidenced as alterations in the metabolic heat release. Given the multiple systemic effects of MetS, the assessment of body composition could be useful, assessing fluid and fat/muscle content. This assessment can be done using bioelectrical impedance vector analysis (BIVA). BIVA is a modality of bioelectrical impedance analysis (BIA) where a reference health population is used to define the reference percentiles 95%, 75% and 50%. This modality has several advantages respect the BIA methods [2], mainly due to the more precise fluid assessment. Since the graphical representation of BIVA is qualitative, it limited success as clinical technique.
The changes in the heat release caused by MetS, display drifts of the natural thermal asymmetry [3]. Intuitively one can rise the hypothesis that if the asymmetric heat release, the natural water vapor release from human skin, and thus the impedance measurements, would have a relationship.
Our interest here is to establish a standard framework to assess the changes induced by MetS, using reference percentiles to introduce quantitative non-invasive markers, of intuitive understanding for the clinical practice.
Methods: For eight control subjects, free from MetS and included in the protocol ICMNSZ REF. 1147, we acquired IR-images, simultaneously with impedance measurements. The IR-images are acquired as described in [3]. In turn the bio-impedance is measured with a bio-impedance meter RJL Systems (Mod. Qunatum IV).
From IR-images we estimated the radiometric asymmetry in a region of interest. In it we use temperature histograms and spatial distribution of temperatures. Thus we compute two indices related to this asymmetry and we defined a framework with these indices using reference percentiles.
Based on the analog methodology, we appreciate that the measured bioelectrical impedance can also be displayed on a percentile chart; and then, the bio-impedance drifts can also be represented in quantitative mode.

Results: Standard framework to assess body composition and alterations in heat release, which incorporate quantitative bioelectrical impedance display, compared with quantitative radiometric asymmetry, extracted from infrared imaging. Both markers are placed as percentiles, in which the measurement drifts, represent the walk-away from the respective reference values.

Conclusions: A standard framework allows a more intuitive interpretation of measurements provided by different techniques and instruments. The big gain is that this information could be read out in a simple way by any person.

References:
[1] Saklayen M.G., 2018. The Global Epidemic of the Metabolic Syndrome. *Current Hypertension Reports*, 20, 12.
[2] Espinosa-Cuevas M.A., *et al*., 2007. Vectores de impedancia bioeléctrica para la composición corporal en población mexicana. *Revista de Investigación Clínica*, 59, 1, 15-24.
[3] Fuentes-Oliver E.I., *et al*., 2019. Anomalous contra-lateral radiometric asymmetry in the diabetic patient. *Biomed. Phys. Eng. Express*, 5, 065015.

Response of BANG3-Pro gel induced by 6 MV X-ray radiotherapy beam

M A Flores-Mancera[1,a], A Rodríguez-Laguna[2,c], MA Poitevin-Chacón[2,d], G Massillon-JL[1,b]
[1]*Instituto de Física, Universidad Nacional Autónoma de México, 04510 Mexico city, Mexico.*
[2]*Departamento de Radioterapia, Hospital Medica Sur, 14050 Mexico City, Mexico.*
[a]*MAFlores@ciencias.unam.mx*, [b]*massillon@fisica.unam.mx*, [c]*arlaguna@ciencias.unam.mx*,
[d]*adepoite@hotmail.com*

Research area of interest: Physics and dosimetry of radiotherapy.
Keywords: 3D dosimetry, BANG3-Pro gel, laser computer tomography.

Introduction: One of the biggest challenges in modern radiotherapy like IMRT and VMAT is the use of high dose gradients to increase the tumor control probability and minimize the normal tissue complication probability [1, 2]. The Quality assurance (QA) of the absorbed dose distribution delivered to each individual patient by the treatment planning system must be performed given the complexity for the dose delivery process by the treatment unit [3]. The QA in conventional 2D dosimetry underestimates high dose gradient near the organs at risk and consequently prevents an adequate evaluation of radiation-induced secondary cancer probability [4]. Therefore, high resolution 3D gel dosimetry offers a novel method determine the dose distribution delivered to patients with acceptable accuracy [5] and minor probability of errors [6]. In this work we investigate the BANG3-Pro gel response to 6 MV x-rays used in the clinic.

Methods: BANG3-Pro gel has been calibrated in order to be used in radiotherapy QA. Firstly, a 6 MV x-ray beam produced by a Varian Clinac iX was calibrated under reference conditions following the IAEA code of practice 398 [6]. For this study, we used three different ionization chambers (IC): an Exradin A12 and two PTW models N23333 and TW30013 calibrated at two different laboratories. Chamber signals were corrected for field factor and tissue-phantom ratio (TPR) were measured. For the field factor correction, the field at the phantom surface was modified according to the IC calibration certificate. Hence, dose rate was estimated at reference depth according to the code of practice 398 [6]. BANG3-Pro gel dosimeter was sealed in several glass spheres and irradiated at the same SSD set-up as the IC to different dose values from 0. 2 Gy, up to 50 Gy. The gel dosimeter was scanned using a laser tomography scanner and the optical density values obtained were used to reconstruct the calibration curve.

Results: Table 1 presents the dose rate and field factors measured with different IC at 10 cm liquid water depth.

IC	Dose rate [cGy/UM]	Field factor	$TPR_{20,10}$
Exradin A12	0.700	1.048	0.672
PTW N23333	0.726	1.066	0.596
PTW TW30013	0.655	0.985	0.670

Conclusions: For the radiotherapy QA, the gel will be used to simulate the patients within the treatment planning system and simultaneously provided the dose received by the tumor volume as well as the organs at risk.

References:
[1]. G Massillon-JL 2010 AIP Conf. Proc. **1310** 23-28.
[2]. J Song 2015 J. Appl. Clin. Med. Phys. **16:6** 263-272
[3]. L J Schreiner 2017 J. Phys. Conf. Ser. **847** 012001.
[4]. J A Moret 2018 J. Appl. Clin. Med. Phys. **19:5** 632-639.
[5]. K B Pulliam 2014 Med. Phys. **41:2** 0121710-6
[6]. IAEA Code of practice **398**.

Acknowledgments: Thank to Alejandro Jiménez and Patricio Vázquez for technical support. Project partially supported by PAPIIT-IN115117 and Royal Society-NA150212.

IMPLEMENTATION OF THE HEXAPOD TABLE IN PATIENTS OF THE OAXACA STATE CENTER OF ONCOLOGY AND RADIOTHERAPY

L. Sánchez-Hernández1[1,a], J. G. Gutiérrez Castillo1[1], E. Hernández-Tellez1[1], I. Vasquez-Baez[1], K. H. Ramírez Vásquez[2]
[1]*Department of Medical Physics, Oaxaca State Center of Oncology and Radiotherapy*
[2]*Department of Radiation Oncology, Oaxaca State Center of Oncology and Radiotherapy*
[a]*slidia0110@gmail.com1*

Physics and dosimetry of radiotherapy
Keywords: HexaPOD table, corrections of translational and rotational errors, treatment time.

Introduction. The HexaPOD robotic treatment table has been developed to correct patient positioning errors with six degrees of freedom [1]. The combination of the CT based image guidance systems and the HexaPOD have allowed position accuracy and correction of patient positioning, showing sub-millimeter accuracy [2]. In our study, we evaluated the average differences in translational and rotational position on the X, Y, Z axes, using the CBCT/HexaPOD combination.

Methods. Fifteen patients participated in this study. The XVI image acquisition system was used to acquire a volumetric kV image cone beam CT (kV-CBCT) of the patient, making the Grey Value register of the reconstructed image with respect to the reference image of the planning CT. To obtain the exact position of the patient, the translational and rotational corrections determined by registration were then transferred to the iGuide system, the software that controls the HexaPOD converted the differences between the position of the reference image and the acquired image with XVI in positioning correction values to reposition the patient (see Figure 1). The corrections of position error between the two images that were analyzed are translation and rotation.

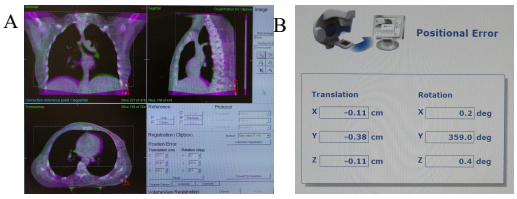

Figure 1. A) VolumeView Registration window, B) HexaPOD dialog box that shows the positional error values.

Results. The Table 1 depicts the differences in average translational positioning (X, Y, Z) of patients treated with HexaPOD were 3 ± 1, 2 ± 3 and 3 ± 1 mm. All rotational differences were below 3º (1.0 ± 0.2°, 1.1 ± 2°, 0.7 ± 0.1°). The additional average time used by the IGRT technique in treatments increased by 25% compared to those where was not used the CBCT/HexaPOD combination, due to acquisition and image registration factors.

Table 1. The average differences from 15 patients in all translational and rotational directions.

	TRANSLATIONAL (mm)	ROTATIONAL (degrees)
X	3 ± 1	1.0 ± 0.2
Y	2 ± 3	1.1 ± 0.2
Z	3 ± 1	0.7 ± 0.1

Conclusions. The differences between planned and actual tumor position in treatment can be calculated with six degrees of positioning freedom using the HexaPOD table. The correction of translational and rotational errors with HexaPOD, were below 3 cm and/or 3°, thus improving the quality of radiotherapy treatments. The average time per treatment session was increased by 25% using the HexaPOD in combination with XVI compared to those sessions where the acquisition of images CBCT was not performed. This can limit the total number of patients in a day.

References

[1] Dhillon, A., et al. (2017). The Impact of Correcting for Translational and Rotational Errors Using the HexaPOD in Head and Neck Stereotactic Body Radiation Therapy Patients. Journal of Medical Imaging and Radiation Sciences, 48, 276-281.
[2] Meyer, J., et al. (2007). Positioning accuracy of Cone-Beam Computed Tomography in combination with a HEXAPOD robot treatment table. Int. J. Radiation Oncology Biol. Phys., 67(4), pp. 1220–1228.

Quality assurance of the calculation algorithm of a radiotherapy treatment planning system before its clinical implementation

Jiménez-Acosta, J.A.[1,a], Pérez-Rodríguez, K.R.[2,b], Rodríguez-Laguna, A.[1,c].
[1]*Hospital Médica Sur, Tlalpan, CDMX,* [2]*Facultad de Ciencias, UNAM, CDMX.*
[a]*jajimenez@ciencias.unam.mx,* [b]*karla_rodriguez@ciencias.unam.mx,* [c]*arodriguezl@medicasur.org.mx*

Research area of interest:
A: Physics and dosimetry of radiotherapy

Keywords: TPS, AAA, eMC.

Introduction: Treatment planning system (TPS) is one of the essential tools in modern external beam radiation therapy. This tool is used to define the set of radiation beams, energies and other modifiers that will be used in the treatment of each patient [1]. For the commissioning of a TPS it is substantial that the parameters of the radiation beam and other modifiers that intervene in the precise calculation of the dose are adequately modeled in the system and verified. Failure to do so could cause, due to a significant difference between the therapeutic and the administered dose, that the treatment does not have the desired effect on the disease and/or that a damage greater than expected in the healthy tissue surrounding the disease be occasioned [1, 2].

Methods: This work was carried out in the radiotherapy service of the Médica Sur Hospital, Tlalpan. The equipment used was a Varian Clinac IX linear accelerator n/s 1227, PTW MP3 water dosimetry system and different models of ionization chambers and electrometers. Eclipse™ Treatment Planning System was employed in this work. The calculation algorithms to which quality assurance were applied were the Analytical Anisotropic Algorithm (AAA) and electron Monte Carlo (eMC). Virtual and physical phantoms were used.

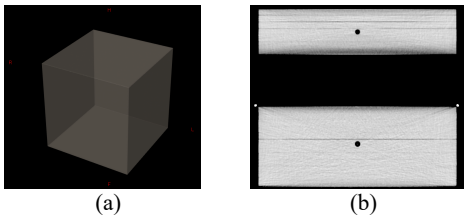

(a) (b)

Figure 1. (a) Virtual and (b) physical phantoms used in the quality assurance of the calculation algorithms.

The basic photon and electron beams dose validation tests described in [2] were completed for each configured beam. The typical setup for the measurement were a static gantry angle pointing directly down with collimator rotated as needed). Additionally, other nonstandard setups were also used. (e.g., oblique incidence, extended SSD and heterogeneous media).

Results and discussion: From the validation of the dose calculation and heterogeneities correction of each algorithm, we have that the comparison between the measured and simulated data in the TPS is within the tolerance range specified in each validation test [2], being the measurements in the low dose regions (penumbra) and the measurements at larger depths the ones that present the greatest disagreement. In the case of the AAA calculation algorithm, in this low dose region an overestimation of the radiation profiles is observed, which is consistent with the results in the literature [2].

Conclusions: The validation of the TPS calculations is a fundamental part in the commissioning of a linear accelerator. The results found in this work allow us to know the strengths and limitations of the dose calculation algorithms used in the TPS for modeling the radiation beams. This knowledge also allows us to define the clinical situations under which the TPS is appropriate and the additional settings required when the software is updated.

References:
[1] Vatnitsky, S. et al., 2007. "Specification and Acceptance Testing of Radiotherapy Treatment Planning Systems". IAEA.
[2] Smilowitz, J. B., et al., 2015. "AAPM medical physics practice guideline 5. a.: commissioning and QA of treatment planning dose calculations-megavoltage photon and electron beams". Journal of applied clinical medical physics, 16(5), 14-34.

Dosimetry response and water influence of delaminated-Gafchromic EBT3 irradiated at kilovoltage

Mauricio Santibañez[1,a], Melani Fuentealba[1,b]

[1]*Departamento de Cs. Físicas, Universidad de La Frontera, Temuco, Chile.*
[a] mauricio.santibanez@ufrontera.cl , [b] mel.fuentealba.mf@gmail.com

Research are of interest:
A. Physics and dosimetry of radiotherapy
Keywords: Delaminated-EBT3, water-influence EBT3, dose enhancement dosimeter.
Introduction: Radiochromic films are widely used in clinical dosimetry applications. According to the manufacturer, the Gafchromic EBT3 film consists of a 30 µm active layer sandwiched between two 125-µm clear polyester covers. Given that the ranges of low energy electron like Photoelectrons and Auger or the heavy ions of few MeV are much shorter than 125 µm of length in polyester, they cannot reach the active layer of the EBT3 and the dose of these particles cannot be readout by this dosimeter [1]. Radiation Dose Enhancement currently is a widely studied process which occurs when a high-Z element infused in a low-*Z* material is exposed to ionizing radiation. This is primarily due to the photoelectric interactions in the high- *Z* element. Some of the photoelectrons and Auger electrons released in the high-*Z* element escape and penetrate into the surrounding low-*Z* medium producing a high increase in the dose [2]. Preliminary relative dose enhancement measurements for Gadolinium and Gold have been reported through Gafchromic films EBT2 and EBT3 [3-5], showing the need of increment the probability of Auger and photoelectrons with energies able to reach the radiosensitive substrate of the Gafchromic film (125 µm of separation). The delamination of the film is a proposed currently in some application like an alpha dosimeter and low energy Heavy Ions, but in these application the Gafchromic Films is not immerse in water, limiting the range of application where the evaluation of different concentration of dose enhancement agents is necessary.
Method: Gafchromic® EBT3 film were carefully unlaminated and evaluated the maintenance of dosimetry properties. 42 Fragments of 1x4 cm2 of EBT3 were cut from the unlaminated film and separated in two groups: 21 fragments for measure doses from 2-8 Gy by triplicate, irradiating directly the 30 µm thick film active layer. The second group was formed by 21 fragments which were immerse 10 minutes inside vials of 4 cm3 fills with water and drying at room temperature at 24 hours. Given the immediately damage which produce the water over the active substrate, a thin film of polyester of 10 µm was adding to the fragments. Later the fragments were used to measure doses from 2-8 Gy by triplicated, irradiating too directly the active layer. All the dosimeter were irradiated by an X-ray equipment Teledyne Model CP160D at 160kV and 5 mA, with a dose rate of 1.25Gy/min. The optical density before the irradiation, after the immersing in water and after the irradiation were measured with a Flatbed Transmission Scanner Epson perfection V370. The sensitivity dose response and the evaluation of the variation among the original, the unlaminated and the unlaminated submerging in water were realizes.
Results and discussion: An effective delamination was achieved by showing that the radiosensitive substrate is not damaged by mechanical force when removing the upper layer. The dose response curve of the delaminated dosimeter does not show significant variations (less than 3% in the optical density for the same dose) with respect to the curve previously obtained for the same batch of EBT3. The delaminated films immersed in water showed the feasibility of being implemented a small coverage (10 µm) that allows to avoid direct damage to the active substrate in 85% of the cases studied, requiring the improvement of the seal at junction points of this new coverage. Films that did not visually show damage to their substrate were evaluated in terms of their dose response curve showing differences within the range of uncertainties observed in delaminated films without immersion in water.
Conclusions: It was possible to delaminate EBT3 films without damage to the radiosensitive substrate, which allowed its subsequent use as a dosimeter in the range of use described by the manufacturer. A new coverage of reduced size (10 µm) was implemented for its use immersed in water that was carried out in 85% of the cases for 10 min immersion times. The films after immersion were shown to maintain dosimetry properties allowing to be used for dose enhancement dosimetry of agents in water solution.
References:
1. C.Y.P. Ng, S.L. Chun, K.N. Yu. Radiation Physics and Chemistry 125 (2016) 176–179.
2. Rakowski, J. T., Laha, S. S., Snyder, M. G., Buczek, M. G., Tucker, M. A., Liu, F. , Mao, G. , Hillman, Y. and Lawes, G. (2015). Med. Phys., 42: 5937-5944.
3. M. Santibáñez, M. Fuentealba, F. Torres, A. Vargas . 2019. Applied Radiation and Isotopes 154, 108857.
4. Ahmad, R., et al. 2016. Phys. Med. Biol. 61, 4537-4550.
5. Cho, J., Gonzalez-Lepera, L., Manohar, N., Kerr, M., Krishnan, S., Cho, S.J., 2016. Phys. Med. Biol. 61, 2562–2581.

Initial characterization of 6X-FFF beam in a Varian C-Series machine and comparison with a TrueBeam linear accelerator

Velázquez Trejo José de Jesús1
[1]*Department of Radiation Oncology, Centro Médico Nacional del Bajío. IMSS*
fis.jesus.velazquez@gmail.com,

Research area of interest: Physics and dosimetry of radiotherapy.
Keywords: FFF-beams, dosimetry, linear accelerator, beam QA.

Introduction: The Varian C linear accelerator series was introduced in the 1990's, it has been upgraded to perform new techniques such as IMRT/VMAT, IGRT, SRS. Recently, Varian upgrade the C series system adding a flattening-filter-free (FFF) beams. This year the Varian iX (this model is part of the serie C) installed at the Centro Médico Nacional del Bajío (IMSS) was upgraded with a new 6X-FFF beam in order to use it with VMAT/SRS techniques. Here are presented the initial beam measurements of this new FFF-beam and the comparison with the Varian TrueBeam reference data, also there were compared the regular 6X beams with flattening filter, all in order to investigate a possible full 6MV beam matching between the C-Series and True Beam systems. Previous works have already performed [1] comparations between no-FFF beams in C and TrueBeam series.

Methods: For a 6X with flattening filter (6X) and the 6X FFF, percent depth dose (PDD) and profiles (inline and crossline) were measured in the Varian iX using a PTW MP3 water phantom with semiflex ion chamber (10 cm x10 cm field size and SSD 100cm). The measurements were compared against measurements from the TrueBeam data provided by Varian [2,3]. The beam analysis and comparations were carried out as follows: for the PDD curves, specific points such a d_{max} and PDD_{10} (depth of the maximum dose and the PDD value at 10 cm) were compared because of their importance as a beam descriptors. Also, in the case of the profiles, the penumbras were compared. All measured curves were compared to the Varian reference data using the gamma index criteria (2%, 1mm).

Results and discussion: The gamma index for the comparison of PDD and profiles between both linacs was less than 1. Values of d_{max}, PDD_{10} , and the penumbra are shown in table I, where it can be confirmed that the difference in PDD_{10} was less than 1.0%, while the difference in d_{max} and the penumbra was less than 2 mm. This could suggest similarities in the filter and machine head construction in both linacs. The measurements also confirm the beam hardening created by the flattening filter in the 6X, this is because both PDD_{10} and d_{max} are greater in the 6X beam.

	6X-FFF		6X	
Parameter	iX	True Beam	iX	True Beam
d_{max} (cm)	1.37	1.30	1.5	1.4
PDD_{10}	63.51	63.50	66.5	66.4
Penumbra	0.8	0.7	0.68	0.68

Table 1: Beam parameters comparison.

Conclusions: This initial characterization suggests that for 6X and 6X-FFF, beam matching is would be possible between the Varian iX C-series and the TrueBeam machines. However, more field sizes and output factor tables need to be compared for final confirmation. At the moment, the beam commissioning process is being carried out, it is expected to have more extensive data in the near future.

References:

[1] Gloria P. Bayer, 2013 "Commissionig measurements for photon beam data on three TrueBeam linear accelerators, and comparison with Trilogy and Clinac 2100 linear accelerators" J. Appl. Clin. Med. Phys. 14-1, pp 273-288.
[2] TrueBeam Representative Beam Data for Eclipse, Varian Medical Systems, Nov 2012.
[3] Zheng Chang et al., 2012 "Commissioning and dosimetric characteristics of TrueBeam system: Composite data of three Truebeam machines" Med. Phys. 39, 6981, pp 6981-7018.

XVI Mexican Symposium On Medical Physics
Physics in Precision Medicine: Advances in Imaging and Therapy

Comments on the precise definition of the concept of absorbed dose

María de los Ángeles Montes-Rodríguez[1], José Trinidad Álvarez-Romero[2]

[1,2] *Ph D student of the ESFM, Instituto Politécnico Nacional,* [2] *SSDL, ININ*

Research area of interest: physics and dosimetry of radiotherapy

Keywords:
Kolmogorov probability theory, Borel σ-algebra, random variable, stochastic process, stationary state, non-equilibrium thermodynamics, electronic equilibrium condition, absorbed dose.

Introduction The absorbed dose D is the fundamental physical quantity that best correlates the physical, chemical and biological effects induced by ionizing radiation. However, its definition given by ICRU 85a lacks rigor in the following aspects, [1]: a) does not use the modern definition of *random variable* of the axiomatic theory of Kolmogorov [2, 3], b) neither does it correctly define the concept of *stochastic variable* [4,5], c) does not explain the electronic equilibrium condition EE to eliminate the temporal dependence of the imparted energy $\varepsilon(r,t)$, considered as a stochastic variable, [5].

Methods. a) Axiomatic definition of Kolmogorov probability. Let, $X = X(e)$, be a function whose domain is the *sample space* E and its image is a subset $S \subseteq \mathbb{R}$, the set of real numbers, therefore $E = X^{-1}(\mathbb{R})$; therefore, a function $X(e)$ defined for all the elementary events of the *probability space:* (E, β, P) in $\mathbb{R}$, it is called *random variable* $\Leftrightarrow \forall\, X \in \mathbb{R}$, the inverse image of the interval $I = (-\infty, X)$ is an event of Borel σ-algebra β; where the sample space E can be countable or uncountable infinity. b) Definition of stochastic variable. Let, $X: I \times \Omega \mapsto \mathbb{R}^d$, be a function of two arguments, $t \in I = [0, \infty) \subseteq \mathbb{R}$ and $\omega \in \Omega$, where $(\Omega, \mathcal{F}, P)$ denotes a probability space; then, $\boldsymbol{X(t)}$ is an $\mathbb{R}^d$-valued random variable on the probability space $(\Omega, \mathcal{F}, P)$ for each $t \in I$, i.e., $X(t) \in \mathcal{F}$ for each $t \in I$, that is $\boldsymbol{X(t)}$ is a *stochastic* variable or *stochastic process* $\mathbb{R}^d$-valued, [3].

Results and discussion Grusell in [3] establishes a *probability space* $(\Omega, \mathcal{F}, P)$ to define the *absorbed dose* in terms of the *energy imparted* ε as a *random variable*; where, the proposed *sample space* is $E = \bigoplus_1^\infty \mathbb{R}$ and $\Omega = \bigoplus_1^\infty E$, for any subset $S \subseteq \Omega \in T$, here T denote the set of all subset of Ω such that T is extended to a Borel field $\mathcal{F}$, with a probability measure P; where: $e_{j,i,min} \leq \varepsilon_{j,i} < e_{j,i,max}$, here $\varepsilon_{j,i}$ is the deposited energy;
However, Grusell does not considered $\varepsilon(r,t)$ as a *stochastic variable*, [4]. Alvarez in [5] states that the temporal dependence of $\varepsilon(r,t)$ is implicitly eliminated with the EE condition, which is a stationary state. In fact, $\varepsilon(r,t)$ is a stochastic variable, i.e. a physical quantity dependent on space and time, which is due to a probability distribution function associated to ε that is strictly a function of time.

Conclusions The definition for D proposed in [3] is incorrect, because he omitted the temporal dependence of the stochastic variable$\varepsilon(r,t)$; therefore, it cannot justify the temporal dependence of $\varepsilon(r,t)$ as stationary process; even more, he cannot interpret it physically from the non-equilibrium thermodynamics, and how to eliminate the time dependence on $\varepsilon(r,t)$.

References

[1] ICRU 85A, (2011).
[2] Kolmogorov N. Foundations of the theory of probability, New York, (1956)
[3] Grusell E., Rad. Phy and Chemistry, 107, 131–135, (2015)
[4] Grigoriu M. Stochastic Calculus, Springer Science+Business Media, LLC, (2002).
[5] Álvarez Romero JT, Revista mexicana de física, 48 suplemento 1, 70-76, (2002)

Determination of α/β for a Mexican Cohort of PCa Patients Treated with External Radiotherapy

Christian Adame González[1], José T. Álvarez-Romero[2], Mario M. y Rodríguez[3]

[1,3] ESFM, Instituto Politécnico Nacional, [2] SSDL, ININ,

Research area of interest: Physics and dosimetry of radiotherapy

Keywords:
Prostate Cancer, Biochemical Relapse Free Survival, Hypofractionation, alpha/beta.

Introduction. With the Kaplan-Meier technique and the Cox proportional hazards model, the biochemical relapse free survival (bRFS) was determined and characterized for a cohort of Mexican patients (n = 595) with prostate cancer (CaP) who received treatment with external radiotherapy [1]. Using these clinical outcomes, the radiobiological parameter α/β is determined.

Methods. The radiobiological parameter α/β is determined with survival curves for different treatment schemes (hypofractioned versus conventional), under the hypothesis that they are radiobiologically equivalent, where the biologically effective dose (BED) is plotted according to of alpha / beta, where its value is given by the point of intersection of both curves [3].

$$BED = dn\left(1 + \frac{d}{\alpha/\beta}\right)$$

Results and discussion. Figure 1 shows the BED values of the 6 treatment schemes used as a function of the α/β ratios: This graph shows that there are four points of intersection; two for a α/β = 2.8, a third of α/β =2.2 and the fourth α/β = 3.5. These values can be explained as follows: a) The bRSF of the schemes do not meet the hypothesis of being equal, b) the absorbed doses given to the patient present an uncertainty that is not considered, c) the α/β for all the schemes have a more probable value of 2.83 ± 0.5 SD. It should be mentioned that in [4] additional considerations are made, such as the number of clonogenic tumor cells, the overall treatment time, the kick-off time for tumor repopulation and the repopulation doubling time.

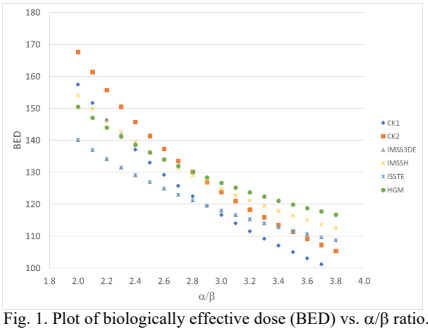

Fig. 1. Plot of biologically effective dose (BED) vs. α/β ratio.

Conclusions. In a first approximation, a radiobiological parameter value of α/β = 2.83 ± 0.53 SD was found for a cohort of Mexican patients with PCa treated with external radiotherapy.

References

[1] C. Adame González, J.T. Álvarez Romero, M. Moranchel y Rodríguez *et al.* bRFS in Patients with CaP treated with External RT: Outcomes obtained at the CMN Siglo XXI Hospital de Oncología, CMN 20 de Noviembre and Hospital General de México of the México City, accepted to publish in Reports of Practical Oncology and Radiotherapy (2019).

[2] R. Miralbell, Stephen A. Roberts *et. al.*, Int. J. Radiation Oncology Biol. Phys., Vol. 82, No. 1, pp. e17–e24, 2012.

[3] Leborgne F., Fowler J., Leborgne J.H, *et. al.*, Int. J. Radiation Oncology Biol. Phys., 2012; 82:1200–1207.

[4] Piernicola Pedicini, Lidia Strigari, Marcello Benassi, Int J Radiation Oncol Biol Phys, Vol. 85, No. 5, pp. e231ee237, 2013

I mparted dose in blood components with a ^{137}Cs irradiator

Alvaro D. Cruz[1,a], Itzel M. Torres[2,b], Luis A. Medina[2,3,c]
[1]*Facultad de Ciencias, Universidad Nacional Autónoma de México,* [2]*Instituto de Física UNAM,*
[3]*Unidad de Investigación Biomédica en Cáncer INCan-UNAM, Instituto Nacional de Cancerología*
[a]alvarodan.crco@ciencias.unam.mx , [b]itzel2606@gmail.com , [c]medina@fisica.unam.mx

Research area of interest:
Physics and dosimetry of radiotherapy.

Keywords: Irradiation of blood components, Radiochromic film dosimetry, ^{137}Cs-irradiator, Spatial dose distribution.

Introduction: Transfusion-Associated Graft-Versus-Host Disease (TA-GVHD) is a fatal complication that occurs when viable donor T lymphocytes proliferate and engraft in susceptible patients after transfusion. This disease manifests itself in patients with congenital immunodeficiencies, principally in bone marrow transplant recipients, as well as in cancer patients treated with chemotherapy or radiotherapy [1]. Irradiation of blood components with ionizing radiation, inactivates T lymphocytes, breaking their DNA molecules to prevent their proliferation and avoid an immune response against the receptor. According with the Mexican regulations (NOM-253-SSA1-2012) [2] blood components must receive 25 to 50 Gy to prevent TA-GVHD. The Blood Donor Center at the National Institute of Cancerology of Mexico implements the irradiation of blood components with a Cs-137 irradiator (BIOBEAM GM 2000; activity: 40.16 TBq 30/10/2019).
In this work we describe the procedure implemented to evaluate the dose imparted in the erythrocyte and platelet components as well as the dose distribution of the radiation field.

Methods: The radiochromic film EBT-XD was used to verify the dose distribution. An Epson Scanner 1200XL Ph was used in the readout of the films. This scanner was previously characterized (stability, reproducibility, uniformity, and resolution) to evaluate its response in film dosimetry. EBT-XD calibration curve was performed with ^{137}Cs Gamma Cell (ICN-UNAM). Film irradiation was performed under CPE conditions using PMMA and water phantoms. Imparted dose in blood components was measured by placing small pieces of films (2x2 cm) at different positions on the bags. Dose distributions were calculated with a homemade Python program that was validated by comparison with DoseLab software.

Results and discussion: Based on the results of the scanner characterization, a film reading protocol was performed. The BIOBEAM GM 2000 irradiation field was not complete uniform; the measured dose in the field was higher (over 40%) than the nominal dose programmed in the irradiator by the manufacturing company.

Conclusions: Dose imparted to the blood components was higher than the nominal dose of 25 Gy (averaging 37 Gy). However, the dosimetric evaluation showed that it complies with NOM-253-SSA1-2012. Based on these results, a new irradiation program will be proposed, to achieve a better dose distribution in the volume of interest. Based on these results, a new irradiation program will be proposed, in order to achieve a better dose distribution in the volume of interest and to ensure that the dose delivered is closer to the nominal dose.

References:
[1] Bahar, B., & Tormey, C. A. (2018). "Prevention of Transfusion-Associated Graft-Versus-Host Disease With Blood Product Irradiation: The Past, Present, and Future".Archives of Pathology & Laboratory Medicine, 142(5), 662–667.
[2] NORMA Oficial Mexicana NOM-253-SSA1-2012, Para la disposición de sangre humana y sus componentes con fines terapéuticos. Publicada el 18 de junio de 2012.

Dosimetry in fractionated irradiation of rat brain to evaluate radiobiological response

Abril D. Iglesias Ojeda[1,5,a], *Monserrat Llaguno Munive*[2,3,b], *Efrén Hernández Ramirez*[4,5,c], *Luis A. Medina Velázquez*[5,6,d].

[1]*Facultad de Ciencias, Universidad Nacional Autónoma de México;* [2]*Posgrado en Ciencias Biomédicas, Universidad Nacional Autónoma de México;* [3]*Laboratorio de Farmacología, Subdirección de Investigación Básica, Instituto Nacional de Cancerología;* [4]*Posgrado en Ciencias Físicas, Universidad Nacional Autónoma de México;* [5]*Instituto de Física, Universidad Nacional Autónoma de México;* [6]*Unidad de Investigación Biomédica en Cáncer INCan/UNAM, Instituto Nacional de Cancerología.*

[a]abril04@ciencias.unam.mx, [b]muniv1250@hotmail.com, [c]efrenhr25@gmail.com, [d]medina@fisica.unam.mx

Research area of interest: Physics and dosimetry of radiotherapy.

Keywords: Fractionated radiotherapy, dosimetry, glioblastoma.

Introduction: The standard treatment for glioblastoma multiforme, the most frequent kind of tumour brain, consists of surgery followed by chemotherapy and radiotherapy [1]. That represents a significant part of the treatment and typically consists of 30 fractions of 2 Gy for a period of about 6 to 7 weeks [2]; however, many different radiation schedules are used and no agreement has been established. The aim of this work is to evaluate brain radiotoxicity from a fractionated irradiation procedure in rat brain to establish a preclinical model that allows the evaluation of the radiobiological response in a model of glioblastoma in rats irradiated with a 6 MV LINAC.

Methods: Male *Wistar* rats were randomized in 3 groups of 5 rats, and irradiated once a week for 3 weeks achieving a total dose of 10, 15 and 20 Gy, respectively. The irradiation was performed using a conic beam (7.5 mm ratio) in isocentric geometry located in the midline of the brain. Brain radiotoxicity was evaluated with histological techniques and microPET molecular imaging using 18-FDG. Radiochromic film EBT-3 located in the top, middle and bottom of a skull phantom, was used for the dosimetric evaluation. The dose distribution was calculated through isocurves obtained with a homemade Python algorithm.

Results and discussion: Dosimetric evaluation showed that the brain receives the highest dose according with the irradiation plan, however, a 17.3 % difference between nominal and irradiation doses was observed. The dose distribution showed dose uniformity at the centre of the irradiation field with dispersion penumbra of 1.7 mm. No significant differences in the 18-FDG uptakes and histological analysis between pre and post- irradiation groups were found.

Conclusions: No significant differences in the radiotoxicity response between different fractionated doses were observed, indicating a favourable result that will be used in the irradiation plan of the tumour model.

References:

[1] Vinchon-Petit, S. et al. 2010. “External irradiation models for intracranial 9L glioma studies”. Journal of Experimental & Clinical Cancer Research.

[2] Jae Ho Kim, M. et al. 1999. “Fractionated radiosurgery for 9L gliosarcoma in the rat brain”. Elsevier Science.

Influence of beam quality on absorbed depth-dose curves in liquid water induced by kilovoltage x-ray beams

A Moreno-Ramírez[1,a], G Massillon-JL[1,b]

[1]*Instituto de Física, Universidad Nacional Autónoma de México*

[a]*adrianamoreno@estudiantes.fisica.unam.mx,* [b]*massillon@fisica.unam.mx*

Research area of interest: A: Physics and dosimetry of radiotherapy

Keywords: Low energy photons, absorbed depth-dose in liquid water, Monte Carlo simulation of absorbed dose to water for low energy x-rays.

Introduction: Kilovoltage x-ray beams are widely used in clinical applications, which include radiotherapy and radiodiagnosis. Radiodiagnosis represents the most important application where 9,549,308 radiological examinations were prescribed for the entire population in Mexico during 2018 [1-2]. Given its transcendence, investigation about the influence of these beam qualities on the photon fluence variation and the high dose gradients, particularly in liquid water, is considered fundamental. The aim of the present work is to evaluate the influence of different beam qualities in the absorbed depth-dose curves in liquid water for some of the NIST M-series x-ray spectra that were previously measured in our lab with a high purity germanium detector [3].

Methods: MC simulations were performed with DOSRZnrc (EGSnrc), $5x10^9$ histories, cut energy Ecut = 1 keV and the M20, M30, M50, M60, M80, M100, M120 and M160 x-ray spectra [3]. Measurements were carried out with a YXLON x-ray unit with 10-160 kV high voltage range and 2-6 mA tube current range, high purity aluminium foils, a homemade water phantom, a farmer ionization chamber type at 61 cm source to surface distance and 1.8 cm diameter field size.

Results and discussion: The Monte Carlo agrees qualitatively with the experiment and differences between them increase as a function of the effective energy or half-value layer (HVL) of the beam. Uncertainties in MC are bigger for those spectra with higher effective energy. Both MC simulation and experimental results show that approximately 5 and 10 cm of liquid water are enough to attenuate 100% of the M20 and M30 beams, respectively. Both beams have effective energies similar to those used in mammography.

Conclusions: Influence of beam quality on absorbed depth-dose curves in liquid water was evaluated through MC simulations and measurements performed with ionization chamber. Results show that the lower the effective energy of the beam, the absorbed dose in water decreases faster, specially for the beams with similar energies to those used in mammography.

Acknowledgments: This project is partially supported by Royal Society - Newton Advanced Fellowship grant NA150212 and PAPIIT- UNAM grant IN115117.

References:

[1] http://sinaiscap.salud.gob.mx:8080/DGIS/ Dirección General de Información en Salud, Sistema de Información en Salud de la Secretaría de Salud, Last update October 2019.
[2] INEGI, September 2019. “Estadísticas de salud en establecimientos particulares 2018”, Comunicado de prensa núm. 472/19, pp. 2.
[3] Hernández-Guzmán A., 2019. “Medida de espectros de rayos-X de bajas energías para la investigación básica y de interés clinico”, Master's Degree Thesis in Science (under revision).

Impact of Detector-specific correction factors in Non-Conventional Radiation Fields for Dose Distribution Calculation in Radiosurgery

Mauricio Missael Sánchez Díaz(1a); Olivia Amanda García Garduño(2b)
(1) Instituto de Ciencias Nucleares; (2)Instituto Nacional de Neurología y Neurocirugíamausandia@gmail.com; *(b)* amanda.garcia.g@gmail.com;

Research area of interest: Physics and dosimetry of radiotherapy.
Keywords: Small Fields Dosimetry,

Introduction: Consistent and traceable reference dosimetry to primary metrological standards is key to the successful of radiotherapy treatment. For conventional radiotherapy has been adopted codes of practice, as Report Series Technicians No. 398 and Protocol TG-51. These dosimetry protocols are based on measurements with reference conditions. [IAEA, 2017]

However currently radiotherapy techniques do not allow this reference conditions because the size of field is less than a 4 cm and the dosimetry is affected as has been extensively discussed in the literature. [IAEA, 2017].

Finally, an international working group of the IAEA in collaboration with the AAPM has developed a guide of standardized recommendations for detectors and dosimetry procedures in small fields based on the absorbed dose in water.

This Code of Practice published in 2017 as "Technical Reports Series No. 483 Dosimetry of Small Static Fields Used in External Beam Radiotherapy"

The methodology proposal to applied a correction factor to the ratio of the detector readings to determine the absorbed dose in water between the clinical and reference fields. These correction factors are of interest because they may modify the dosimetry data used to commissioning treatment planning system (TPS), Garcia-Garduño, et. al. has shown the use of factors for Tissue Maximum Ratio (TMR) and Off-Axis Ratio (OAR) does not have an important impact on the calculated dose distribution by the TPS iPlan RT with the Clarkson algorithm (v.4.1.1, BrainLAB, Germany) with just a simulation spherical lesion.

However, the use of factors for total scattering factors (TSF) has an important impact on monitor units calculations.

Then it is proposed to develop a project to test the impact of the specific detector correction factors in the calculation of dose distributions proposed by the TRS 483 over a several patients treatment and verify the importance of its use in clinical practice in radiosurgery using non-conventional fields radiation.

Methods:

The development of the project involves the simulation of 25 treatment plans with the algorithms available in the INNN, these are: the Clarkson and Pencil Beam method developed by BrainLab. Each treatment plan will be carried out using the specific detector factors proposed by the IAEA and will be repeated disregarding the factor.

A statistical analysis will be carried out to demonstrate the existence of some difference in the dosimetric data in each simulation. The analysis consists of evaluating the dose distributions with the gamma factor; measure and analyze the histograms dose volume, dose distribution, homogeneity index; It is of particular interest to analyze the total dispersion factors and monitor units obtained with the simulations because they are directly related to the dose deposited to patients.

References:

1. IAIEA (2017). Technical Report Series No. 483. Viena.
2. Garcia-Garduño OA, et. al (2018) Detector-specific correction factors in radiosurgery beams and their impact on dose distribution calculations. PLoS ONE 13(5): e0196393

Audit of non-conventional radiation fields applying AAPM/IAEA 483 formalism

Daniel Nolasco Altamirano[1]; Teodoro Rivera Montalvo[1]; Olivia Amanda Garcia Garduño[2]

Centro de Investigación en Ciencia Aplicada y Tecnología Avanzada[1]; Instituto Nacional de Neurología y Neurocirugía[2]

dnalexus89@gmail.com[1]; riveramt@hotmail.com[1]; Amanda.garcia.g@gmail.com[2]

Area of interest: Physics and dosimetry of radiation therapy.

Keywords: Dosimetry of small fields, nanodots.

Introduction: The use of non-invasive procedures such as radiosurgery and stereotactic radiation therapy has helped us to treat tumors, which are based on the application of ionizing radiation to target to treat, whose practice code is given by the IAEA TRS-398[1].

But the development of new equipment for these treatments has benefited in the use of non-conventional radiation fields, which have a great benefit as it reduces the irradiated field in the patient.

However, these non-conventional fields carry dosimetry problems such as the lack of laterally charged particle balance, among others which are not considered in the above codes of practice, which is why the AAPM in conjunction with the IAEA have published a new code of practice, in the series of technical reports No. 483[2],which proposes the use of specific detector correction factors to correct those problems.

One way to corroborate the good use of this formalism is with a quality control such as audits, which are to verify that the absorbed dose delivered by the x-ray generating equipment using some reference detector is according to a 3 % the dose calculated by the planning algorithms.

This work consists of establishing a methodology for conducting an audit using nanodot type detectors, in conventional fields and non-conventional radiation fields.

Methodology:

Development consists of the characterization of nanodots for both conventional and non-conventional fields of radiation.

A 6 MeV Truebeam STX linear accelerator will be used for nanodot irradiation and a MicroStar reader will be used for reading.

The data obtained for conventional radiation fields, as well as those obtained for non-conventional fields, shall be evaluated and the specific detector factors referred to in CoP 483 shall be applied.

Its statistical analysis will be done and compared with the information obtained from the planning systems used in the INNN.

References:

[1] IAEA (2000), TRS-398, Austria.

[2] AAPM/IAEA (2017), TRS-483, Viena.

Emulation of Gynecological Brachytherapy Doses with External Beam

Erich Schnell[1a], Spencer Thompson[1], Terence Herman[1],
Salahuddin Ahmad[1], Tania De La Fuente Herman[1]
[1]*Department of Radiation Oncology, The University of Oklahoma Health Sciences Center*
[a]*Erich-Schnell@ouhsc.edu*

Research area of interest:
A: Physics and dosimetry of radiotherapy
Keywords: High dose rate (HDR), high-risk clinical volume (HR-CTV), organs at risk (OARs), Volumetric Modulated Arc Therapy (VMAT), Intensity Modulated Proton Therapy (IMPT), dose heterogeneity.
Introduction: HDR brachytherapy is standard for boosting dose to cervical cancer after external beam radiation. In the past 20 years, its use slowly declined in favor of advancing external beam technology and SBRT, but outcomes have worsened. Brachytherapy boosted patients showed cause specific and overall survival rates 12.8% and 12.0% better than external beam, respectively. [1] This worse performance by external beam may be due to differences in dose heterogeneity between external beam and brachytherapy plans. Brachytherapy treatments have substantial portions of target volume receiving 200% and 300% or more of the prescription dose Rx, while external beam plans are limited to 110% maximum. The effect on the radiation biological equivalent uniform dose (EUD) when utilizing this level of dose heterogeneity has been calculated to be in the range of 1.15 to 1.30 when compared to uniform dose coverage. [2] This investigation evaluated the performance of external beam therapy methods at emulating the dose heterogeneity in brachytherapy plans. This study was approved by the IRB for use of patient data.
Methods: Data from three patients who received external beam radiation and brachytherapy boosts were utilized. Target volumes from brachytherapy plans were copied to external beam CT scans without applicator and corrected by a physician for accuracy. Two plans per patient utilizing two VMAT arcs were optimized to the target, with one plan achieving a uniform dose coverage, and one attempting to match the V200% and V300% of the brachytherapy plan. Additionally, IMPT plans utilizing a pencil beam scanning system and two lateral beams were optimized with the same set of goals. Additional Proton plans were created to evaluate settings of robustness Single-Field-Optimization (SFO) vs Multi-Field-Optimization (MFO). Comparisons included differences in percentage dose coverage to 90% and 100% of the HR-CTV (D90, D100), doses to 2 cm^3 of each OAR (D2cc), volumes of normal tissues covered by 20% and 50% isodose levels (V20%, V50%), and finally the percent of the target covered by the 200% and 300% Rx isodose levels (V200%, V300%). The greater biologic effect when using proton beam when compared to photon was addressed by the planning system itself, with units of cGy (RBE equivalent) used for an apples-to-apples comparison. When comparing external beam (MV) to Ir192, the interaction is similar for both energy spectrums, and the dose rate for a single fraction delivery in all 3 modalities is similar.
Results and Discussion: All plans had target D90 coverage at or above the Rx dose. The D100 coverage was superior for external beam plans. Critical structure dose changes were mixed, and owed more to geometry differences between CT scans than planning differences, when evaluating the 2 cm^3 volume. The V50 was similar for brachytherapy and escalated photon arc plans, while it was greatly increased for escalated proton plans. Conversely, V20 was similar for proton and brachytherapy plans, while it increased greatly for photon plans. (Figure 1) The V200% doses were matched or better for two patients, with proton performing slightly better. The V300% was not met for any patient, with coverage between 1-5% for external beam and between 10-27% for brachytherapy. Photon plans performed better for the V300% metric.
Conclusion: Although the volume to 200% of the Rx may be matched, the extreme doses in the center of the brachytherapy plan are still unique to that modality. While external beam methods are popular for brachytherapy replacement, and may show some potential for emulating the brachytherapy distribution, brachytherapy should remain gold standard for boosting gynecologic cancer patients.

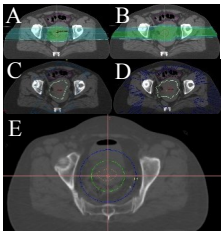

Figure 1. Green is 50% and blue is 20% isodose lines surrounding target volume for a single patient using: a uniform coverage proton plan (A), an escalated dose proton plan (B), a uniform coverage photon plan (C), an escalated photon plan (D), and the original brachytherapy plan (E).

References:
[1] Han K, *et.al*. Trends in the utilization of brachytherapy in cervical cancer in the United States. International Journal of Radiation Oncology, Biology, Physics. 2013;87(1):111-119.
[2] Dale R, Coles P. Allowance for the radiobiological effects of dose gradients in gynaecological applications. Radiotherapy and Oncology. 2001;60:S7.

Out-of-Field Dosimetry in IMRT with OSL

Rojas-López J A [1,2,a], Agüero H [2,b], Mancuzo A [2,c], and Binia S [2,d]
1 Instituto Balseiro, Universidad Nacional de Cuyo, 8400 San Carlos de Bariloche, Argentina
2 Fundación Escuela de Medicina Nuclear, 5500 Mendoza, Argentina
a alexrojas@ciencias.unam.mx, *b* haguero2626@gmail.com *c* arielmancuzo@gmail.com,
d sergiobinia@gmail.com

Research area of interest:
A: Physics and dosimetry of radiotherapy

Keywords: OSL, IMRT, radiotherapy, low dose.

Introduction: Accurate radiation dose measurements at non-target tissues in external beam radiation oncology treatments has become a relevant issue in modern clinical practice. In these cases, doses are less than 20% the prescribed dose to planning target volume (PTV). Huang *et al.* [1] showed dose underestimation in 50% in out-of-field doses measured with TLD and calculated by the treatment planning system (TPS) Pinneacle's Reverse Planning Machine Direct Parameter Optimization (DMPO) algorithm. Howell *et al.* [2] showed dose underestimation in 40% by Eclipse's analytical anisotropy algorithm (AAA). In this work we compare dosimetric response of the OSL nanoDot versus ionization chamber (IC) and TPS MIRS v.5.1 semi-empirical scatter integrator algorithm and Eclipse (AAA) in cases of water phantom, anthropomorphic phantom CIRS and *in vivo* measurements.

Methods: Calibration curve (low and high doses) was established following TG-191 AAPM international guideline. OSL nanoDots (10x10x2 mm3) were exposed in three sets of experiments: I) in a water tank phantom for a perpendicular orientation to 6 MeV photon beam (Varian Clinac iX). Exposures (SSD 100 cm, depth 10 cm, field size 10x10cm2) were carried out with open field and adding a scatter element (wood's metal compensator filter) at 1.5, 3.5 and 6.5 cm from field edge. II) in anthropomorphic thorax CIRS phantom for an IMRT plan with compensator filters. Measurements were made at 4 cm out-of-treatment field. Measured doses were compared with the TPS calculated doses: MIRS v.5.1 and Eclipse and IC Farmer 2571 measured dose. III) in IMRT plan for 14 *in vivo* intracavitary measurements were carried out (on average 9 cm distance out-of-treatment field). Dosimeters were placed in oral cavity and rectum. Measured doses were compared with TPS MIRS 5.1 calculated doses.

Results and discussion: I) In water phantom, OSL out-of-field measured doses followed with good agreement IC measured doses. Absolute differences (evaluated as $\frac{Dose-Dose(CI)}{Dose(CI)} \times 100$) showed that both TPS MIRS and Eclipse underestimated doses up to 55% and 40% respectively in presence of scatter elements up to 6.5 cm from field edge (figure 1). II) In anthropomorphic phantom, in terms of absolute differences, OSL measured dose followed IC up to 3%. MIRS underestimated doses up to 35%. III) for *in vivo* measurements, mean difference between OSL and TPS MIRS showed absolute difference dose underestimation of 42%.

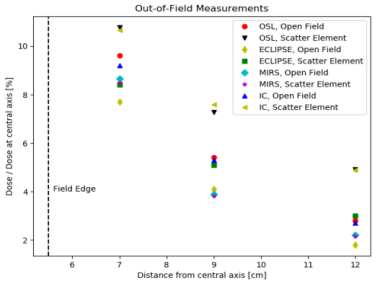

Figure 1. Case I: Water phantom. Comparison between OSL and TPS MIRS and Eclipse dose ratio out-of-field and at central axis. Measurements are shown with and without scatter element. Exposures were carried out on Varian Clinac X6.

Conclusions: Different experiments showed a reliable response of OSL nanoDot versus IC. Both TPS MIRS and Eclipse showed limitations to determine and to model out-of-field dose with differences up to 55%. It is remarkable that unlike Bordy *et al.* [3] we did not find over-estimation of dose by OSL due to spectral changes (at low energies) presented in out-of-treatment field. It is important to continue researching dosimetry in anatomical regions at low doses due to probable long-term biological effects.

References:
[1] Huang JY, Followill DS, Wang XA, Kry SF, (2013). J Appl Clin Med Phys 14(2): 186-197.
[2] Howell RM, Scarboro SB, Kry SF, Yaldo DZ, (2010). Phys Med Biol 55(23): 7009-7023.
[3] Bordy JM, Bessieres E, d'Agostino C, Domingo F, *et al.* Radiat Meas 57:29-34

Implementation of total body irradiation using VMAT

Erika Muñoz-Moral[1,a], Alejandro Rodríguez-Laguna [2,b], Jose Alejandro Jiménez-Acosta[2,c]
[1]*Facultad de Ciencias, Universidad Nacional Autónoma de México, CDMX.* [2]*Médica Sur, Tlalpan, CDMX.*
[a] erika.mm@ciencias.unam.mx, [b] arlaguna@ciencias.unam.mx, [c] jajimenez@ciencias.unam.mx

Research area of interest: Physics and dosimetry of radiotherapy.
Keywords: TBI, VMAT, radiochromic film dosimetry.

Introduction: Total body irradiation (TBI) is well-established component of several conditioning regimens required prior to bone marrow or hematopoietic stem cell transplantation. The 2-field technique at an extended SSD, which is the conventional way to impart it, has serious inconvenient. For example, lack of reproducibility, poor dose homogeneity and technical difficulties to reduce the lung dose. The aim of this work is to validate the imparted doses in TBI technique using VMAT in Médica Sur.

Methods: An anthropomorphic phantom ATOM 702-D, CIRS (Norfolk, Virginia) was used. We added the upper extremities of the phantom using a homemade water equivalent material, (Fig. 1A). The phantom was scanned using a CT scanner GE 580RT (General Electric Company). The TBI-VMAT was calculated and optimized using the treatment planning system (TPS) Eclipse™ V.11.031 (Varian Medical Systems, Palo Alto, CA).

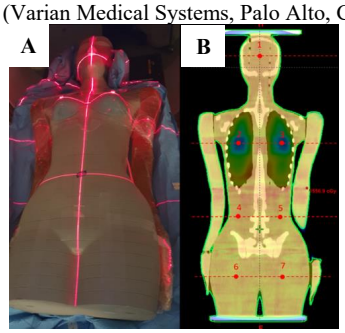

Figure 1. (A) Anthropomorphic phantom ATOM 702-D, CIRS (Norfolk, Virginia) (B) Coronal view of TBI-VMAT planned dose distribution; red dots indicate isocenters.

We used and adapted the VMAT plan configuration proposed by Springer et al. [1]. The planned doses were compared with the imparted doses in the phantom using Gafchromic EBT3 film (Ashland ISP, Wayne, NJ). Film was calibrated in water using a 6 MV photon beam of a Varian Clinac iX linear accelerator n/s 1227 (Varian Medical Systems, Palo Alto, CA) in a dose range of 0-3 Gy. Films were digitized using Epson® Expression® 11000XL flatbed scanner. Red channel calibration curve was fitted using a grade-3 polynomial function. EBT3 film were placed inside the phantom in planes corresponding to head, lungs, liver and pelvic region, and were irradiated with one single fraction (2 Gy) of the achieved TBI-VMAT plan.

Results and discussion: Arms mean HU was 112 ± 8.5 HU, consistent with mean HU of a human arm considering fat, muscle and bone tissues. The resulting TBI-VMAT plan consisted in 7 isocenter (Fig. 1B), 2 full arcs and 16 half arcs covering the PTV comprising the whole phantom. According with TPS dose-volume histograms, 97.8% of the PTV received 95% of the planned dose (12 Gy in 6 fractions). The planned mean dose to the phantom lungs was 10.03 Gy. These values were consistent with those reported in reference [1]. Figure 2 shows TPS and measured film doses. In the selected phantom planes, lungs mean doses were 168.2±15.9 cGy (TPS) vs. 168.2 ± 12.5 cGy (EBT3 film); head, liver and pelvis mean doses were, 226.3 ± 6.3 cGy (TPS) vs. 220.3 ± 13.4 cGy (EBT3 film). Film dose uncertainties were calculated according with Devic S. et al [2].

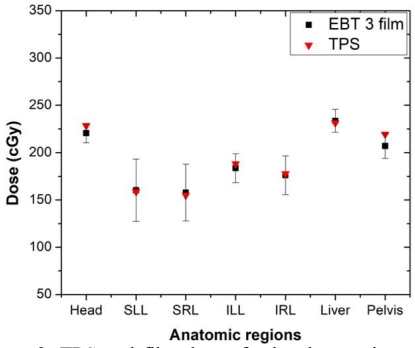

Figure 2. TPS and film doses for head, superior portion of left (SLL) and right (SRL) lung, inferior portion of left (ILL) and right (IRL) lung, liver and pelvis.

Conclusions: TBI-VMAT plan that was achieved provides a satisfactory dose coverage, dose distribution and effective lung dose sparing. Plan optimization and dose calculation took roughly 30 h. This work demonstrates consistency between doses shown by the TPS and measured doses with EBT3 film, and the viability of implementing clinically TBI using VMAT in Médica Sur.

References: [1] Springer, Andreas, et al. "Total body irradiation with volumetric modulated arc therapy: dosimetric data and first clinical experience." Radiation Oncology 11.1 (2016): 46. [2] Devic S. et al., "Dosimetric properties of improved GafChromic films for seven different digitizers", Med. Phys. 31 (9): 2392-2401, (2004).

Personal dose assessment using thermoluminescent dosimetry

Concepción Laura Silva Fierro[2,a], David Cortés Elvira[2,b], Eduardo López-Pineda[1,c] and María-Ester Brandan[1,d]

[1]*Instituto de Física, UNAM,* [2]*Facultad de Ciencias, UNAM*

[a] laura_silva@ciencias.unam.mx, [b] david_cortes@ciencias.unam.mx, [c] edlope@fisica.unam.mx, [d] brandan@fisica.unam.mx

Research area of interest:
F. Radiation protection and health physics
Keywords: Thermoluminescent dosimetry, personal dosimetry

Introduction: The radiation levels received by occupationally exposed personnel (OEP) need to be monitored. The recommended magnitude to quantify the exposure is the Effective Dose (E), which considers the spatial distribution and radiation type received by the individual; its special unit is called Sievert (Sv). E can be determined from measurements of air kerma (K_{air}), considering of the type and energy of the radiation field, and appropriate conversion coefficients. The International Commission on Radiological Protection has established a yearly limit of 20 mSv for working personnel and 1 mSv for the general public [1]. We present the development of two dosimetry systems that determine E and the effective photon energy.

Methods: Two personal dosimetry devices were elaborated, using thermoluminiscent dosimeters TLD-100 or a TLD-100/TLD-300 combination. Both devices consisted on dosimeters inside small plastic boxes (5.5 x 3.2 x 0.7 cm^3). The first device was divided into 4 regions, each region having 2 TLD-100 under different filters (1 and 0.6 mm Cu, 1 mm Al and air). This device was calibrated from 0.1 to 2.2 mGy of K_{air} using different beams with energies between 15.1 and 1250 keV. The ratios between the signals of the dosimeters, beneath different filters, were used as an energy detector; taking advantage of the energy and material dependence of attenuation. The second device, called Koph/Shin, had 4 dosimeters (2 TLD-100 and 2 TLD-300). This device was calibrated at K_{air} from 0.1 to 40 mGy for photon energies between 13.5 and 63.4 keV. The shape of the glow curve of the TLD-300 was used as an energy detector [2]. The glow curve was analyzed by 3 methods.

TLDs were annealed at 400°C for 1 hour (TLD-100/TLD-300) followed by rapid cooling to room temperature and annealing at 100°C for 2 hours (TLD-100). Dosimeters were read in a Harshaw 3500 reader, under N_2 flux, from room temperature to 300°C (TLD-100) and 400°C (TLD-300) at 8°C/s rate.

Results and discussion: The first device enabled to determine E with about 35% relative expanded uncertainty (k=2); it was used by personnel at a nuclear medicine department of a national medic center in Mexico City, and the measured energies were similar to the nominal energies prevailing at the working place (26% relative expanded uncertainty and 30% maximum difference).

The Koph/Shin device allowed to determine E with about 14% relative expanded uncertainty (k=2) and energy was determined with 24% uncertainty. Currently, a calibration of the Koph/Shin device is being completed to get better performance and include a wider range of energies.

Conclusions: We have developed a pair of personal dosimetry devices to determine E using TL dosimetry. Results have shown the viability of both methods complying with ICRP, which recommends that uncertainty (k=2) must be between -33% and +50%).

References:

[1] Petoussi-Henss, N., et al. "Conversion coefficients for radiological protection quantities for external radiation exposures." Annals of the ICRP 40.2-5 (2010): 1-257.

[2] Muñoz, I. D., et al. "Evolution of the CaF_2: Tm (TLD-300) glow curve as an indicator of beam quality for low-energy photon beams." Physics in Medicine & Biology 60.6 (2015): 2135.

Dosimetric evaluation of a dental 70 kV X-ray tube

Sandra A. Hernández[1,a], Eduardo López Pineda[2,b], Luis Alberto Medina[2,3,c].
[1]*Facultad de Ciencias, UNAM;* [2]*Instituto de Física UNAM;* [3]*Laboratorio de Física Médica e Imagen Molecular, Instituto Nacional de Cancerología.*
[a]sandra.hg@ciencias.unam.mx, [b]edlope@fisica.unam.mx, [c]medina@fisica.unam.mx.

Research area of interest: Physics and dosimetry of radiotherapy.

Keywords: kilovoltage x rays, dosimetry, dental X-ray tube, cell culture irradiation.

Introduction:

Photons from x-rays tubes of medium and low kV have been used to evaluate its effect in cell cultures and small experimental animals. The dose estimation requires the implementation of dosimetric methods. The TG-61 protocol establishes the procedures to implement a dosimetry for kilovoltage x rays (tube potential: 40–300 kV) using calibrated ionization chambers in terms of air (air kerma or exposure) to determinate experimentally the dose to water and air kerma.

Here we report the dosimetric characterization of an X-ray tube, used in dental radiology, in terms of dose to water and aire kerma.

Methods: The characterization of a dental X-ray tube of 70 kVp was made based on the AAPM's TG-61 protocol, using a parallel flat ionization chamber (Radcal 20X6-6M) to measure exposure values and estimate dose to water rate, air kerma rate and HVL (half value layer) at a fixed SSD. The uniformity of the radiation field was characterized using radiochromic film XR-QA2.

Results and discussion: Experimental procedures determined an air kerma rate of 4.69 mGy/s and dose to water rate of 5.67 mGy/s, with a HVL = 1.69 mm Al with an effective energy of 28 +/- 0.2 keV. The radiation field was uniform with minimal penumbra. The results showed a limited dose of 17 mGy in the longest time period allowed for the equipment (3 sec) in a single shot that could be useful to evaluate radiation effects at low dose in cell cultures. Evaluation of the effectiveness of this x-ray tube will be studied in future experiments with cancer cell cultures.

Conclusions: The dosimetric characterization of this 70 kVp x-ray tube, designed for dental radiology, shows potencial for it use in cell culture irradiation for preclinical research.

References:

[1] López E. Reporte interno FE085 2017. Calibración Cruzada de una cámara de ionización Radcal para Mamografía. Instituto de Física, Universidad Nacional Autónoma de México.

[2] Ma, C. M., Coffey, C. W., DeWerd, L. A., Liu, C., Nath, R., Seltzer, S. M., & Seuntjens, J. P. (2001). AAPM protocol for 40–300 kV x-ray beam dosimetry in radiotherapy and radiobiology. Medical physics, 28(6), 868-893.

[3] Niroomand-Rad, A., Blackwell, C. R., Coursey, B. M., Gall, K. P., Galvin, J. M., McLaughlin, W. L., & Soares, C. G. (1998). Radiochromic film dosimetry: recommendations of AAPM radiation therapy committee task group 55. Medical physics, 25(11), 2093-2115.

Functional network of patients with temporal lobe epilepsy: characterization of the database

Wady. A. Ríos[1,2,a], Ana Leonor Rivera[1,2,b], Jose F. Barruecos[3,4,c], Horacio Sinties[5,d], Alejandro Frank[1,2,e] and Markus Müller[1,6,f]
[1] Centro de Ciencias de la Complejidad, Universidad Nacional Autónoma de México.
[2] Instituto de Ciencias Nucleares, Universidad Nacional Autónoma de México.
[3] Instituto Neurológico de Colombia, Medellín, Colombia.
[4] Universidad del CES, Medellín Colombia.
[5] Instituto Nacional de Ciencias Médicas y Nutrición Salvador Zubirán.
[6] Centro de investigación de Ciencias, Universidad Autónoma del Estado de Morelos.
[a]wadyarh@hotmail.com, [b]ana.rivera@nucleares.unam.mx, [c]jfzb78@gmail.com,
[d] sentiesmadridh@gmail.com, [e]alejandro.frank@gmail.com, [f]muellerm@uaem.mx

Rersearch area of interest: Biological physics, physiological measurements and mathematical methods in medical physics**.**

Keywords: electroencephalogram (EEG), electrocardiogram (ECG), time series analysis, temporal lobe epilepsy.

Introduction:
Despite 80 years of research in EEG related to epilepsy, the brain dynamics during a seizure has not been entirely explored.
There are many controversies about the different methods of analysis, measurement techniques and theoretical hypothesis. Therefore, epilepsy phenomena are still an issue of vivid ongoing research.
The goal of this project is to contribute constructively to this area, formulating specific questions, applying different measurement techniques and quantitative analysis based on recent findings.

Methods:
In the present project, a database of EEG and ECG recordings of patients with temporal lobe epilepsy was generated, with the support of the Colombian Neurological Institute and the National Institute of Medical and Nutrition Sciences Salvador Zubirá of Mexico.
The records were classified by expert neurophysiologists in the area. The records of EEGs and ECGs were properly pre-processed [1,2] for their respective quantitative analysis. We studied the variability and the time evolution of the peri-ictal transition of the functional network. Additionally, we investigated if the heart rate time series may serve as a reliable biomarker for the early warning of epileptic seizures.

Results and discussion:
We expect that the outcome of this project will help to deepen and widen the scope about the brain dynamics before, during and after an epileptic seizure. Moreover, to set the feasible link between epileptic seizures and sleep disorders in order to find a biomarker for seizures via ECG recordings.

Reference:
[1] Ríos-Herrera, W.A., Joaquín Escalona, Daniel Rivera López, and Markus F Müller. On the estimation of phase synchronization, spurious synchronization and filtering. Chaos: An Interdisciplinary Journal of Nonlinear Science, 26(12): 123106, 2016.

[2] Rios-Herrera, W.A., Olguín-Rodriguez, P.V., Corsi-Canrera, M., Escalona, J., Marín-García, A.O., Rivera-López, A.L., Rivera-López, D., Zapata-Berruecos, J.F., Müller, M.F., The influence of EEG references on the analysis of spatio-temporal interrelation patterns, submitted to Frontiers in Neuroscience, 2019.

Parkinson´s Disease Image Analysis

R.I. Rojas-Jiménez[1, a], A. Muñoz-Diosdado[1, b], J.A. Martínez-Castro[2, c], M. Rubio-Osornio[3, d].

[1]Unidad Profesional Interdisciplinaria de Biotecnología, Instituto Politécnico Nacional, [2] Centro de Investigación en Computación, Laboratorio de Simulación y Modelado, Instituto Politécnico Nacional, [3] Instituto Nacional de Neurología y Neurocirugía Manuel Velasco Suárez, Mexico City, Mexico.

[a]rodrigoroji.97@gmail.com, [b]amunozdiosdado@gmail.com, [c]macj@cic.ipn.mx, [d]ruomnd@yahoo.com.mx

Research area or interest:
D. Biological physics, physiological measures and mathematical methods.

Keywords: Parkinson, image analysis, mathematical methods, central nervous system, neurodegenerative damage.

Introduction: Parkinson´s disease (PD) is classified as the second neurodegenerative disease (NDD) with higher incidence in Mexico, after Alzheimer. It affects the central nervous system, specifically the locus coeruleus (LC) and substantia nigra (SN) in brainstem nuclei. PD is characterized for its motor symptoms such as bradykinesia, rigidity and tremors. Non-motor symptoms include: depression, hyposmia and dementia [1-2].

Many of the clinical symptoms are attributed to neurodegenerative damage (ND) caused by early death of dopaminergic cells located in SN. Necrosis occurs when α-synuclein proteins become intracellular abnormal aggregates in nervous cells (Lewy bodies). Some authors highlight the importance of iron and copper molecules in this process and associate it with neurodegenerative [2-3]. In recent years, the use of computational tools and mathematical methods have become popular in medical sciences, opening possibilities for new and multidisciplinary analysis, such as image analysis of histological images [4].

Methods: In the present project we implement image analysis to fit images from histological cuts of SN, obtained from threated mice with microinjections of iron nanoparticles. Later, we used those images to compute an artificial intelligence algorithm, with a convolutional neural network (CNN) architecture, which uses the input images for supervised training, using a Haar cascade algorithm. Thus, a simple mathematical model was developed, for further analysis and future research.

Results and discussion: After the training step, the algorithm was capable of identifying iron aggregates linked with ND. Furthermore, mathematic models give the opportunity to partially simulate biological systems, this could be a new approach to such problems.

Conclusions: The merge between medical sciences, computational sciences and medical physics eases the histological analysis and provides new tools for diagnostic, further analysis of these data involves a multidisciplinary approach, this implies new ideas for the diagnosis of PD.

All applicable international, national, and/or institutional guidelines for the care and use of animals were followed.

References:

[1] Estrada, I., Martínez, H., 2009. “Diagnóstico y tratamiento de la enfermedad de Parkinson”, Avances No. 25 vol. 8.

[2] Kalia, V., Lang, A., 2015. “Parkinson´s disease”, Lancet 386: 896-912.

[3] Zecca, L., et al., 2004. “The role of iron and copper molecules in the neural vulnerability of locus coerlus and substantia nigra during aging”, PNAS No. 26 vol. 101.

[4] Höfner, H., et al., 2018. ”Deep learning nuclei detection: A simple approach can deliver state-of-the-art-results”, Elsevier, Computerized medical imaging ang graphics 70(2018) 43-52.

ECG Peak-Detector and Waveform Analysis Algorithm

R.I. Rojas-Jiménez[1, a], A. Muñoz-Diosdado[1, b], J. A. Zamora-Justo[1, c].
[1]Unidad Profesional Interdisciplinaria de Biotecnología, Instituto Politécnico Nacional, Mexico City, Mexico.
[a]rodrigoroji.97@gmail.com, [b]amunozdiosdado@gmail.com,
[c]zamora.justo@outlook.com

Research area of interest:
D. Biological physics, physiological measures and mathematical methods.
Keywords: ECG, waveforms, time interval, time series, signal analysis.

Introduction: Electrocardiogram (ECG) signals come from the combined action potential of the cardiac muscle tissue, it begins in the sinoatrial node and ends in the Purkinje cells. This potential travels to the skin and can be captured by electrodes placed in the Einthoven triangle. ECG serves as a diagnostic method for cardiovascular disease (CVD), physicians use the waveforms and interval between complex R-R and QRS to determine possible CVD [1-2].

Various authors use common signal analysis methods such as Fast Fourier Transform (FFT) and correlation coefficients (CC) to analyze ECG time series, which is a signal-perspective of the problem. Nevertheless, peak-detecting algorithms could be useful for physicians to diagnose bradycardia, tachycardia and arrythmias [2-3].

Methods: In the present work, we developed a peak-detector algorithm to measure the time between each waveform, thus to compute the integral of each one, and providing physicians with a powerful tool to analyze ECG time series more efficiently. Thus, obtaining relevant data for possible diagnostics and further mathematical analysis using multifractal and complex networks technics.

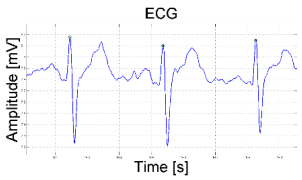

Figure 1. ECG sample.

Results and discussion: ECG time series were obtained by a Holter monitor with sample frequency of 1000, each waveform was labeled individually and the time interval between R-R and S-T intervals was computed. Furthermore, complex analysis was performed, using methods of non-linear dynamics, such as multifractal analysis.

Conclusions: ECG waveform analysis is critical for CVD diagnosis, computing the process of peak-detection and counting peaks increases the tools which physicians can use and reduces error and analysis time. Additionally, mathematical analysis can be performed in the obtained data.

All procedures performed involving human participants were in accordance with the ethical standards of the institutional and/or national research committee and with the 1964 Helsinki Declaration and its later amendments or comparable ethical standards.

Informed consent was obtained from all individual participants involved in the study.

References:

[1] Khan, G., 2006. "Encyclopedia of heart diseases", Elsevier, California, pp. 1-3.
[2] Ranji, R., Kaur, I., 2013. "Electrocardiogram Signal Analysis – An Overview", International Journal of Computer Applications, (0975-8887), Vol. 84 no. 7.
[3] Shim, E., et al., 2004. "Mathematical Modeling of Cardiovascular System Dynamics using a Lumped Parameter Method", Japanese Journal of Physiology, Vol. 54, 545-553.

Sleep in Crayfish: Relationships between Brain Electrical Activity and Autonomics Variables

Mireya Osorio-Palacios, Laura Montiel-Trejo, Iván Oliver-Domínguez, Jesús Hernández-Falcón and Karina Mendoza-Ángeles
Departamento de Fisiología, Facultad de Medicina, UNAM, México
palaciosmireya11@gmail.com, lau.montiel21@gmail.com, i.oliver.dom@gmail.com, jesushf@unam.mx, xolotlk@gmail.com

Research area of interest: D. Biological physics, physiological measures and mathematical methods
Keywords: Invertebrate, behavior, electrophysiology, respiration, cardiovascular, wavelet transform.
Introduction: In vertebrates like mammals and birds two types of sleep have been described: rapid eye movement (REM) sleep and no-REM sleep. Each one has a specific brain electrical activity and is accompanied by changes in cardiac and respiratory frequencies. Slow wave sleep has been described in some invertebrates [1,2]. Crayfish sleep fulfills behavioral and electrophysiological criteria defined for vertebrates [3]. In this animal, heart and respiratory frequencies are modified by diverse changes in its environment during wakefulness [4]. However, we do not know if this animal has sleep phases and what is the behavior of cardiorespiratory activity during sleep. The main goal of this work was to search for sleep phases in crayfish, and if there is any correlation with cardiorespiratory activity.
Methods:
Biological material: We used adult male crayfish *Procambarus clarkii* in intermolt. In cold anesthetized animals we implanted electrodes on deutocerebrum, both gills chambers and cardiac sinus. After two days of recovery, we recorded, simultaneously, behavioral and electrical activity. All the experiments involving animals have been approved by the Commission of Investigation and Ethics of Facultad de Medicina, UNAM (Project number 023).
Behavioral Recordings: To determine crayfish positions, we videotaped them continuously during periods of 8 h.
Behavior Analysis: We analyze the video tapes considering the animal position (walking, immobile or lying on one side) and the day hour, and then we associated each one with the electrophysiological state.
Electrical Recordings: We recorded brain electrical and cardiorespiratory activity using a sampling frequency of 2000 Hz. To analyze brain electrical activity, we used wavelet transform.
Results and discussion:
We measured cardiac and respiratory rates during all recording conditions. We found that crayfish can sleep lying on one side or when it is motionless.
The depth of sleep (measured as the power of electroencephalographic activity) changes over time and is accompanied by oscillations in cardiorespiratory frequency.
Conclusions: The analysis of brain electrical activity and autonomic variables such as cardiorespiratory frequency indicate that in crayfish there are phases of sleep.

References:
[1] Mendoza-Angeles K, Cabrera A, Hernández-Falcón J, Ramón F. 2007, Slow waves during sleep in crayfish: A time-frequency analysis. *Journal of Neuroscience Methods* **162**(1-2):264-271.
[2] Mendoza-Angeles K, Hernández-Falcón J, Ramón F. 2010, Slow waves during sleep in crayfish. Origin and spread. *Journal of Experimental Biology* **213**(12), 2154-2164.
[3] Ramón F, Hernández-Falcón J, Nguyen B, Bullock TH. 2004, Slow wave sleep in crayfish. *Proceedings of the National Academy of Sciences USA* **101**(32):11857-11861.
[4] Schapker H, Breithaupt T, Shuranova Z, Burmistrovd Y, Cooper, Robin L. 2002, Heart and ventilatory measures in crayfish during environmental disturbances and social interactions. *Comparative Biochemistry and Physiology* **131**: 397-407.

XVI Mexican Symposium On Medical Physics
Physics in Precision Medicine: Advances in Imaging and Therapy

Facial Palsy Estimation Algorithm

Martínez-Angeles W. L.,* Castellanos-Alvarado E. A., and García-Ramírez M. A.†
Research Centre for Applied Science and Technology, Universidad de Guadalajara,
Blvd. Marcelino García Barragán 1421, 44430, Guadalajara, Jalisco, México
(Dated: December 12, 2019)

Reserch area of interest:
D. Biological Physics, Physiological Measurements and Mathematical Methods in Medical Physics.
Keywords: Facial Palsy, Motor Fibers, Cranial Nerve, Quantification, Muscle Trajectory.

Introduction: The facial nerve is a mixed nerve that performs motor sensory and parasympathetic fibers. It is one of the most common cranial nerves implicated in disorders that considers congenital, traumatic, infectious, inflammatory and neoplastic disorders [1]. As a consequence, a quantification method for facial palsy, a disease that results from the abnormal state of the facial nerve, was developed. The method that we propose uses the muscle trajectory information in order to perform a comparison between the right and left side of the face starting from the sagittal plane. In addition, a statistical analysis is performed and thus it is possible to obtain information about the muscle trajectory that will allow us to know the state of the facial nerve.

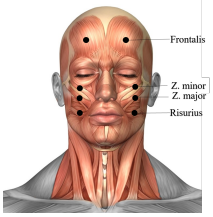

FIG. 1. Facial muscles front view. The circles show the location of the sensors (on the frontal muscles, minor zygomatic, risorius and the major zygomatic). Illustration by StockTrek Images

Methods: To obtain information in regard to the facial palsy, we propose an algorithm that will read a series of sensors distributed across the face in order to read the state of the muscle in real-time. In here, the algorithm takes 500 samples of the muscle trajectory in 6.06 sec. Once we have obtain the state of the nerve, a statistical analysis that encompassed the standard deviation as well as mean for each muscle is obtained. Furthermore, the correlation for the muscle, thresholds, facial asymmetry and muscle trajectory correlation are normalized as shown in Fig. 2.

Results and discussion: Once the algorithm has analyzed the muscle trajectory, it will depict bits of the face muscle in which it is possible to infer if the person has some damage (See Fig. 2a) and it here the person has some issues due to facial palsy (see Fig. 2b). Figure 2a) display a swift slope that indicates that the muscles are healthy. In contrast, Fig. 2b) shows that the slope grows slowly and a hectic behaviour is displayed indicating that the face has had an issue at muscular level. According to the graphs generated by the algorithm when the face is in a normal state, on average, the response speed from the point of maximum relaxation, to the point of maximum contraction is 2.49 sec while for the injured muscles it was 3.52 sec. It was also observed in the experimental data that when the correlation is high, the data dispersion increases as shown in Fig. 2a).

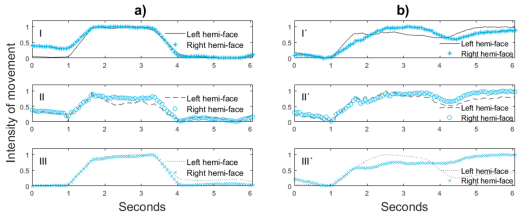

FIG. 2. Algorithm readings depicts the intensity of the frontal muscle movement in a healthy a) and unhealthy b) person. The signals are normalized and plotted as a function of time. In both graphs are defined "I" the components in "x" of the muscular trajectory, "II" the components in "y" and in "III" the components are presented in "z". It is possible to infer the behaviour for the healthy person and the odd for the ill one.

Conclusions: Accurate facial palsy measurement plays a key role in the disorder treatment. According to the results provided by the system, healthy faces must show a high correlation as well as a large standard deviation, correlation coefficient and statistical mean. This is why, the face symmetry will display a healthy behaviour otherwise the symmetry will be severely affected displaying an abnormal and hectic behaviour.

References:

[1] Al-Zwaini, I. J., & Hussein, M. J. (2019). Introductory Chapter: Facial Nerve-An Overview. In Selected Topics in Facial Nerve Disorders. IntechOpen.

* wendylmtz07@gmail.com
† Corresponding author: mario.garcia@academicos.udg.mx

Dominant vs Submissive: Autonomic-like responses in crayfish

Iván Oliver-Domínguez, Aidee Lashmi García-Kroepfly, Mireya Osorio-Palacios, Jesús Hernández-Falcón, Karina Mendoza-Ángeles.

Departamento de Fisiología, Facultad de Medicina, UNAM.

i.oliver.dom@gmail.com, lashmig@gmail.com, palaciosmireya11@gmail.com, jesushf@unam.mx, xolotlk@gmail.com

Research area of interest: Biological physics, physiological measures and mathematical methods.

Key words: autonomic responses, heart rate, heart rate variability, time series analysis, crayfish interactions.

Introduction: Under laboratory conditions, the social interactions between triads of crayfish result in the establishment of a hierarchical order with one animal being the dominant and the others becoming submissive (1 and 2 respectively) [1]. Some authors [2][3] have reported changes in the cardiorespiratory electrical activity associated with social interaction. This seems to indicate that crayfish presents autonomic-like responses during agonistic encounters, as it happens in vertebrates, but without an autonomic nervous system being reported. A tool that allows the study of the autonomic nervous system of vertebrates and the adjustments made in physiological conditions is the analysis of heart rate time series [4]. In particular, the heart rate variability (HRV), which is based on the study of the intervals between each beat and whose fractal and nonlinear characteristics contribute to a detailed description of the cardiac dynamics [5].

The aim of this work was to analyze cardiorespiratory electrical activity of adult crayfish *Procambarus clarkii* during social interactions in order to compare the dynamic of these variables between dominants and submissive.

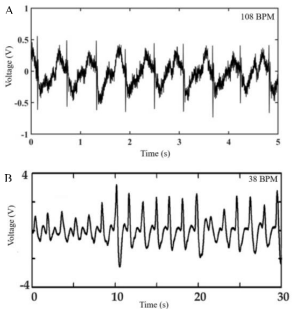

Figure 1. Cardiorespiratory electrical activity of resting crayfish; (A) Cardiac electrical activity for a period of 5 seconds; (B) Respiratory electrical activity for a period of 30 seconds.

Methods

Biological preparation: Triads of adult crayfish (*Procambarus clarkii*) in intermolt, with a weight and size difference less than 5%, were used. Triads were implanted with Pt-Ir electrodes in the cardiac sinus and one branchial chamber (animals were cold anesthetized). Behavioral and electrophysiological recordings were made simultaneously. All the experiments involving animals have been approved by the Commission of Investigation and Ethics of Facultad de Medicina, UNAM (Project number 023).

Behavioral recordings: Triads were placed in an arena and videotaped during one hour. After obtaining the recording of the social interaction, the behavior was analyzed and the hierarchical order of the triads members was determined.

Electrophysiological records: The electrical activity of the heart and respiratory muscles was recorded. The signals were processed by standard methods. Data was stored on a computer for the analysis.

Results and discussion: The dynamic of the cardiorespiratory electrical activity of adult crayfish *Procambarus clarkii* during social interaction is different between dominants and submissive.

Conclusions: Crayfish presents autonomic-like responses during agonistic encounters that seem to depend on the hierarchical order.

References:

[1] Delgado-Morales G, Hernández-Falcón J & Ramón F. (2004) Agonistic behaviour in crayfish: the importance of sensory inputs. Crustaceana, 77(1), 1-24.

[2] Schapker H, Breithaupt T, Shuranova Z, Burmistrov Y & Cooper RL. (2002) Heart and ventilatory measures in crayfish during environmental disturbances and social interactions. Comparative Biochemistry and Physiology Part A: Molecular & Integrative Physiology, 131(2), 397-407.

[3] Hernández-Falcón J, Basu AC, Govindasamy S & Kravitz EA. (2005) Changes in heart rate associated with contest outcome in agonistic encounters in lobsters. Cellular and molecular neurobiology, 25(2), 329-343.

[4] Fossion R, Rivera AL & Estañol B. (2018). A physicist's view of homeostasis: how time series of continuous monitoring reflect the function of physiological variables in regulatory mechanisms. Physiological measurement, 39(8), 084007.

[5] Rivera AL, Estañol B, Sentíes-Madrid H, Fossion R, Toledo-Roy JC, Mendoza-Temis J & Frank A. (2016) Heart rate and systolic blood pressure variability in the time domain in patients with recent and long-standing diabetes mellitus. PloS one, 11(2), e0148378.

High dose-rate effect (1200 MU min^{-1}) on delay expression of cytokine pro-inflammatory IL-1β in rats brain.

Ramiro Humberto Aguirre-Maldonado[1a], Paola Ballesteros-Zebadúa[2b], Alejandro Rodríguez-Laguna[3c], Mercedes Rodríguez-Villafuerte[1d], Javier Franco-Pérez[2e].

[1]*Instituto de Física – Universidad Nacional Autónoma de México,* [2]*Instituto Nacional de Neurología y Neurocirugía "Manuel Velasco Suárez",* [3]*Hospital Médica Sur.*

[a]rh.aguirre15@gmail.mx, [b]paolabz@innn.edu.mx, [c]alejandro.rodriguez.laguna@gmail.com, [d]mercedes@fisica.unam.mx, [e]jfranco@innn.edu.mx

Research area of interest: Biological Physics, physiological measures and mathematical methods.

Keywords: Dose Rate, whole-brain irradiation, cytokine, neuro-inflammation, IL-1β, radiobiology, ELISA.

Introduction: Modern radiotherapy now routinely utilizes fluence modifying techniques that has revolutionized the field. The flattening filter-free FFF beams by removing the flattening filter allow a significant decrease in treatment times by increasing the dose-rate of the accelerator as 2 to 4 times [1, 2]. However, questions have been raised about the radiobiological consequences of this treatment modality [1]. Radiation-induced late brain injury has been described in patients subjected to cranial radiotherapy for brain tumors. Consequential inflammatory and immune reactions [3] like the expression of the pro-inflammatory cytokine interleukin-1β have previously been found after whole-brain irradiation. Cytokines such as IL-1β mediate the adhesion and trafficking of leukocytes across endothelial cell monolayers into inflamed tissues of the central nervous system, and there is evidence that this may be an early indicator of cognitive dysfunction secondary to aspects of late inflammatory response [4, 5]. It has been reported noticeable changes in this expression 30 days after irradiation and is also consistent with the symptoms observed in patients that may only appear approximately 4 weeks after irradiation [5]. The purpose of this study was to investigate the radiobiological effects of FFF photon beams with high dose rates on the expression of IL-1β after whole-brain irradiation in rat model.

Methods: All procedures were approved by the Institutional Animal Care and Use Committee of the Neurological and Neurosurgery National Institute "Manuel Velasco Suárez" (Protocol Number 160/19) in compliance with the National Ministry of Health guidelines for the care of laboratory Animals. We used 9 male Wistar rats weighing 280-310 g. All rats were anesthetized with Ketamine and Xylazine and placed in a stereotactic frame and were irradiated with a prescription dose of 12 Gy and divided in two groups according to dose rate of 600 UM min^{-1} and 1200 UM min^{-1}. The rats were irradiated using high energy X-Rays from a dedicated linear accelerator TrueBeam STx (Varian Medical System). The procedure allowed to precisely locating the radiation target using tomography images and the treatment planning software Eclipse (Varian Medical System). The rats were decapitated 30 days after irradiation and brain tissue was processed; the IL-1β concentration was measured by BCA (Bicinchoninic Acid Protein Assay) and ELISA (The Enzyme-linked Immunosorbent Assay) analysis.

Results and Discussions: No statistical differences were seen in the expression of IL-1ß between conventional dose-rate (600 UMmin^{-1}) and high dose-rate (1200 UM min^{-1}) in the frontal cortex (p=0.386) and the hippocampus (p=0.248).

Conclusions: In our work, no differences in the expression of IL-1β were detected due the change on dose rate at same prescription dose in frontal cortex and hippocampal region of rat brain 30 days after irradiation. Nevertheless is it still necessary to increase the number of subjects and to further evaluate other structures that previously show neuro-inflammation like hypothalamus. Future work in this area includes the evaluation of higher dose-rates with clinical relevance.

References:

[1] King, R.B. et al., 2013 "An in vitro study of the radiobiological effects of flattening free radiotherapy treatments" Phys. Med. Biol.

[2] Y, Xiao et al., 2015 "Flattening filter-free accelerators: A report from the AAPM Therapy Emerging Technology Assessment WorkGroup". Journal of Applied Clinical Medical Physics.

[3] K. Lumniczky and T. Szatmari., 2017 "Ionizing Radiation-Induced Immune and Inflammatory Reactions in the Brain". Front. Immunol.

[4] P. Ballesteros et al., 2012 "Radiation-induced Neuroinflammation and Radiation Somnolence Syndrome." CNS and Neurological Disorders.

[5] Ballesteros, P. et al., 2014 "Whole-brain irradiation increases NREM sleep and hypothalamic expression of IL-1B in rats" Int. J. of Rad. Biol. pp. 142-148

Measurement of activity concentration of polonium-210 in species of the phylum Mollusca from Mexico

C.D. Mandujano-García[1,a], A.R. Nava-Huerta[2,b], P.-L. Ardisson[2,c], J. Huerta-García[1,d], I. Vioque[3,e] and R. García-Tenorio[3,f]

[1]*Environmental and Molecular Biology Laboratory, Autonomous University of Zacatecas, 98060 Zacatecas, Mexico*
[2]*Departmento de Recursos del Mar, Cinvestav, 97310 Mérida, Yucatán, Mexico*
[3]*Applied Nuclear Physics Group II, University of Seville, 41012 Seville, Spain*
[a]*cmandujano@fisica.ugto.mx,* [b]*ruth_an22@hotmail.com,* [c]*pedro.ardisson@cinvestav.mx,* [d]*jhuga@msn.com,* [e]*ivioque@us.es,* [f]*gtenorio@us.es*

Research area of interest: D. Biological physics, physiological measures and mathematical methods.
Keywords: Radioecology, gastropods, bioaccumulation, radioactivity, bivalves.

Introduction: Radioecology is a specialized branch of environmental sciences that studies how radioactive substances interact with the environment, as well as the mechanisms and processes that affect the migration of radionuclides in an ecosystem [1]. Some human activities release to the environment materials enriched with radioactive elements, as polonium, which may represent a radioecological risk. This paper explores the presence of polonium-210 in soft tissue from various gastropods and bivalve species that inhabit environments exposed to industrial activities from Mexico.

Methods: In the present project, we use the alpha-particle spectrometry technique for the quantification of polonium in soft mollusc tissue. A total of 890 samples of mollusc specimens were collected from an environment exposed to human activities that generate naturally occurring radioactive materials. The molluscs were identified, washed with distilled water, and then the soft tissue from each specimen was removed. For each species, a composed sample of soft tissue was dried in a convection oven for 48 h at 60 °C. For isolation of polonium from the matrix of the dried samples, the radiochemical process described in [2] was followed. This process is including an acid digestion of the samples, co-precipitation of actinides with iron hydroxide and source preparation by auto-deposition of polonium in cupper metallic plates. The measurements were performed in an Alpha Analyst System from Canberra. This spectrometric system uses passivated implanted planar silicon detectors and the software Genie 2000. Ethical issues were considered by following the indications in all the authorizations for collection and exportation of biological material provided by CONAPESCA, SENASICA and SEMARNAT, from Mexico as well as MAGRAMA from Spain.

Results: Preliminary data show that mollusc biocumulate polonium-210 with an average level of 158 Bq/kg. Molluscs from the taxonomic class Bivalvia presented a polonium-210 average value of 244 Bq/kg, meanwhile molluscs from the taxonomic class Gastropoda presented a polonium-210 average level of 42 Bq/kg. Figure 1 shows some values of polonium-210 obtained in several species of Mollusca.

Figure 1. Polonium-210 activity concentration (Bq/kg) in several species of molluscs from Mexico.

For comparison, reported concentrations of polonium-210 in molluscs from Kuwait; including different species of snails, clams and cockes, cover values from 10-215 Bq/kg [3]. On the other hand, in soft tissues of mussel species from India, the overall polonium-210 activity concentration varied from 156-928 Bq/kg [4].

Conclusions: The activity concentration values of polonium-210 in species of the phylum Mollusca from Mexico are very similar with those reported internationally. A further study on the mechanisms of migration and bioaccumulation of polonium in these organisms is recommended.

References:

[1] Brit Salbu, 2009. "Challenges in Radioecology", J. Environ. Radioact. 100, 1086–1091.
[2] Díaz-Francés I., et al., 2016. "210Po in the diet at Seville (Spain) and its contribution to the dose by ingestion", Radiat. Prot. Dosim., Vol. 168, No. 2, pp. 271–276
[3] Uddin et.al., 2015. "Radioactivity in the Kuwait marine environment — Baseline measure-
ments and review" Marine Pollution Bulletin 100, 651-661.
[4]Feroz Khan M., et al., 2014. "Polonium-210 in marine mussels (bivalve molluscs) inhabiting the southern coast of India" Journal of Environmental Radioactivity 138, 410-416.

FROM PLANNING TO OPERATING OF AN ABT BG-75 SELF-SHIELDING CYCLOTRON SERVICE

K. Vazquez[1 2], L. Rojas [1], M. Saucedo[1,2], A. Rivera[1,2].
[1,] Grupo Vitalmex, [2,] Imagen Tomográfica y Molecular.
Katya.rivera@vitalmex.com.mx, Luis.rojas@vitalmex.com.mx

Research area of interest: Education and profession

Keywords: Cyclotron, Planning, Commissioning, Acceptance, Licensing

Introduction: The low offer and the logistical operational requirements for purchasing radiopharmaceuticals for PET-CT services in Mexico, specifically the Mexican South-East is the biggest motivation for this project.

The implementation in Mexico of the first integrated service in nuclear medicine in the Mexican Peninsula, including Vitalmex' first Cyclotron service in the region, has presented great challenges in all stages of development.

Among the challenges that presented themselves along the way the most representative during the initial stages was the Cyclotron setup: project and business planning, construction site planning and licensing.

Methods: With a client focused, integrated decision making between financial technical and logistical professionals, the medical physicist played a key role between the organizations involved in this project and also the professionals needed to sort out the obstacles and official requirements.

A wide range of resources to develop this project were occupied by the professional team, lead by the medical physicist such as: professional advisors, Mexican Official Regulation (NOM), international guidelines in radiation safety, best practice documents and a lot of patience.

With specific logistical guidelines to drive the project onwards, we create a mindset around which to focus the efforts of the team involved.

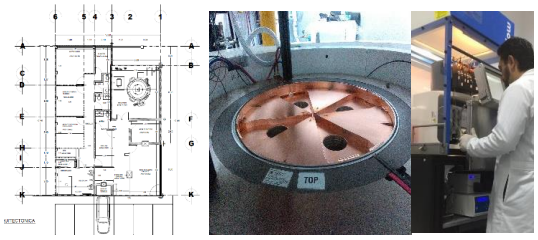

Figure 1. Planning, installation and acceptance

Results and discussion: The project now stands, regarding the cyclotron, on completed stages of financial projections, planning and construction, developing standard operational procedures and acceptance test; currently focusing on wrapping up operational licensing.

The PET-CT service is currently fully operational.

Conclusions: The development of this project has been a great professional experience for all those involved within the company regardless of its complexities.

It is important to have a solid logistics plan, on business project and construction, coordinate with authorities and decision makers and keep changes mid project to a minimal.

References: [1]. Ávila-Rodríguez MA, et al (2019) "Estado actual y perspectivas de la imagen molecular PET en México" Gaceta Medica de Mexico. 155.
[2]. Porter, M. (2002). "The Competitive Advantage: Creating and Sustaining Superior Performance". Mexico
[3]. Criterios para el licenciamiento y requisitos de inspección con ciclotrones para producción de radioisótopos utilizados en aplicaciones e investigaciones médicas, FORO, 2013.

Turning undergraduate research assistants into scientific researchers: a wooden-block based method

Mariela A. Porras-Chaverri[1,2], Marco A. Rodríguez-Jirón[1]
[1]*Escuela de Física, Universidad de Costa Rica, San José, Costa Rica, mariela.porras@ucr.ac.cr*
[2]*Centro de Investigación en Ciencias Atómicas, Nucleares y Moleculares (CICANUM), Universidad de Costa Rica, San José, Costa Rica.*

Research area of interest:
E. Education and professsional issues
Keywords: scientific training, active learning, STEM education

Introduction: In addition to limited funding, one of the limitations of scientific research in developing countries with a small population, such as Costa Rica, is the lack of human resource with the expertise needed to tackle research challenges. This is particularly the case for emerging fields such as Medical Physics. At the University of Costa Rica (UCR), much of the support to research projects comes from undergraduate students. The main challenge for the principal investigators (PI) is to train these undergraduates to be able to develop not only their assigned tasks, but also their critical thinking skills and knowledge of the field, in order to contribute meaningfully to the research. [1] This work presents the experiences of the Computational Medical Physics Laboratory (FIMEC, Laboratorio de Física Médica Computacional) in training undergraduate students (sophomore and up) for advanced scientific research using innovative educational resources and experiences. All research conducted at FIMEC requires knowledge of graduate level topics and methods in Medical Physics, particularly for the development of Monte Carlo simulations of radiation transport.

Methods: Incoming students undergo an induction training including the reading of textbook chapters, scientific articles and theses, with topics in basic concepts on radiation physics, statistics, and anatomy fundamentals. Students undergo a series of tutorials on the computer languages to be used as part of their work (C++, Fortran and others). The training activities are organized in a sequence of increasing difficulty by the PI, to allow the gradual development of skills and knowledge in the students according to their research topic. The students meet regularly with the PI to present their progress and discuss their work. Scientific discussions are aided with the use of educational materials, such as wooden blocks, anatomical models, and board games. These educational materials have been selected to help illustrate and discuss topics related to Monte Carlo modeling. The materials are also used in the design of experiments and the discussion of results. All students are given a laboratory book in which to keep their notes from meetings and their individual work. All exiting students are required to provide documentation on their work, including code manuals, usage guides and a summary of their results.

Results and discussion: Since this methodology was implemented at FIMEC in early 2019, 9 undergraduate students have been involved with the laboratory. Three of those students have submitted original work to an international peer-reviewed conference during 2019. Two of those abstracts were derived from work started in 2018 and one of the abstracts was proposed by students who started working at FIMEC in 2019. Two new internal research grants were submitted to UCR for 2020 based on the preliminary work of two other students. In all these works the students involved participated actively in the experiment design, development of software, analysis of results and submission process. In our experience, the use of wooden blocks has resulted to be particularly useful in the discussion of simulation geometries and the analysis of results, as it helps convey ideas both from and to the students in a direct and unequivocal fashion. The remaining students are currently at different stages of their initial training.

Conclusions: The implementation of a learning environment where students undergo a series of organized learning activities allows undergraduate students to obtain a minimum of necessary knowledge to become active participants in scientific research. The use of educational materials as aids in the discussion of abstract technical concepts and experimental design facilitates the transference of ideas between the PI and the students, and provides a way in which students can convey their own ideas.

References:

[1] Tiruneh et al., 2016. "Systematic design of a learning environment for domain-specific and domain-general critical thinking skills", Education Tech. Research Dev. 64:481-505.